QUANTIFYING RIPARIAN CANOPY ENERGY ATTENUATION AND STREAM TEMPERATURE USING AN ENERGY BALANCE APPROACH

A Thesis presented to the

faculty of the Graduate

School at the University of

Missouri-Columbia

In Partial Fulfillment of the

Requirements for the Degree

Master of Science

---

by

EDWARD BULLINER
Dr. Jason Hubbart, Thesis Advisor
May 2011

The undersigned, appointed by the dean of the Graduate School, have examined the thesis entitled

QUANTIFYING RIPARIAN CANOPY ENERGY ATTENUATION AND STREAM TEMPERATURE USING AN ENERGY BALANCE APPROACH

presented by Edward Bulliner, a candidate for the degree of Master of Science and hereby certify that, in their opinion, it is worthy of acceptance.

Dr. Jason A. Hubbart

Dr. Steven G. Pallardy

Dr. Neil I. Fox

DEDICATION

This thesis is dedicated to my mother and father. Your love and support is never forgotten and will always be appreciated.

ACKNOWLEDGMENTS

I would like to thank, to start with, everyone who has helped me to get where I am today. My family and friends have always been there to help me, up to and through my graduate education, and for that I am extremely grateful. Particular thanks goes to my parents, who have given me their unconditional love and support through my whole life in so many ways – I would not have been able to write this thesis without them.

I would especially like to thank my advisor, Dr. Jason Hubbart, for his guidance, support, encouragement, and insight throughout the past two and a half years. He has always been willing to grant help and new ideas when needed. Moreover, his willingness to challenge me and push me to do my best has made me grow not only as a scientist, but as a person, for which I am extremely grateful.

Special thanks should also go to my committee members, Drs. Steven Pallardy and Neil Fox. Their insights into my research have proved invaluable, as have their revisions in helping to write this document. Extra thanks goes to Dr. Fox, whose atmospheric physics course provided me with tremendous insight into the physical processes discussed in this research. Additionally, extra thanks goes to Dr. Pallardy and Kevin Hosman, who were very generous in helping to provide reference data from a nearby project used in this work. General thanks also goes to all faculty members at the University of Missouri who have instructed me in my coursework, providing me with the broad, interdisciplinary knowledge base needed to write this thesis.

I would also like to acknowledge everyone who has helped with field work related to this research. This has been a field work intensive research project, and I would have not been able to collect all of the data that I have without the help of others, including, but not limited to, Greg Hosmer, Pennan Chinnasamy, Graham Freeman, Thomas Stokely, Dan Scollan, and Malia Volke.

Finally, special thanks go to the Environmental Protection Agency, which provided funding for this research.

TABLE OF CONTENTS

LIST OF ILLUSTRATIONS

Figure Page

LIST OF TABLES

Table Page

QUANTIFTYING RIPARIAN CANOPY ENERGY ATTENUATION AND STREAM TEMPERATURE USING AN ENERGY BALANCE APPROACH

Edward Bulliner

Dr. Jason Hubbart, Thesis Advisor

ABSTRACT

Forested riparian buffers play an important role in modulating stream water quality, including temperature. Few studies have quantified the relationship between stream temperature and canopy cover in the climatologically distinct deciduous forests of the central U.S. Hydroclimate data were collected from two intensively instrumented stream reaches of opposite orthogonal compass orientation in a semi-karst watershed on the border of southern Missouri's Ozark region, USA, during the 2010 water year. Data were compared to above canopy reference measurements to calculate an energy budget for each stream reach. Average leaf area index (LAI) during the year was 2.64 in the riparian zone adjacent to the E-W oriented reach, and 2.43 in the N-S reach riparian zone. Air temperature and relative humidity transect data analysis indicated that riparian microclimate was significantly different (α=0.01) from the stream edge 25 or 40 meters away for 3 of 4 transects. Average stream discharge was 0.15 m^3/ and 0.25 m^3/s within the E-W and N-S reaches respectively. Mean stream temperature was greatest in August and was 24.4 °C in the E-W reach and 24.0 °C in the N-S reach. Net shortwave radiation was the primary energy flux causing stream heating (average 44.7 W/m^2 for E-W reach and 46.8 W/m^2 for N-S reach). Results suggest that riparian management practices in Missouri should potentially be altered to include wider buffers (40 meters) with less thinning (density dependent on stream size and discharge) to maintain pre-harvest stream temperature regimes.

CHAPTER I:

INTRODUCTION

Water temperature is an important biophysical controlling variable of aquatic ecosystem health (Allan and Castillo, 2007; Brooks, 2003). In-channel biological, physical, and chemical processes are affected by stream temperature (Caissie, 2006). Most aquatic organisms require specific temperature regimes to survive (Moore and Miner, 1997). Increased temperature can adversely affect many stream water quality parameters, for example dissolved oxygen concentration (Lane *et al.*, 1949; LeBosquet Jr and Tsivoglou, 1950; Webb *et al.*, 2008). Lower water temperature was shown to be related to higher total taxa richness of invertebrates (Wallace and Eggert, 2009). In many regions, streams have warmed as a result of changes in land use and management practices (Moore *et al.*, 2005a; Webb *et al.*, 2008). Forested riparian buffers protect stream aquatic ecosystems by supporting streamside vegetation resulting in buffered stream temperature regimes thereby improving or maintaining stream ecosystem health (Bunn *et al.*, 1999). This research seeks to improve the understanding of forested riparian zone form and function by quantifying riparian canopy ability to attenuate energy and thus ameliorate stream water heating. Project results and syntheses will characterize energy exchange processes at the stream surface and riparian canopy attenuation of the parameters controlling stream heating.

Quantifiable understanding of the capacity of riparian canopies to attenuate stream temperature by shading is limited. In particular, there is a lack of research in headwater systems of the ecologically and climatologically distinct deciduous forests of the central United States. Enhanced understanding of fundamental physical processes controlling stream temperature within riparian systems will provide land managers with improved information and tools (i.e. models) to sustainably manage these ecologically diverse and complex systems.

BACKGROUND

Processes Controlling Stream Temperature

To best understand forested riparian buffer impacts on stream water temperature first requires a fundamental understanding of the processes governing stream water temperature. Hereafter, any references made to stream temperature will refer to the temperature of water within the stream. Studies conducted by Brown (1969) and Pluttowski (1970) were among the first to attempt to quantify the energy fluxes in to and out of stream reaches with the goal of understanding the major factors influencing the thermal regime of stream water. Both studies established an energy balance based on local climate measurements for individual stream reaches over short (~1 day) time scales. An energy balance, also referred to as an energy budget, is an adaptation of the basic conservation equation as follows (Dingman, 2002):

$$\text{Amount in} - \text{Amount Out} = \text{Change in Storage} \qquad (1.0)$$

With regard to the stream energy balance, changes in stream water temperature (e.g. thermal energy storage) for a given reach are determined by quantifying the energy fluxes acting on the reach. Stream temperature fluctuations are thus driven by differences in the energy balance between stream water and the surrounding environment (Dechert and Woodruff, 2003). Energy balance models for streams generally predict change in stream temperature as a function of flow distance. Among the first energy balance models to predict stream warming was that proposed by Brown (1969), known as the Brown equation:

$$\Delta T = ((\Delta H * A)/Q) * 0.000267 \quad (1.1)$$

This equation is a physical model which calculates the maximum possible change in temperature (ΔT, units $^{\circ}F$) through a stream reach where H is the total energy input rate per unit surface area of stream (btu), A is the surface area of stream through the reach (ft^2), Q is stream discharge (ft^3/s), and 0.000267 is factor to convert cubic feet per second to pounds per minute so that change in temperature ($^{\circ}F$) can be expressed by btu. In this model, H includes net radiation, evaporative, conductive, convective, and advective energy exchanges.

Energy fluxes influencing stream temperature include net radiation, latent heat exchange (from evaporated or condensed water), sensible heat exchange with the overlying air, conductive exchange with the stream bed, advected energy (including thermal energy from precipitation, tributary streams, and groundwater/hyporheic

exchange), and friction (Caissie, 2006; Moore and Miner, 1997; Thompson, 2005). With the exception of friction, all fluxes can either be positive or negative, thereby either adding or removing energy from the stream.

In recent years there were numerous investigations designed to better quantify fundamental physical processes, or energy fluxes, controlling stream and river temperature and their relative importance (Bravo *et al.*, 1993; Brown, 1969; Hannah *et al.*, 2008; Hannah *et al.*, 2004; Jeppesen and Iversen, 1987; Mohseni *et al.*, 1999; O'Driscoll and DeWalle, 2006; Story *et al.*, 2003; Webb and Zhang, 1997). Studies indicated varying influences of energy fluxes to stream heating. In a recent review of stream and river temperature research, Webb (2008) hypothesized that differences between studies may be largely attributable to variations in climate and local physiography, indicating a need for regionally specific studies. Not surprisingly, relative contributions of energy balance terms were shown to vary seasonally in longer duration studies (Hannah *et al.*, 2008; O'Driscoll and DeWalle, 2006; Webb and Walsh, 2004). Ultimately, studies that integrate long-term comprehensive data, complex physiography and canopy interactions are critically needed to identify the primary drivers of stream temperature regime within specific systems for regional improvement of stream and riparian management.

Multiple studies showed that net radiation is the primary energy flux controlling stream temperature. Webb and Zhang (1997; 1999) measured heat fluxes for 33 river reaches in the U.K., mainly in Southwest England, over multiple years. For a short stream reach, they suggested a stream energy balance of the form:

$$Q_n = Q^* + Q_h + Q_e + Q_b + Q_f + Q_a \quad (1.2)$$

Where Q^* is net radiation, Q_h is sensible heat flux, Q_e is latent heat flux, Q_b is bed conduction, Q_f is frictional heating along the stream bank, and Q_a is advected heat. Neglecting advective heat fluxes such as precipitation and groundwater flux, they found the main drivers of thermal energy to a stream to be shortwave and longwave radiation incident on the stream surface, accounting for 70% of energy input, while main losses of energy were via longwave radiation emitted by stream water (36.8%) and latent heat via evaporation (33.3%). In a similar energy balance study in Scotland, net radiation was found to be the major energy input during summer for both a forested (deciduous) and an unforested stream, while latent heat loss was a major negative energy flux (Hannah *et al.*, 2008). It is noteworthy that in some streams, net radiation was shown to account for up to 99% of stream heating, as was observed in an Antarctic stream with no riparian canopy (Cozzetto *et al.*, 2006).

Stream thermal dynamics are often confounded by interaction with a stream's substrate (Johnson, 2004; Moore and Miner, 1997; Story *et al.*, 2003; Webb *et al.*, 2008), including conduction of heat to the streambed (Evans *et al.*, 1998), groundwater flux (Story 2003), and hyporheic exchange (Johnson and Jones, 2000; Poole and Berman, 2001). The prevalence of these processes depends both on the geology around the stream as well as the climate above the stream. In a study in Antarctica, Cozzetto *et al.* (2006) found hyporheic exchange accounted for six to 21% of stream cooling. Moore *et al.*

(2005b) showed that cooling via hyporheic exchange offset up to 25% of energy gains from net radiation for a headwater stream within a clearcut located in British Columbia. Story *et al.* (2003) found that groundwater inflow accounted for 40% of observed cooling in a coniferous-forested stream reach located downstream from a clearing, while localized hyporheic exchange and bed conduction accounted for the other 60%. In a stream energy balance study for a karst watershed in Pennsylvania, USA, O'Driscoll and deWalle (2006) determined groundwater was both a source and sink of thermal energy to a groundwater fed stream. In the winter, groundwater was a net source of thermal energy, as the subsurface temperature was warmer than stream temperature, resulting in a stream that was warmer overall than had there been no mixing with groundwater. In the summer, groundwater was a net sink of thermal energy, as the subsurface was cooler than stream temperature.

Groundwater flux, precipitation, and hyporheic exchange influence the volume of water flowing through a reach. Hyporheic exchange and groundwater exchange are different concepts in regards to stream energy flux calculations (Evans *et al.*, 1998). Hyporheic exchanged groundwater is generally thought of as water which was in the stream at some point, then infiltrated into the hyporheic zone below and adjacent to the stream. The water then travels a short distance within the hyporheic zone before returning to the stream. Groundwater exchange is water which enters (or leaves) the stream from the groundwater aquifer underlying the stream (Evans *et al.*, 1998).Change in flow volume from groundwater and hyporheic exchange complicate the calculation of an energy balance for a stream through a reach, in particular advected energy flux. Webb

and Zhang (1997) addressed the problem by using a mixing ratio to account for advected heat flux. Groundwater contribution to streamflow through a reach was calculated as the difference between measured upstream and downstream discharge, and groundwater temperature was assumed to be temperature measured 30cm below the streambed. Modeled downstream temperature was calculated accounting for the relative volumes and temperatures of both stream surface and groundwater contributions. Using this approach, modeled change in temperature from the inlet of a reach to its outlet influenced by advected sources is defined as the temperature of advected sources multiplied by the proportion of water at the outlet coming from advected sources added to the temperature of water at the inlet multiplied by the proportion of water at the outlet not from advected sources. This relationship is essentially an integrated version of the second or third terms to the right of the equal sign in equation 1.3 below (note that equation 1.3 separates advected energy from groundwater and hyporheic exchange, not computed by Webb and Zhang). Polehn and Kinsel (2000) proposed an energy balance model to account for changes in flow volume with advected fluxes, according to the following relationships:

$$\frac{dT_w}{dx} = \frac{\Sigma Q}{\rho C_p v D} + \frac{F_{gw}}{F}\left(T_{gw} - T_w\right) + \frac{F_{hyp}}{F}\left(T_{hyp} - T_w\right) \quad (1.3)$$

Where $\frac{dT_w}{dx}$ is change in stream temperature with distance downstream; $\frac{\Sigma Q}{\rho C_p v D}$ is the sum of non-advective heat fluxes divided by the density of water (ρ), specific heat capacity of water (C_p), stream velocity (v), and local mean depth (D); $\frac{F_{gw}}{F}\left(T_{gw} - T_w\right)$ is the flux of

groundwater (F_{gw}) divided by stream discharge (F) and multiplied by the temperature difference (T_{gw}-T_w) between the two mass fluxes; and $\frac{F_{hyp}}{F}(T_{hyp} - T_w)$ is the rate of hyporheic exchange (F_{hyp}) divided by stream discharge (F) and multiplied by the temperature difference (T_{hyp}-T_w) between the two mass fluxes.

Sensible and latent heat exchange with the air overlying the stream's surface also play an important role in stream thermal dynamics. Generally, latent heat exchange was shown to result in stream water cooling (Brown and Krygier, 1970; Webb *et al.*, 2008; Webb and Zhang, 1999), while sensible heat exchange can both add and remove energy from a stream reach, resulting in heating and cooling of the stream water, respectively (Hannah *et al.*, 2008).

A general quantification of change in stream temperature through a stream reach most relevant to this study is expressed as per Story *et al.* (2003):

$$T_{ds} = \frac{q_{us}T_{us} + L[q_{gw}T_{gw} + q_{hyp}(T_{hyp} - T_{us}) + \beta Q_u + \beta Q_c]}{q_{ds}} \quad (1.4)$$

where T_{ds} represents stream temperature at a downstream location; q_{us} and T_{us} represent stream discharge and temperature, respectively, at an upstream location; L represents the distance along the stream between the upstream and downstream points, q_{gw} represents average groundwater flux to or from the stream between the upstream and downstream locations per unit stream length; T_{gw} represents the average temperature of groundwater within the reach; q_{hyp} represents the average rate of hyporheic exchange per

unit stream length; T_{hyp} represents the temperature of the hyporheic zone; β represents the average width of channel through the reach divided by the specific heat of water ($4.18x10^6$ J/$m^{3\circ}$C); Q_u represents the net energy flux across the stream surface per unit area; Q_c represents the net energy flux across the streambed per unit area; and q_{ds} represents stream discharge at the downstream location within the reach. While notably not all terms in the above model are accounted for in this work, use of this model will provide insight into how stream surface energy exchanges influence stream temperature and give insights as to the importance of advected energy sources that are not quantified. Models such as these are one-dimensional; they assume that water temperature varies only as a function of distance downstream and not with depth or position across the stream channel; such assumptions are typically acceptable for low order, headwater streams (Sridhar *et al.*, 2004).

In practice, stream energy budget models are useful for identifying mechanisms of stream temperature change within forested riparian ecosystems, thereby helping to improve recommended riparian management practices (Moore *et al.*, 2005a). Figure 1 below illustrates energy fluxes into and out of a hypothetical riparian stream reach.

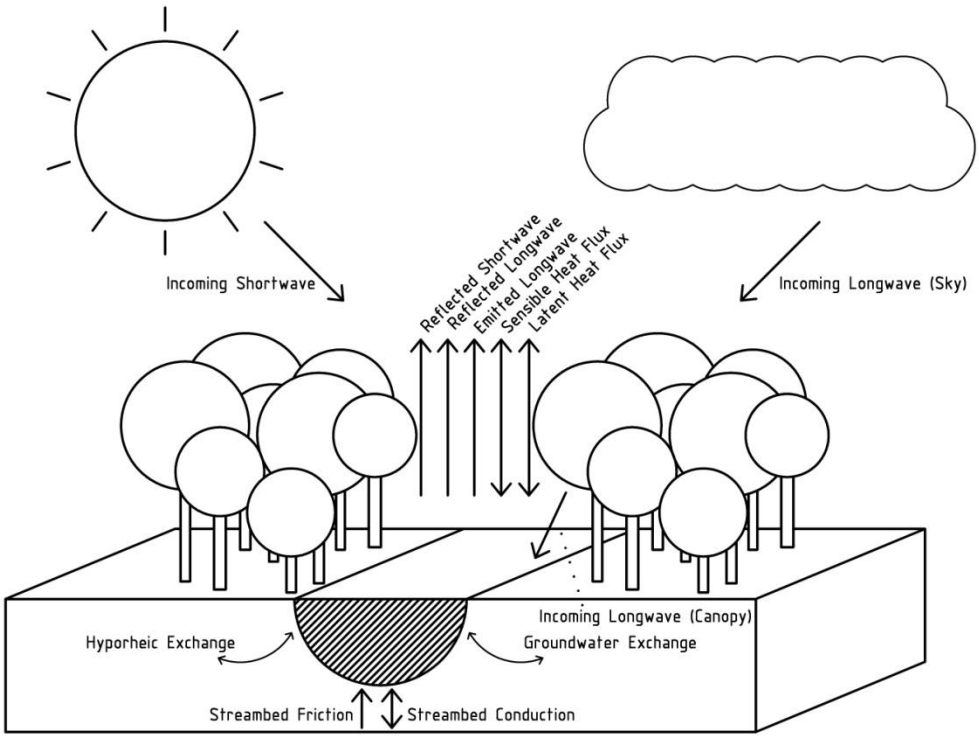

Figure 1: Components of the stream energy balance.

Correlations of stream temperature with climate variables also provide insight to processes driving stream temperature. In the absence of more detailed, reach-scale measurements, stream temperature is often estimated based on correlations to air temperature using various regression models (Smith, 1981; Webb *et al.*, 2008). Air temperature is used as an approximation of the equilibrium temperature, or stream temperature at which no net heat exchange occurs between water and the overlying air (Edinger *et al.*, 1968). A number of previous studies used simple linear regression models for air and stream temperature correlation (Crisp and Howson, 1982; Johnson, 1971; Mackey and Berrie, 1991; Neumann *et al.*, 2003; Smith, 1981; Webb and Nobilis, 1997).

More recently, nonlinear models were used at weekly time scales to correlate air temperature to stream water temperature (Mohseni *et al.*, 1999; Mohseni *et al.*, 2003; Mohseni *et al.*, 1998). Mohseni *et al.* (1999) suggested that an s-shaped (logistic) function is more effective for characterizing stream temperature as a function of air temperature. The logistic function accounted for upper limits of stream temperature due to evaporative cooling and lower limits due to advected inputs. Accounting for increases in evaporative cooling with increases in stream temperature, Bogan *et al.* (2006) estimated a mean upper boundary for stream temperature of 27.63°C with a standard deviation of 4.97 °C based on temperature data from 720 USGS gauging stations. Bogan *et al.*'s research was motivated partially by a desire to predict the impacts of climate change on stream temperature; air temperature increases of 1.0 °C are predicted on average to increase stream temperature by 0.16 °C (average for all stations), with streams that are already warmer tending to heat less due to evaporative cooling.

Riparian Zones

Riparian zones exhibit unique hydrologic and ecological characteristics that set them apart from many other aquatic and terrestrial ecosystems. Understanding the impact of forested riparian zones on stream temperature necessitates understanding what a riparian zone is, as well as an understanding of the varying terminology used in relation to riparian zones. In general, riparian zones are interfaces of terrestrial and aquatic ecosystems characterized with distinct biological communities (Naiman and Decamps, 1997). It is somewhat surprising that there is no universally (i.e. interdisciplinary)

accepted definition for what constitutes a riparian zone or how to delineate one. Terminology used to refer to riparian areas is inconsistent in scientific literature. This confusion largely occurs due to different priorities for riparian zones across disciplines, e.g. the functional extent of a riparian zone for a hydrologist studying sediment may be different than when viewed by a biologist studying wildlife habitat (Fischer *et al.*, 2000).

Typically, riparian areas have elevated water tables and higher soil moisture when compared to upland areas, resulting in distinct forest cover and understory vegetation (Moore *et al.*, 2005a). Riparian zones are generally described as extending from the stream edge to the uplands where vegetation is no longer influenced by elevated water tables, flooding, and soil moisture capacity associated with the stream (Naiman and Decamps, 1997). Though they are often only a small portion of land in an area, riparian zones are critically important because they form the linkage between terrestrial and aquatic ecosystems, and can therefore significantly affect exchanges of mass and energy between the two (Gregory *et al.*, 1991).

Among the terms used to refer to biotic communities associated with water bodies is ‘riparian wetland’. This particular term can be confusing as the term wetland often implies legal specifications and definitions, and thus environmental protection as established by the U.S. Army Corps of Engineers (ACOE) and Environmental Protection Agency for the U.S. as part of the Clean Water Act (US ACOE, 1987). The ACOE has sole authority for the determination of land areas designated as wetlands. To be considered a jurisdictional wetland, certain requirements must be met, namely vegetation adapted to hydric environments, hydric soils, and hydrologic conditions such that the

area is continuously inundated for at least five percent of its growing season (DuCharme, 2001; US ACOE, 1987). Jurisdictional wetlands can occur in riparian zones, but generally only account for a small portion of the zone, meaning a large portion of riparian zones are not afforded special wetland legal protection (Fischer *et al.*, 2000). Regardless of legal assignations, there is no argument that riparian zones are functionally distinct from upland forests and, like wetlands, play a fundamental role in modulating aquatic ecosystem health (Gregory *et al.*, 1991). In the state of Missouri, a study by the Department of Natural Resources concluded that most rivers in Missouri do not flood frequently enough to produce wetland hydrology within adjacent riparian zones (DuCharme, 2001). Regardless, riparian zones are identified as critical to stream health in Missouri (Whitledge *et al.*, 2006). On this basis, further study, quantification and validation of current Best Management Practices (BMP's) in Missouri forested riparian ecosystems is critical to optimally manage these highly productive and biologically diverse ecosystems.

Riparian Impact on Stream Temperature

It is widely accepted that riparian vegetated canopy cover influences energy fluxes governing stream thermal dynamics (Dechert and Woodruff, 2003; Ice, 2001; Moore *et al.*, 2005a; Pluhowski, 1972; Webb *et al.*, 2008). Canopy cover was generally shown to be associated with streams that are cooler with lower diurnal temperature variations; streams with harvested riparian zones remained four to six degrees warmer five years after harvest, and daily temperature range changed from 1.0 to 1.3 ˚C before

harvest to 2 to 3 °C post harvest for coniferous forests in British Columbia, Canada and Washington, U.S.A. (Ice, 2001; Macdonald *et al.*, 2003). The influence of riparian buffers on energy flux, and thus stream aquatic ecosystem health, depends upon multiple factors including stream geomorphology, riparian soil attributes, vegetative species composition, canopy structure and density, and land-use management (Broadmeadow and Nisbet, 2004; Moore *et al.*, 2005a). However, specific processes and mechanisms by which forested riparian buffers affect stream temperature and how buffers should be managed with regard to stream temperature remains a matter of intense debate (Beschta, 1997; Ice *et al.*, 2004; Johnson, 2004; Larson and Larson, 1996).

Microclimate beneath the riparian canopy influences energy exchange at the stream surface (Dechert and Woodruff, 2003; Johnson, 2004; Moore and Miner, 1997; Moore *et al.*, 2005a). In riparian zones, close association to free water surfaces may alter some energy flux variables important for stream water heating. While many studies have characterized microclimate underneath forest canopies, studies were not always conducted within riparian zones, which can be climatologically distinct. Previous research showed that, in general, forested canopies tend to reduce solar radiation, wind speed, and precipitation, and increase incident longwave radiation at the soil surface (Chen and Franklin, 1997; Chen *et al.*, 1999; Moore *et al.*, 2005a; Rambo and North, 2009). Lower wind speeds and dampened temperature variations beneath riparian forest canopies were shown to reduce latent and sensible heat exchange with streams (Brown, 1969; Story *et al.*, 2003; Webb and Zhang, 1997).

Many authors identified shading from solar radiation provided by forested riparian canopies to be the primary means limiting stream heating (Beschta, 1997; Johnson, 2004; Sugimoto *et al.*, 1997). For example, peak daytime net radiation incident on a stream can be up to five times greater for an unshaded stream reach versus a forested reach (Brown, 1969). An experiment conducted in Oregon, USA, showed that artificial stream shading lowered daily maximum stream temperatures, but did not have a large effect on either minimum or average stream temperatures (Johnson, 2004). Some authors, however, argue that shading is not the primary means by which riparian zones influence stream temperature; rather air temperature (i.e. sensible heat) is the dominant factor (Larson and Larson, 2002; Larson and Larson, 1996). For example, riparian vegetation removal was shown to increase streamside temperature by up to 4.4 °C (Dong *et al.*, 1998). Notably, both air temperature and shading are influenced by riparian vegetation canopy density.

Many studies have focused on stream temperature within forested riparian systems in relation to timber harvest in an attempt to better understand the impact of forest canopy thinning on stream thermal dynamics. Generally, forest harvesting increases solar radiation reaching the stream surface, thus influencing air, soil, and stream substrate and water temperature (Moore *et al.*, 2005a). Most studies focused on comparing pre-harvest calibration monitoring to post harvest monitoring in the Pacific Northwest of the U.S. and Canada. Johnson and Jones (2000) reported an increase in summer weakly mean stream temperature of 5.4 °C after harvest with a clearcut of all riparian vegetation. Macdonald *et al.* (2003) observed an increase in weekly average

stream temperatures of 2.5 °C after harvest with riparian buffer widths ranging between 10 and 30 meters, where all trees greater than 20 cm diameter at breast height (dbh) were harvested from within the buffer, resulting in canopy density ranging from 5-15% during the study period.

Studies of streams within riparian zones affected by wildfires have also provided useful information about the impact of reduced riparian forested vegetation (i.e. canopy) on stream temperature. A large number of trees can die during a wildfire, reducing stand density and canopy cover and thus attenuation of energy reaching a stream surface. Post-fire stream temperatures were shown to increase for streams in British Columbia, Canada following a fire in which 75% of the study catchment was burnded, resulting in riparian zones composed primarily of dead standing cottonwoods and coniferous species. (Leach and Moore, 2010a; Leach and Moore, 2010b). Increases in maximum water temperature after fire were found to be as high as ten degrees Celsius (Amaranthus *et al.*, 1989). Following a wildfire in Montana, USA, daily maximum stream temperatures within a riparian zone exceeded those from a nearby control stream, while daily minimum temperatures between the two corresponded closely (Hitt, 2003). Dunham *et al.* (2007) found elevated stream temperatures in multiple streams for up to 10 years following wildfires. Streams with altered morphology after fire, namely those with widened channels and decreased hyporheic exchange from increased runoff and debris, were associated with warmer temperatures, suggesting a relationship between channel disturbance and stream heating. Stream temperature was observed to increase by an average of two degrees Celsius after fire in a stream in British Columbia, Canada, relative

to a nearby control stream (Leach and Moore, 2008). However, the authors noted that stream-groundwater interactions can produce a large degree of spatial heterogeneity in stream temperature, influencing the effects of riparian disturbance. After fire, standing dead vegetation may still provide some energy attenuation; a recent study reported that dead trees following a wildfire reduced net radiation at a stream surface by approximately 50 percent compared to reaches where dead trees had been removed (Leach and Moore, 2010a).

The width and density of forested riparian buffers necessary to prevent heating of stream water is a matter of debate (Moore *et al.*, 2005a). Most studies focused on how microclimate variables were altered by increasing buffer width or distance from a stream. For example, humidity was shown to increase and solar radiation decrease exponentially with increasing distance from a stream in coniferous forest riparian buffers of the Pacific Northwest; climate gradients stabilized within 30m from the stream edge (Brosofske *et al.*, 1997). Sridhar (2004) reported that buffer widths greater than 30m did not significantly alter stream temperature in coniferous forests of the Pacific Northwest. In nine of 12 study transects within coniferous forests in the Eastern Cascade Mountains off Oregon, relative humidity was significantly higher than upland conditions for only the first five meters from the stream edge (Danehy and Kirpes, 2000). A large number of studies agree that most changes in microclimate within the riparian zone take place within one tree length of the buffer from the stream bank (Brosofske *et al.,* 1997; Hagan and Whitman, 2000; Ledwith, 1996). Orientation of buffer edges is also important; a study in Australia found that sunlight penetrating a riparian canopy horizontally from its

edge decreased rapidly after 10 meters for all orientations, but sunlight received 10 meters from the edge was significantly higher for edges facing the equator (e.g. south facing edges in the northern hemisphere) (Dignan and Bren, 2003). Another (northern hemisphere) study showed differences in light penetration and temperature from forest harvest edges between different edge orientations, with south and west oriented edges reaching maximum temperatures (measured within the first ten meters from the edge) up to six degrees Celsius higher than east and north oriented edges (Heithecker and Halpern, 2007). Orientation is also important for attenuation of wind and its associated advected energy exchange-wind was observed to penetrate further into forest edges facing the direction of the wind, with gradients not stabilizing until 40 meters into the forest (Davies-Colley *et al.*, 2000).

STATEMENT OF NEED

Riparian ecosystem management, in particular for water quality, is increasingly important as fresh water resources become increasingly impacted and development near streams becomes more likely (Baird and Maddock, 2005). To properly manage complex riparian ecosystems, best management practices (BMP's) are necessary to maintain water quality (MCC, 2006). Riparian forest BMP's usually include recommendations for minimum forest stand density, including leaving trees of particular size and density adjacent to the stream. Of as much importance is establishing proper management practices for reestablishing forested buffers in previously clearcut streamside zones (MCAF, 2005; Schultz *et al.*, 1995). Quantifiably validating the most effective catchment and reach scale forest buffer designs is critical to achieve economic and riparian zone

natural resource sustainability (Richards *et al.*, 1996; Rios and Bailey, 2006). Forest riparian buffers that are too narrow may provide inadequate protection to the stream, and buffers that are too wide reduce the area of available timber harvest (and thus margin of profitability), and potential area for agricultural crops (Broadmeadow and Nisbet, 2004).

Continued research is necessary to fill gaps in understanding and clarify assumptions pertaining to riparian forest buffer protection of stream water quality with respect to temperature dynamics (Hannah *et al.*, 2008; Johnson, 2003; Malcolm *et al.*, 2004; Moore *et al.*, 2005b; Webb *et al.*, 2008). There is an expressed need to quantify optimal riparian buffer width (Johnson, 2003), temporal variability of stream water temperature in small headwater catchments (Malcolm *et al.*, 2004), and the capacity for riparian forested buffers to influence stream water quality in terms of temperature. There is a particular need for more research in the central U.S., as the majority of previous stream temperature studies were undertaken in the northwestern U.S. (Anderson *et al.*, 2007; Danehy *et al.*, 2005; Johnson, 2003; Moore *et al.*, 2005b; Richardson and Danehy, 2007; Story *et al.*, 2003) or outside the U.S. (Bourque and Pomeroy, 2001; Hannah *et al.*, 2008; Malcolm *et al.*, 2008; Webb and Zhang, 1997) where, aside from geophysical differences, there are notable differences in both riparian forest composition, structure and climate. Furthermore, most previous energy balance studies were conducted within coniferous stream reaches, with only one study undertaken in a mixed deciduous forest, which produced different results (Hannah *et al.*, 2008). Additionally, to date, there was limited work characterizing thermal dynamics of headwater streams in the central U.S. A study that modeled stream temperature for an Ozark stream indicated increases in riparian

shading would result in more habitat capable of supporting smallmouth bass (Whitledge *et al.*, 2006). However, that work examined higher order streams and not headwater systems. Notably, there is increasing concern about the effects of climate change on stream thermal behavior, thus necessitating improved understanding of the physical processes controlling stream temperature (Caissie, 2006; Cooter and Cooter, 1990). Results from the current work will improve the understanding of a riparian hardwood forest's role with regard to energy attenuation and exchange with a stream water surface resulting in improved forest management practices in Missouri and the central U.S.

Currently there are no statewide mandatory regulations for riparian buffers in Missouri. Current timber harvest BMP's include recommendations for a 25ft wide primary buffer strip, followed by a secondary buffer strip of varying width depending on the slope of the land (Table 1); there is no mention of stream orders to which these recommendations apply. The combined buffer area is hereafter referred to as the streamside management zone (SMZ).

Table 1: Recommended riparian zone width according to current harvesting best management practices (MCC 2006).

Slope of Land [%]	Width of Buffer Strip for Common Logging Areas [ft]
0	50
10	50
20	65
30	85
40	105
50	125
60	145

Within designated riparian buffers, at least one-third, and preferably one-half to three-quarters, of trees should be left unharvested such that the basal area within the SMZ is at least 40 ft^2/acre. Basal area refers to the cross sectional area of wood in standing trees measured at four and one half feet above ground. Management recommendations specify that most trees on stream banks should not be harvested, and a closed canopy (no recommended leaf area index, LAI) within the SMZ should be maintained (MCC 2006). It is worth mentioning that current recommended Missouri BMPs are designed for erosion control and have not been validated with respect to canopy energy attenuation and stream water heating. Furthermore, recommendations do not apply to intermittent streams in the uplands of forested watersheds. Information is therefore critically needed to quantify the forested riparian buffer canopy density required to holistically sustain riparian and aquatic natural resources. The current research increases process understanding of stream thermal dynamics and relations between canopy density and stream temperature in the ecologically and climatologically distinct Ozark border region of the central U.S. Results should be immediately applicable to better management of

freshwater resources and riparian systems in the state of Missouri and throughout the distinct Ozark mixed-deciduous forest region.

OBJECTIVES

The overall objective of this study was to quantify the attenuation of light and energy flux to a stream surface via its adjacent forested riparian canopy. Specific energy fluxes (i.e. net radiation, sensible heat, and latent heat) controlling stream temperature dynamics within a second-order riparian stream reach will be characterized using the stream water energy balance approach. The attenuation the riparian canopy exacts on net radiation, sensible heat exchange, and latent heat exchange were quantified by comparison of differences in microclimate between study sites relative to an above canopy reference site as well as betweens stream reach orientations, thus quantifying how riparian buffer canopies modulate stream water temperature and ameliorate stream heating. In addition, this work sought to characterize temporal and spatial variation in headwater stream temperature. This research began to assess the influence of buffer width and stand density on water quality, supplying much needed science based information for future management practices within the state of Missouri. Specific objectives of this study included:

1. Quantify the extent of a forested riparian canopy's ability to attenuate the climate variables driving changes in stream temperature, accounting for spatial and temporal variability in canopy structure, as well as edge effects.

2. Given results from objective one, quantify the key energy fluxes affecting stream temperature over one hydrologic year. Key energy fluxes are assumed to be influenced primarily by microclimate, aspect, and landscape physiography.
3. Characterize variability in stream water temperatures between reaches of opposite orientation, accounting for spatial variations in topography and stream morphology, as well as temporal and spatial changes in canopy cover and microclimate.

HYPOTHESES

Specific hypothesis addressing each of the previous Objectives are as follows:

1.

Ho: Riparian canopy will attenuate stream temperature.

Ha: Riparian canopy will not attenuate stream temperature.

2.

Ho: Key energy fluxes will be influenced by microclimate, aspect and landscape physiography.

Ha: Key energy fluxes will not be influenced by microclimate, aspect and landscape physiography.

3.

Ho: Spatial variations in topography and stream geomorphology will influence stream water temperature.

Ha: Spatial variations in topography and stream geomorphology will not influence stream water temperature.

In agreement with previous studies, it was expected this work would show that the riparian canopy buffers the stream from incoming radiation and consequently buffers water temperature (Chen and Franklin, 1997; Chen *et al.*, 1999; Moore *et al.*, 2005a; Rambo and North, 2009). Attenuation of energy should be highly correlated to the canopy's leaf area index (LAI), which is an indirect measurement of canopy density. Because energy is attenuated by the canopy, there is less energy reaching the stream. Therefore, dampened radiative, latent, and sensible heat exchanges with the stream water are expected through each study reach relative to the above canopy reference site.

Variations in attenuated energy and energy exchange with the stream were expected between study sites. It was hypothesized that differences between the E-W and N-S reaches will occur primarily as a result of solar orientation to the canopy gap above the stream. Maximum stream heating will occur at midday for a N-S stream reach when the sun is directly above the canopy gap created by the stream. For an E-W stream, there will likely be less heating as the creek will be shaded by a portion of the streamside canopy for the entire day (Ice, 2001).

This work also sought to characterize spatial variability in riparian microclimate as a function of distance from stream edge. Previous studies showed that most microclimate gradients within a riparian zone stabilize within 30 meters of stream edge (Brosofske *et al.*, 1997; Ledwith, 1996). Additionally, major outside climate influences from clearcut edges diminish within approximately one tree height from the edge (15-60

meters) (Chen *et al.*, 1999; Davies-Colley *et al.*, 2000; Hagan and Whitman, 2000; Moore *et al.*, 2005a). Previous researchers combined distance from stream edge required for climate to stabilize to distance of penetration from outside edges and recommend a width of 45 meters for riparian buffers (Brosofske *et al.*, 1997). Notably, that research was conducted in coniferous forests of the Pacific Northwest, the coniferous forests of which can have canopy densities around twice that of the deciduous forests of Missouri (Breda, 2003). However, based on these results, current recommended buffer widths for Missouri may not be sufficient to attenuate incoming energy and prevent stream heating.

Stream water temperature changes were expected to be highly correlated to energy exchange processes at the stream surface (e.g. net radiation, latent, and sensible heat). Previous studies showed that net radiation is the most important factor determining stream water temperature change (Webb *et al.*, 2008). However, within forested reaches, groundwater cooling and substrate effects are also important. It is expected that results of this study will be similar to previous studies in that most stream water heating should occur as a result of net radiation. However, due to natural heterogeneity of deciduous canopies (including those of this study), reach orientation and seasonal variation of canopy cover, we expected variations in relative contribution of energy fluxes. We also expected advected sources of energy (groundwater and hyporheic exchange) to confound interactions between stream water temperature and modeled energy fluxes (i.e. net radiation, latent heat exchange, sensible heat exchange, and streambed conduction).

CHAPTER II:

MATERIALS AND METHODS

SITE DESCRIPTION

This research was conducted on two reaches of Brushy Creek located within the Baskett Wildlife Research and Education Area (BREA) (Figure 2). The BREA is an 890 ha wildlife reserve located in central Missouri, USA, owned and managed by the University of Missouri, consisting primarily of second-growth hardwood forests ranging in age from 85 to 170 years. Land use within the watershed is dominated by forests in the southern extent of the watershed and pasture (primarily for cattle) in the northern extents. According to 2005 land use surveys, the watershed consists of 1.3% impervious and light urban land use, 21.7% cropland, 32.1% grassland, 42.9% forest, and 2.0% open water and wetlands (MoRAP, 2009). According to the Strahler method (Strahler, 1952), Brushy Creek is a second order stream. Brushy creek has an average slope of 0.94% through the BREA. Each stream reach flows over alluvial bed material consisting of coarse gravel. The BREA includes a 4.9 ha lake (Ashland Lake) along Brushy Creek, created by a man-made dam, which aerial photographs (Figure 2) show has existed since at least 1939. The lake is located 2.4 km upstream from the E-W study reach. Ashland Lake has likely altered the hydrologic regime of Brushy Creek. There is also an open culvert on the bottom of the dam that was observed to have a very small flow contribution during a time of low spillway discharge. Thus, for drier periods during the year, water flowing in

Brushy Creek within the study reaches likely flows from a combination of the culvert at the base of the dam, groundwater from the surrounding terrain, and groundwater seepage from the dam. During higher flow periods, stream water flows from a combination of the aforementioned sources, terrestrial surface runoff, as well as surface discharge from the lake over the spillway. Water discharged over the spillway may be warmer during summer, as residence time in the lake may have allowed for energy/heat absorption; alternatively increased heat loss and cooling may occur during the winter. Relative to the stream water, the surface lake water may be closer to equilibrium temperature, where evaporative cooling balances warming from sensible heat and net radiation (Edinger *et al.*, 1968). Determining the proportions of groundwater, culvert discharge, spillway discharge, and seepage from the lake within Brushy Creek at each study site would require additional experimentation such as isotope studies which are beyond the scope of the current work. Downstream from the dam, Brushy Creek flows through a densely forested second growth riparian zone ranging from approximately 30 to 180 meters wide and forested hillslopes with slopes ranging from 25 to 55%.

The BREA was used for agriculture before becoming publicly owned in the 1930's. The total area of the property used for agriculture prior to public ownership is not known as clearings made in the forest were scattered and largely uncataloged. Notably, 1939 aerial photos showed much of the upland forests to be relatively open with evidence of previous selective thinning and clear cutting (Pallardy *et al.*, 1988). The BREA is geographically located on the border of southern Missouri's Ozark region, a transitional area between the central hardwood forest and central grassland regions of the United

States (Thom and Wilson, 1980). Vegetation of the BREA consists of a combination of Northern dominated and Southern subdivision oak-hickory forest species (Belden and Pallardy, 2009), including American sycamore (*Platanus occidentalis),* American elm (*Ulmus Americana),* and black maple (*Acer nigrum)* dominated riparian reaches (Belden and Pallardy, 2009). Understory species within the riparian zones include sugar maple (*Acer Saccharum*), flowering dogwood (*Cornus florida*), and black cherry (*Prunus serotina)* (Reed, 2010).

Figure 2: Comparison of 1939 (left) and 2007 (right) aerial photographs from Baskett Wildlife Research and Education Area, central Missouri, USA.

Within the riparian zone, low-lying areas that channel water to the stream become inundated with water during high flow events immediately following precipitation. Stream discharge is in general flashy, such that low-lying areas are normally inundated for no more than 12 hours. There are likely local areas within the riparian zone that are covered for a cumulative total of 8 days, which falls within the minimum required for jurisdictional wetland status in the state of Missouri (DuCharme, 2001). However, areas of standing water within the riparian zone were not quantified in this work. Furthermore, marginal wetland areas make up a relatively small portion of the watershed riparian zone such that the area taken as a whole should not be considered a jurisdictional wetland.

Climate in the BREA is classified as humid continental. Mean January temperature of -2.3 °C, July temperature of 24.3 °C, and annual mean precipitation of 1023 mm were recorded between the years 1971 and 2000 at the Columbia Regional Airport, located 8km to the North of BREA (Belden and Pallardy, 2009). For the period 2005-2008, on site average annual temperature (from flux tower described below) was 13.5 °C and average precipitation 969.8 mm versus 13.2 °C and 1023 mm at the Columbia Regional Airport.

The entire study area overlies limestone bedrock, resulting in a hydrologically distinct semi-karst system. A recent study of nearby (Bonne Femme and Bass Creek Watersheds, Boone County, MO) karst systems characterized one recharge area as having extensive development of large sub-surface water conduits (Lerch *et al.*, 2005). If present within this study site, such conduit development could result in significant groundwater exchange with the stream. The presence and influence of karst features in the BREA is

currently unknown, and is beyond the scope of the current study, but supplies impetus for future work. Hills surrounding each study reach are a mix of Clinkenbeard-Gasconade-Rock Outcrop and Bardley-Clinkenbeard soil complexes, USDA soil map units 60009 and 60012, respectively. These complexes are well-drained mixtures of residuum and slope-alluvium derived from limestone (Young *et al.*, 2001). Soil within riparian zones consists of a mix of Cedargap and Dameron soil complexes (USDA soil map unit 66017). Soils were previously classified as well-drained, frequently flooded soils of alluvial parent material, with average bulk density of 1.2 to 1.4 g/cm^3 (Young *et al.*, 2001).

Data were collected from hydroclimate stations located along two forested riparian stream reaches (Table 2), hereafter referred to as Site 1 and Site 2 (Figure 2), as well as from a flux tower (Ameriflux project, described below) located approximately 930 meters Northeast of Site 1. Vegetation at the reference site is a second-growth upland oak-hickory forest which includes white oak (*Quercus alba*), black oak (*Quercus velutina*), shagbark hickory (*Carya ovata*), sugar maple (*Acer saccharum*), and eastern redcedar (*Juniperus virginiana*) (Gu *et al.*, 2006). Site 1 was located at UTM15 coordinates 568922E 4288008N, elevation 177 meters, along an East-West stream reach approximately 90 m in length and 15m wide at bankfull. The stream within the E-W reach diverged into two channels during times of peak flow; this divergence was assumed to not impact study findings (explained in results section) Site 2 was located approximately 660 m S-SE of Site 1 at UTM15 coordinates 569137E 4287352N, elevation 174 meters along an approximate N-S reach 157 m in length and 10 m wide at bankfull.

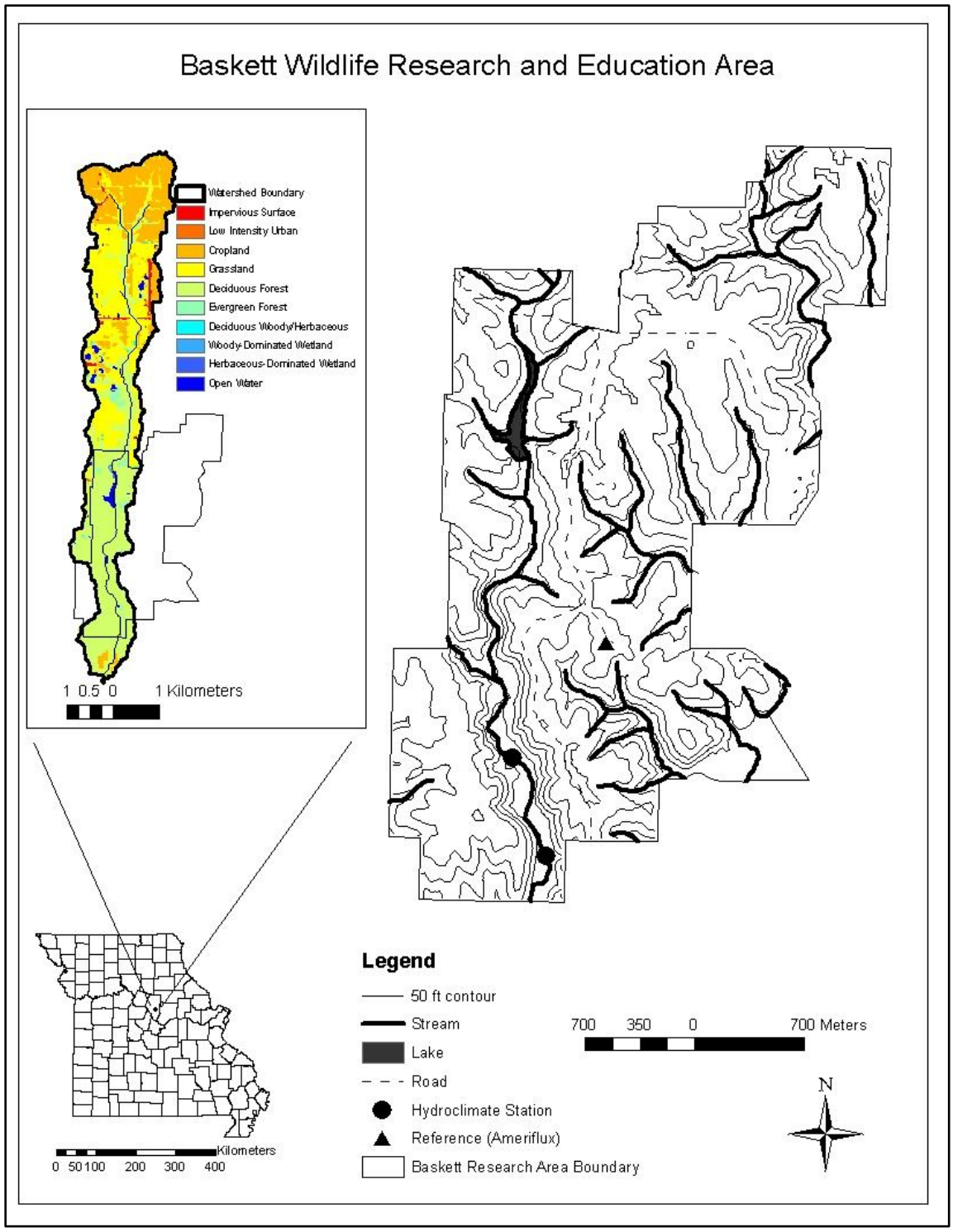

Figure 3: Map of hydroclimate station and above canopy reference site located in Baskett Wildlife Research and Education Area along second order stream Brushy Creek, central Missouri USA.

Data Collection

Each hydroclimate station consisted of an array of instrumentation that supplied necessary site specific data to quantify mass and energy fluxes through the riparian zone. Climate stations were located along the above described reaches approximately four meters from the stream edge-north of the stream at site 1 and east of the stream at site 2. Microclimate variables measured at each climate station included air temperature, relative humidity, wind speed, incoming shortwave radiation, net shortwave radiation, net longwave radiation, soil temperature at depths of 15 and 25 cm, precipitation, stream stage, and stream temperature at each climate station as well as approximately 45 meters upstream and downstream. Air temperature, relative humidity, wind speed, and radiative fluxes were measured approximately 2.5 meters above ground and 3 meters above the stream surface. Table 2 lists instruments used and relative error for each. Data at each climate station was measured at 10 second intervals, and averages were recorded in 15 minute intervals. Data were collected over the 2010 water year, October 1 2009 through September 30 2010. Climate stations were maintained at least biweekly. During maintenance, instruments were checked for damage and cleaned if necessary, data were downloaded, and desiccant packs within the stations' dataloggers were replaced as necessary.

Each climate station was complemented with a transect of iButton Hygrometer temperature/humidity sensors (Hubbart *et al.*, 2005). Transects are oriented perpendicular to the direction of the stream. The transect at the upstream site (Site #1) was oriented directly north-south and the transect at the downstream site (Site #2) was oriented

directly east-west. Each transect consisted of sensors extending both directions away from the stream. Sensors were housed in constructed radiation shields (Figure 4). On each side of the stream, a sensor was located at 0, 5, and 10 meters from the stream bank. After the initial three sensors on each side of the stream, spacing between sensors increased to 15 meters continuing to the edge of the riparian zone. This design was selected to characterize attenuation of energy horizontally through the canopy close to the stream edge in higher spatial resolution, while still covering the entire width of the riparian zone. There were a total of 19 sensors (iButtons, temperature and humidity) in the transect at Site #1 and 10 iButtons in the transect at Site #2. Hubbart *et al.* (2005) conducted an iButton accuracy assessment and found that that the sensors are within ±0.21 °C of a calibrated mercury thermometer (i.e. temperature standard).

IButtons were housed within an inexpensive fabricated radiation shield as designed and tested by Hubbart *et al.* (2005). The shield was built to effectively shed precipitation. It is comprised of a 6 oz and 8 oz white funnel assemblage. A clear plastic (plastic hose) spacer is placed over the end of the perforated 6 oz funnel to maintain separation between the two funnels and allow passive airflow. A 40 cm wire is run through the entire assemblage with a plastic cap positioned over the top that prevents precipitation from entering the shield. At the end (inside the 6 oz funnel) of the wire hangs a Key Fob that holds the Thermocron iButton. Total cost of this assemblage (discounting Key Fob and iButton) is approximately U.S. $4.00. Figure 4 below illustrates the design of the radiation shield. Performance of the radiation shield was

previously assessed by Hubbart (unpublished). Results from this experiment are provided in Appendix A.

Figure 4: Home built shield used to house iButton temperature and relative humidity sensors from radiation and precipitation, designed by Hubbart (2005). Photo by J.A. Hubbart.

IButtons were also buried within the streambed in the middle of the channel within each study reach at depths of 5 cm, 15 cm, and 25 cm. IButtons were housed in commercially available waterproof iButton housings. These iButtons logged stream temperature at 15 minute intervals starting in April 2010 and continued through September 30, 2010.

Additionally, reference data were collected from a flux tower on top of a forested ridge near the stream reach sites, UTM15 coordinates 569523E 4288716N, elevation 238 m. The flux tower is part of the U.S. Department of Energy funded AmeriFlux project and has been collecting on-site data since 2004 (Gu *et al.*, 2006). Half-hour averages for all sensed parameters were collected via a public ftp server (ftp://ftp.atdd.noaa.gov/pub/GEWEX/2009/mo/). Flux tower data complemented climate

station data. To allow for comparison to 15 minute averages recorded at the hydroclimate stations, averages were linearly interpolated between each logged value.

Table 2: Instrumentation of hydroclimate stations and above canopy reference (flux tower), Baskett Research and Education Area, Central Missouri USA.

Hydroclimate Station	Flux Tower	Variable Sensed	Location of Sensor (Hydroclimate / Flux)	Error of Sensor (Hydroclimate / Flux)
Keller America Acculevel Pressure Transducer	-	Water Depth [m]	2±1 cm above streambed/-	±0.25% total error band / -
Campbell Scientific, Inc. TE525WS Texas Electronics Rain Gauge	Campbell Scientific, Inc. TE525WS Texas Electronics Rain Gauge	Precipitation [mm]	2.8 m above surface/30 m above surface	±1% for rates up to 1 in./hr
Campbell Scientific, Inc. 034-B Met One Wind Set	R.M. Young 04101 Wind monitor	Wind Speed [m/s]	2.8 m above surface/32 m above surface	±.11 m/s when < 10.1 m/s / ±.5 m/s when <10 m/s
Kipp & Zonen's CNR2 Net Radiometer	Kipp & Zonen CNR1 Net Radiometer	Incoming and Outgoing Short and Long Wave Radiation [W/m^2]	2.7 m above surface/25.5 m above surface	<10% in daily totals / ±10% of daily total
LI200X LI-COR Silicon Pyranometer	LI200 LI-COR Pyranometer	Incoming Short Wave Radiation [W/m^2]	2.7 m above surface/30 m above surface	±5% maximum / ±5%
Campbell Scientific, Inc. 107 Temperature Sensor	YSI 44034 Thermistor	Temperature of Soil and Stream Temperature [°C]	2±1 cm above streambed, 15 cm below surface, 25 cm below surface/16 cm below surface	±0.2 ˚C / ±0.2 ˚C
Campbell Scientific, Inc. CS616-L Water Content Reflectometer	Delta-T Devices PR1/6 Soil Moisture Sensor	Soil Volumetric Water Content [%]	10 cm below surface/10 cm below surface	±2.5% / ±3%
Thermochron DS1923 Hygrochron iButton	-	Air Temperature [°C] and Relative Humidity [%]	3±0.4 m above surface/-	±0.5 ˚C, ±5% RH / -

Monthly measurements of leaf area index (LAI) were collected using two methods beginning in April 2010 and continuing through November 2010. As the goal of leaf area index measurements was to quantify stream shading, measurements were taken above the level of ground vegetation, which does not significantly shade the stream, and only accounted for the mid-story and canopy. The first method consisted of using two ceptometers, Decagon Devices LP-80, which measure photosynthetically active radiation (PAR) along an array of 80 sensors mounted on a one meter light bar. One ceptometer was set on a tripod approximately 1.6 meters above ground within a clearing to log reference PAR every minute. Measurements of PAR within the clearing were compared to measurements collected beneath the canopy. Leaf area index was calculated based on the ratio of the two measurements (Decagon Devices, 2006; Gower *et al.*, 1999; Law *et al.*, 2001). Computation of leaf area index from the ratio of the devices is discussed in data analysis, below. Ceptometer measurements were collected at three locations surrounding each climate station, at each iButton temperature humidity site within the riparian zones, at 20 randomly selected permanent locations within the riparian zone adjacent to each reach, and at seven locations within the stream along each reach. A PAR reading was recorded with the instrument oriented in each cardinal direction at all measurement locations, for a total of four samples per location, per time-period (i.e. monthly). Measurement locations are shown in Figure 5 below.

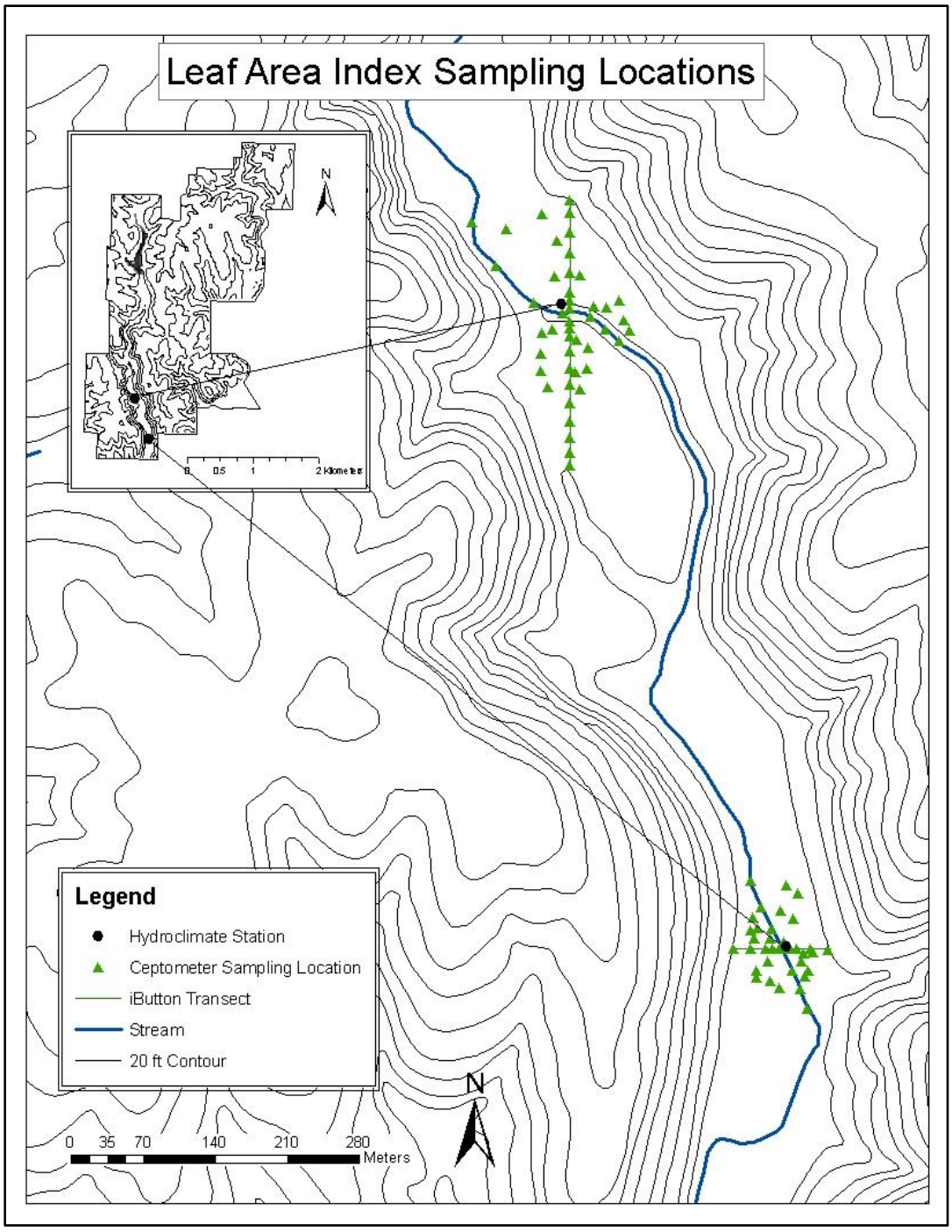

Figure 5: Locations of leaf area index (LAI) measurements at Baskett Research and Education area, Central Missouri USA

Leaf are index was also estimated using hemispherical photography at the same monthly intervals using a Nikon D60 digital slr camera with a Sigma 4.5 mm F2.8 EX DC circular fisheye lens. Photos were collected at the same time and locations as the ceptometer with the exception of the random points, which were not measured. Photographs were collected with the lens pointing vertically upward and camera base mounted 1.3 meters above ground. An aperture of f5.6 was used for all photographs. Exposure settings were determined manually by pointing a telephoto lens at a clear portion of sky and using the camera's aperture priority setting to determine the necessary exposure for given lighting conditions for an aperture of f5.6. The camera was then set two shutter speeds slower in order to overexpose the sky, creating greater contrast between leaves and the sky. A previous study showed that these exposure settings produced results with an R^2 of 0.95 (y=0.9961x-0.2332) and RMSE of 0.38 relative to a ceptometer (Zhang *et al.*, 2005). Analysis of hemispherical photos is described in data analysis below.

Missing data were filled using linear regression models. Coefficient of variation (R^2) values were over 0.91 in all cases. Included in the modeling was streambed temperature for the first half of the water year, as streambed temperature sensors were not installed until April.

DATA ANALYSIS METHODS

Quantifying Riparian Canopy Attenuation of Energy Fluxes

Comparisons between measurements from the stream-side climate stations and the reference flux tower provided necessary data to quantify the attenuation of energy flux through the riparian canopy. The influence of riparian canopy on net radiation, in particular attenuation of incoming solar (shortwave) radiation, is of primary interest due to its importance in stream heating, and dependence on canopy structure and density (Moore and Miner, 1997). Given the dependence on canopy density, it was important in this work to quantify the density of the riparian canopy to accurately estimate the net radiation received at the stream surface. Additionally, canopy density plays a key role in the attenuation of sensible and latent heat exchanges with the stream as these fluxes are driven primarily by air temperature, vapor pressure and wind speed, all of which are influenced by forest canopies (Chen and Franklin, 1997; Chen *et al.*, 1999; Moore *et al.*, 2005a; Rambo and North, 2009).

Even though incoming shortwave radiation was measured adjacent to each stream reach, it may not be appropriate to assume that those point measurements are representative of shortwave radiation incident at the stream surface. Canopy cover along the study stream reach differs both as a result of the canopy gap created by the stream as well as a result of spatial variability in vegetation in the riparian buffer. Furthermore, canopy cover varies seasonally with tree foliation/defoliation processes. Therefore, net radiation at the stream surface will vary spatially (varying canopy structure and density along stream reach), and temporally at daily (change in solar position through the day),

and seasonal scales (seasonal change in solar path and canopy density) (Ice, 2001). This variability must therefore be accounted for in energy balance derived stream energy (and thus temperature) computations.

Leaf Area Index

One method commonly used to approximate canopy density is by leaf area index (LAI), defined as the one-sided surface area of leaves per unit ground area (Campbell and Norman, 1998). The amount of photosynthetically active radiation (PAR) that is transmitted through a vegetative canopy is a direct function of canopy structure and density, characterizable by the canopy's leaf area index. To calculate LAI based on transmitted PAR underneath the forest canopy, the following equations were used (Decagon Devices, 2006):

$$\tau = exp\left\{\frac{A(1-0.47f_b)L}{\left(1-\frac{1}{2K}\right)f_b-1}\right\} \tag{2.1}$$

where τ is the fraction of PAR transmitted through the vegetative canopy, f_b is the fraction of incoming radiation that is direct beam, L is leaf area index, K is an extinction coefficient for the canopy, and A is a function of leaf absorptivity in the PAR wavelengths, calculated as follows:

$$A = 0.283 + 0.785a - 0.159a^2 \tag{2.2}$$

where α is leaf absorptivity for PAR, usually assumed to be approximately 0.9 (Decagon Devices, 2006). Equation 2.1 can be inverted to calculate L based on the amount of PAR transmitted as follows:

$$L = \frac{\left[\left(1-\frac{1}{2k}\right)f_b - 1\right]\ln\tau}{A(1-0.47f_b)} \tag{2.3}$$

Equation 2.3 above implies that measurements for LAI obtained via transmitted PAR are dependent on the fraction of radiation on top of the canopy which is direct beam as opposed to diffuse. When the direct beam radiation fraction is close to 0 parts of equation 2.2 become negligible and the equation simplifies to:

$$L = \frac{-\ln\tau}{A} \tag{2.4}$$

To assure accuracy of equation 2.3 to calculate LAI, all ceptometer measurements were collected during mostly cloudy to overcast conditions when the contribution of direct beam radiation is assumed negligible.

Canopy density can also be quantified in terms of LAI by use of hemispherical photo analysis. Hemispherical photos were analyzed using the program "Gap Light Analyzer" (Frazer *et al.*, 1999). The algorithms in the Gap Light Analyzer software, and other similar analyses platforms generally relate gap fraction (percent open sky seen at a point versus obstructions such as leaves) to leaf area index, and rely on an inversion of

Beer's law with the assumption that leaves in the canopy are randomly distributed. Beer's law characterizes radiative transmission through a medium (in this case, a forest canopy) and is written as follows (Campbell and Norman, 1998):

$$\varphi = \varphi_0 \exp(-kz) \tag{2.5}$$

Where φ is radiative flux density (W/m^2) at a given depth through a medium , φ_0 is unattenuated radiative flux density (W/m^2), z is the distance traveled through the medium (m), and k is the extinction coefficient (m^2/m^3). Since the penetration of direct light through a forest canopy is a function of leaf density through which light travels, LAI (a function of leaf density) can be calculated by quantifying the amount of light penetrating the canopy as seen from a given location. This relationship is characterized in the following equation (Stenberg *et al.*, 1994):

$$L = 2\int_0^{\pi/2} -2\ln[T(\theta)]cos\theta sin\theta d\theta \tag{2.6}$$

Where L is leaf area index, T is amount of light transmitted, and θ is zenith angle. This equation assumes that for a hemispherical photograph, leaf area index is a function of transmitted light, or gap fraction, integrated across zenith angles from 0 to 90 degrees. This integration was performed using the aforementioned Gap Light Analyzer software. Within the software, each photograph was manually assigned a threshold value that best contrasted sky from the canopy in each photograph. Pixels above this threshold value

were considered to be sky (transmitted light) and used by the program to compute LAI (Frazer *et al.*, 1999).

Gap Fraction Analysis and Incident Radiation Model

Incident solar radiation beneath forested canopies can also be calculated using mathematical functions that take into account canopy structure and density and that are dependent on the canopy's gap fraction (Ringold *et al.*, 2003). Gap fraction for beam radiation, g(t), varies with time as a function of both solar position over the course of a day as well as canopy density over the course of a year; gap fraction for diffuse sky and longwave sky radiation varies only over the course of a year as it is not dependent on solar position. Furthermore, these gap fractions vary spatially along the stream reach. Moore (2005b) provided the following equation (2.7) to express incident radiation at a given location beneath a forest canopy given temporally variable solar position and canopy gaps. In this equation, radiation is divided into diffuse shortwave, direct (beam) shortwave, and longwave radiation as these fluxes are attenuated differently by the riparian canopy. Incident radiation forms one component of net radiation (Q_r) for a reach. Average net radiation varies as a function of time (t) and can be characterized as follows:

$$Q_r = (1-\alpha)[D(t)g(t) + S(t)f_v] + \left[f_v\varepsilon_a + (1-f_v)\varepsilon_f\right]\sigma(T_a + 273.15)^4 - \varepsilon_w\sigma(T_w + 273.15)^4 \quad (2.7)$$

where α is stream albedo (varying as a function of zenith angle), D(t) is direct (beam) solar radiation above the canopy, g(t) is the canopy gap fraction for beam radiation between the stream and sun at time t, S(t) is diffuse sky radiation above canopy at time t, f_v is sky view factor from the stream surface, ε_a is atmospheric emissivity, ε_f is canopy emissivity, ε_w is emissivity of the stream, and T_a and T_w are air and water temperatures. Analysis of hemispherical photos collected over the course of the study allowed for quantification of gap fractions which of course changed temporally. Partitioning of diffuse and beam radiation was based on the clearness index and is discussed below (Erbs *et al.*, 1982; Leach and Moore, 2010a). This equation was the basis for modeled net radiation using the hemispherical photographs.

Canopy gap fraction (g(t)) for a given solar position and sky view factor (f_v) were estimated using hemispherical photography and Gap Light Analyzer (discussed in the previous section), resulting in expressions of radiative transmission as a function of time that can be applied across the entire dataset (Frazer *et al.*, 1999); contrasting sky from canopy pixels is described above in the LAI measurement section. While application of a threshold value is a somewhat subjective step, previous work has shown that modeled net radiation is relatively insensitive to threshold value used (Leach and Moore, 2010a). For an individual photograph, the software divided the picture's area into five degree sections for both altitude and azimuth angles. Fraction of sky pixels (beam radiation can pass through) versus total pixels was calculated for each section, as well as summed for the entire picture to calculate view factor for diffuse sky radiation. To calculate incident shortwave radiation for a given time, the solar position was used to select the appropriate

5˚x5˚ section within the photograph. Gap fraction within this section was multiplied by the above canopy beam radiation, and gap fraction for the entire photo was multiplied by above canopy diffuse sky radiation.

Solar position was computed using the following equations (Campbell and Norman, 1998):

$$\sin\beta = \sin\varphi \times \sin\delta + \cos\varphi \times \cos\delta \times \cos[15(t - t_0)] \quad (2.8)$$

Here, β is solar altitude in degrees, δ is solar declination in degrees, φ is latitude in degrees, t is time of day in hours, and t_0 is time of solar noon, in hours. These variables remain the same for the following equations. δ was calculated as follows:

$$\sin\delta = 0.39785 \times \sin[278.97 + 0.9856J + 1.9165 \times \sin(356.6 + 0.9856J)]$$

J is day of the year, with January first equal to one. Time of solar noon, t_0, was calculated as:

$$t_0 = 12 - LC - ET \quad (2.9)$$

LC is the longitude correction factor, and is +1/15 hour each degree east of the nearest standard meridian, or -1/15 hour each degree west. Standard meridians are multiples of 15˚. LC was determined to be -0.15 hours. ET is the equation of time (hours), and varies according to day of the year as per the following equation:

$$ET = \frac{-104.7\sin f + 596.2\sin 2f + 4.3\sin 3f - 12.7\sin 4f - 429.3\cos f - 2.0\cos 2f + 19.3\cos 3f}{3600}$$

Where:

$$f = 279.575 + 0.9856 \times J \quad (2.10)$$

Here, f is in units degrees, and again J is day of the year. Azimuth (AZ) was calculated as follows:

$$\cos AZ = \frac{-(\sin\delta - \cos\psi \sin\varphi)}{\cos\varphi \sin\psi} \quad (2.11)$$

ψ is solar azimuth angle in degrees, and is simply equal to 90-β.

Relative contributions of above canopy diffuse sky radiation and direct beam radiation were not measured on site. These fractions were therefore modeled. The ratio of diffuse to total shortwave radiation, k_d, is dependent on the clearness index, k_t. k_t is the ratio of shortwave radiation incident on a surface to extraterrestrial solar radiation (total radiation that would be incident on the surface were it not scattered by the atmosphere). It was calculated as follows (Erbs *et al.*, 1982; Leach and Moore, 2010a):

$$k_t = \frac{R_{in}}{1379 \times \cos\psi} \quad (2.12)$$

Where R_{in} is measured incoming shortwave radiation at the reference flux tower. 1379 is the solar constant (W/m^2) and represents irradiance at the extent of the earth's atmosphere, and is multiplied by the cosine of the solar zenith angle according to Lambert's cosine law to quantify the radiation spreading over a surface which is not perpendicular to its source. For each 15 minute timestep, k_d was calculated as follows (Erbs *et al.*, 1982; Leach and Moore, 2010a):

For $k_t \leq 0.22$:

$$k_d = 1.0 - 0.09k_t \quad (2.13)$$

For $0.22 < k_t \leq 0.80$:

$$k_d = 0.951 - 0.1604k_t + 4.388{k_t}^2 - 16.638{k_t}^3 + 12.336{k_t}^4 \quad (2.14)$$

For $k_t > 0.80$:

$$k_d = 0.165 \quad (2.15)$$

Since canopy density varies through the year, a linear interpolation model was developed within the software package Matlab to compute gap fraction for both beam and diffuse components of solar radiation incident on the stream surface for all 15 minute timesteps of measurements collected during the 2010 water year. The code applied solar position as computed above and selected for each time step the appropriate section (containing the solar coordinates for the given timestep) within the hemispherical photo analysis grid. A value for gap fraction within that section was then linearly interpolated between the two nearest measurement dates for that section for five of the seven hemispherical photos collected within the stream reach (the furthest upstream and downstream photos were not included in this analysis as they were considered too far from the sensors measuring stream temperature). These five values were then averaged to calculate beam gap fraction for that timestep. Total gap fraction for the entire image to calculate diffuse sky attenuation was also interpolated at each time step. Finally, for each time step, beam shortwave radiation was multiplied by computed beam gap fraction, and diffuse sky shortwave radiation was multiplied by total gap fraction. Combined, the two quantities represent modeled incident shortwave radiation at the stream's surface, expressed in the following equation:

$$S_{in} = (1 - \alpha)[D(t)g(t) + S(t)f_v] \quad (2.16)$$

where α is stream albedo (varying as a function of zenith angle), D(t) is direct (beam) solar radiation above the canopy, g(t) is the canopy gap fraction for beam radiation between the stream and sun at time t, S(t) is diffuse sky radiation above canopy

at time t, and f_v is sky view factor from the stream surface. Multiplying this value by stream albedo resulted in estimation of net shortwave radiation at the stream surface.

The above described method was replicated for three images collected around each hydroclimate station. Values from this model were compared to shortwave radiation measured at each hydroclimate station to assess accuracy of the method, and also used to compute net longwave radiation incident on the stream surface. Incoming longwave radiation L_{in} was calculated as follows:

$$L_{in} = f_v \times L_{ref} + (1 - f_v) \times \varepsilon_f \times \sigma \times (T_f + 273.15)^4 \quad (2.17)$$

Here, f_v is sky view factor, L_{ref} is incoming longwave radiation as measured at the reference site above the canopy, ε_f is canopy emissivity, σ is the Stefan-Boltzman constant, and T_f is canopy temperature in ˚C. Canopy temperature was assumed to equal air temperature as measured at the hydroclimate stations, and canopy emissivity was assumed equal to 0.97, a typical value for most natural surfaces (Campbell and Norman, 1998).

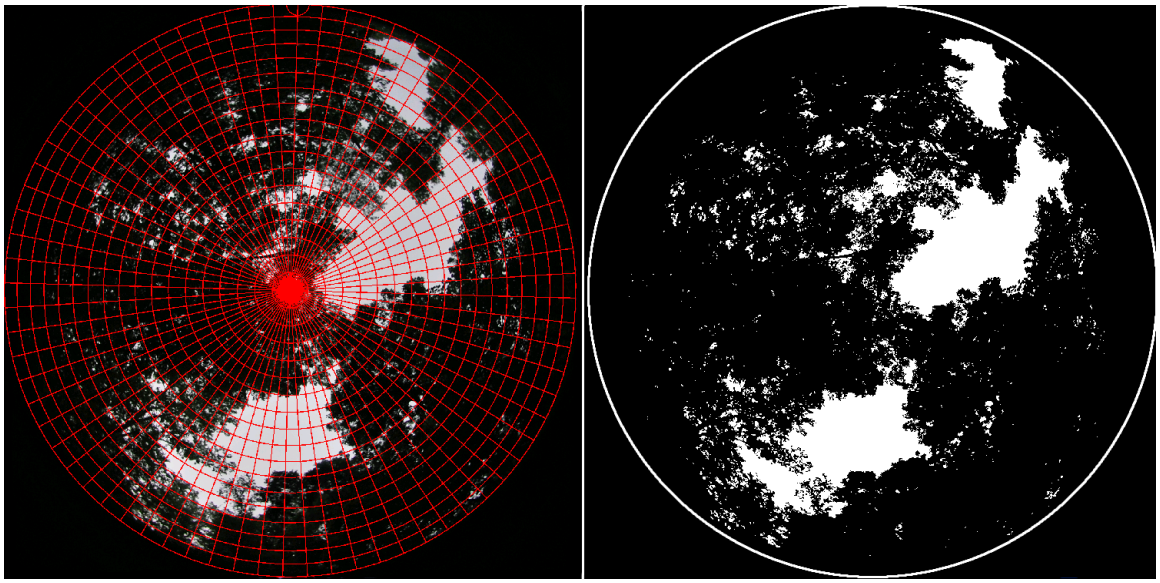

Figure 6: Example of hemispherical photo used for gap fraction analysis and quantification of incoming shortwave and longwave radiation. The photograph is divided into 5˚ segments of azimuth and altitude (left). A threshold value is applied to differentiate sky and canopy to determine sky view factor (right).

Modeled shortwave radiation values were compared to measurements collected in stream during the period September 2 2010 through September 30 2010. During this time, an Apogee SP-110 pyranometer was installed in the middle of each stream channel approximately 0.75 meters above the streambed to validate the best method for quantifying incident radiation on the stream water surface (Figure 7). These sensors were connected to dataloggers that logged 30 minute averages of incoming shortwave radiation for September 2 through September 30, the end of the study period. This method was used to validate how well incident radiation modeled through the reach correlated with radiation measured at one point. This is the general method used to estimate incident radiation on a stream reach in stream energy balance studies (Leach and Moore, 2010a).

As most stream energy balance studies have used radiation sensors mounted directly above stream (Hannah *et al.*, 2008; Johnson, 2004; Moore *et al.*, 2005b; Webb and Zhang, 1997), which we did not have at this study site for most of the water year, it was necessary to find the best approximation.

Figure 7: Pyranometer installed approximately 0.75 meters above streambed near middle of canopy gap created by N-S stream reach, Brushy Creek, Baskett Research and Education Area, Central Missouri USA.

Shortwave radiation data collected using the Apogee pyranometers from September 2 through September 30 were compared to three other methods for quantifying incident shortwave radiation on the stream's surface.

1. The first method was based on the assumption that transmitted light did not vary significantly spatially between the riparian zone and stream reach. Therefore incident

shortwave radiation as measured at each hydroclimate station was assumed to be characteristic of shortwave radiation incident on the stream surface within each reach, and radiation values measured at each climate station were compared directly to measurements from the in-stream apogee pyranometers.

2. The second method was to use the previously described hemispherical photo model (equation 2.16), reliant on gap fraction estimates, solar position, and above canopy estimates of diffuse sky and direct beam radiation to model incident shortwave radiation on the stream surface and compare to measurements from the in-stream apogee pyranometers.
3. The third method was to solve equation 2.4 for shortwave transmissivity, which shows transmissivity as a function of leaf area index (as measured by ceptometer) and leaf absorptivity (assumed to be 0.9, the absorptivity for green leaves) (Decagon Devices, 2006). Above canopy shortwave radiation measurements were multiplied by this transmissivity to model incident shortwave radiation at the stream surface.

For method 3, LAI values measured within the stream reach with the ceptometer method were averaged for each measurement date, and timesteps in between each measurement were filled by linear interpolation to create a continuous time series of values for the entire study period. Measurements from the streambed pyranometers were interpolated using Microsoft Excel to 15 minute time steps to allow for direct comparison to the other methods. The 15 minute averaging period was selected as it was closest to the short averaging period used by recent stream energy balance studies (Hannah *et al.*, 2008; Leach and Moore, 2010a).

Modeled values were compared to measurements using several metrics. A similar study by Leach and Moore (2010a) used root mean square error (RMSE) and mean bias error (MBE). These metrics were also used for this study. MBE was calculated as follows:

$$MBE = \frac{1}{n}\sum_{i=1}^{n} x_i - x_{true} \quad (2.18)$$

where n is the sample size, x_i is the modeled value for a given time step, and x_{true} is the measured value for a given time step. RMSE was calculated as follows:

$$RMSE = \sqrt{\frac{1}{n}\sum_{i=1}^{n}(x_i - x_{true})^2} \quad (2.19)$$

where all variables are the same as the MBE calculation.

Modeled values were also compared to measurements with linear regression, similar to a previous study that compared hemispherical measurements of solar exposure to canopy density measurements with a densitometer (Ringold *et al.*, 2003). Ringold *et al.* (2003) concluded there was a strong correlation between densitometer readings and hemispherical photo estimates of solar exposure, with R^2 values between reach scale averages of hemispherical and densitometer readings ranging from 0.53 to 0.94.

Horizontal Variation Attenuation of Energy by a Forest Canopy

Also of interest in understanding the riparian canopy's ability to attenuate light and energy is the change in climate spatially into the riparian zone from the stream edge. Change in temperature (˚C) and relative humidity (%) through the riparian zone was quantified by examining spatial variation of these parameters along the previously

described iButton transects, and by quantifying how the variables changed when moving from the stream edge (gap) to the interior of the riparian zone. The analysis further quantified energy flux attenuation by the riparian canopy by examining edge effects and spatial change in microclimate moving away from the stream. The objective of this investigation was to determine the extent to which the stream and associated canopy gap influenced climate within the riparian zone. Measurements of air temperature and relative humidity were compared using a pairwise analysis of variance test (ANOVA), analogous to the work of Brosofske *et al.* (1997) who investigated microclimate gradients within coniferous riparian forests. A basic ANOVA table is presented in Table 3:

Table 3: Summary of statistics for ANOVA analysis.

Source of Variation	Degrees of Freedom	Sum of Squares	Mean Square	f
Regression	1	SSR	SSR	$\frac{SSR}{MSE}$
Error	n-2	SSE	$MSE = \frac{SSE}{n-2}$	
Total	n-1	SST		

f=f-test statistic

where: SSR=Sum of Squares Regression: Measure of variation explained by linear relationship, SSE=Sum of Squares Error: Measure of unexplained variation, and SST=Sum of Squares Total: Total of SSE and SSR. The sample size is represented by n. Correlation between different treatments (e.g. distance from stream) was tested by conducting an F test and concluding correlation if the test statistic $f \geq F_{\alpha,1,n-2}$, where α is the probability of a type I error and n is the number of samples (Devore, 2000). Tukey's test to compare means was used to select iButtons which had significantly different mean temperatures and relative humidities (Brosofske *et al.*, 1997; Devore, 2000).

Stream Energy Balance

All major energy balance terms affecting stream temperature through each reach were quantified either via direct measurement or mathematical models. In some cases, energy fluxes were calculated based on measurements collected at a single point. However, previous studies assumed that for short reaches (<200m), energy exchanges

calculated at a single point are representative of the entire reach (Hannah *et al.*, 2008; Story *et al.*, 2003). Therefore, all calculated energy fluxes were conceptualized as acting across the entire reach. For this study, the following fluxes across the water surface (Q_u) were considered, following the stream energy balance terms identified by Webb and Zhang (1997) that characterize the major energy fluxes acting on a stream:

- Q_r=Net radiation (including shortwave and longwave fluxes) above the water surface (W/m^2)
- Q_e=Latent heat flux via evaporation and condensation (W/m^2)
- Q_h=Sensible heat transfer via convective and conductive exchange of energy with air overlying stream surface (W/m^2)

Energy flux at the streambed, following the stream energy balance terms identified by Webb and Zhang (1997) includes:

- Q_{fc}=Heat flux due to bed friction (W/m^2)
- Q_{hb}=Heat flux due to bed conduction (W/m^2)

The summation of these terms to represent non-advected energy exchange within the stream reach yields the following equation, where Q_u represents the total non-advected energy available for stream heating or cooling.

$$Q_u=Q_e+Q_h+Q_r+Q_{fr}+Q_{hb} \quad (2.20)$$

Advected heat fluxes are accounted for in equation 1.4 from Story (2003) above. Advection from precipitation, and advected energy from evaporating water molecules (this term refers to actual sensible energy contained in evaporated water molecules in the form of water temperature as opposed to the latent energy which causes evaporation to occur discussed below) are not included as they were shown to have negligible impacts on stream water temperature relative to the above fluxes (Evans *et al.*, 1998).

Webb and Zhang (1997) used a modified Penman equation to quantify latent heat flux from the stream's surface:

$$E_v = 0.165 * \left(0.8 + \frac{U}{100}\right) * (E_w - E_a) \quad (2.21)$$

Here, E_v is the evaporative flux of water in mm/day, U is wind speed in km/day, E_w is saturation vapor pressure at the temperature of water within the stream reach, and E_a is the actual vapor pressure of the air above the stream (both vapor pressures in units mbar). Saturation vapor pressures were calculated according to the following equation:

$$E_w = 0.611kPa \times e^{\left(\frac{17.502T}{T+240.97°C}\right)} \quad (2.22)$$

where T is the temperature in degrees Celsius. Actual vapor pressures were calculated by multiplying the saturation vapor pressure by relative humidity.

Previous studies used wind speed measured two meters above the stream surface for evaporative flux calculation (height specified by model for calculations) (Hannah *et al.*, 2008; Moore *et al.*, 2005b). Since wind speed was measured 2.8 meters above the

ground surface, which is itself approximately one meter above the stream water surface at each site, measured values would not be comparable to previous studies. Therefore, measured values were used to model wind speed two meters above the stream water surface, which equals one meter above the ground surface. To do so, the following equation was used:

$$u(z) = \frac{u^*}{0.4} \ln \frac{z-d}{z_m} \quad (2.23)$$

where u is wind speed (m/s), u^* is called the friction velocity (m/s), z is the height above a surface (m), d is called the zero plane displacement (m), and z_m is called the roughness length (dependent on the roughness of surface) (m). Generally, this equation expresses wind speed above a canopy; however within the first 10% of a canopy above ground the relationship also holds (Campbell and Norman, 1998). In this case, the zero plane displacement is zero and the roughness length used is characteristic of the underlying soil. A roughness length of 0.09 meters was selected to match the surface underneath the forest canopy (Campbell and Norman, 1998). For all timesteps, the friction velocity was calculated based on the measured wind speed 2.8 meters above the riparian zone's surface (3.8 meters above stream surface) according to equation 2.23. Calculated friction velocity was then used again in equation 2.23 to calculate wind speed one meter above the riparian zone's surface (2 meters above the stream surface).

Using evaporative flux calculations, the latent heat flux from a stream surface can be calculated using the following equations, from Webb and Zhang (1997).

$$Q_e = E_v * \lambda * p \quad (2.24)$$

$$\lambda = 2454.9 - 2.366 * T_a \quad (2.25)$$

Q_e is latent heat flux (W/m^2), λ is latent heat of vaporization for water, and ρ is density of water.

The Bowen ratio, B, is defined as the ratio of sensible heat flux to latent heat flux from a free water surface (Bowen, 1926).

$$B \equiv \frac{Q_h}{Q_e} \quad (2.26)$$

This ratio was estimated using the formula (Webb and Zhang, 1997):

$$B = \left[0.61 * P * \frac{T_w - T_a}{E_w - E_a}\right] / 1000 \quad (2.27)$$

Since latent heat flux is calculated using the Penman-style equation (equation 2.21), calculating the Bowen ratio provided necessary information to estimate the sensible heat flux, Q_h to or from the stream's water surface. This method of calculating sensible heat flux from the stream surface is a accepted standard for stream energy balance studies (Hannah *et al.*, 2008; Johnson, 2004; Leach and Moore, 2010a; Moore *et al.*, 2005b; Webb and Zhang, 1997).

Net radiation, Q_r was measured directly adjacent to each stream reach at the climate stations with a net radiometer. However, vegetated canopy density varies spatially within the riparian zone of each study reach, particularly above the stream, where there is a canopy gap. Quantifying the incoming shortwave and longwave radiation at the stream surface was estimated using a variety of methods and values compared by examining differences between summary statistics as well as root mean square error, mean bias error, and R^2 coefficients (see Results). Energy from incident solar radiation is generally transmitted to the surface of the streambed. However, because water is very effective at conducting heat away from the streambed, the effective absorptivity of water for solar radiation is very high (Ice, 2001). Therefore, it is assumed that the effective transmission of radiation within the stream is low, and all incident radiation on the stream that is not reflected at the stream surface is absorbed by the water-either directly or by absorption and reemission by the streambed.

The flux of longwave radiation emitted from the stream surface is expected to be slightly different than that emitted from the forest floor, as emitted longwave radiation is a function of a surface's temperature and emissivity (Campbell and Norman, 1998). Longwave radiation (L) emitted from the water surface was quantified using the Stefan-Boltzman Law:

$$L = \varepsilon\sigma \times T^4 \tag{2.28}$$

where ε is surface emissivity (unitless), σ is the Stefan-Boltzman constant (5.67×10^{-8} W/m^{2}K^4), and T is temperature in Kelvin.

The surface emissivity of water was estimated as 0.96, which is a standard value for water bodies (Campbell and Norman, 1998). Shortwave reflectivity of incident radiation is different between the climate station and water surface; the shortwave reflectivity (albedo) of the water surface varies according to solar elevation angle and ranges from 0.05 for 60° to 0.60 for 5° (Dingman, 2002).

The energy flux from fluid friction ($Q_{f)}$ was estimated using the empirical equation (Theurer *et al.*, 1984):

$$Q_f = 9805\left(\frac{q}{W}\right) \times S \tag{2.29}$$

Here, q is stream discharge in m^3/s, W is average wetted stream width in m, and S is channel slope (unitless).

Streambed conduction was estimated via measurement of streambed temperature under each reach. Bed conduction can be calculated using the following equation (Moore *et al.*, 2005b):

$$Q_{hb} = k_c(T_w - T_b)/x \tag{2.30}$$

Here, k_c is the thermal conductivity of the stream substrate, T_w is water temperature, T_b is temperature measured within the streambed, and x is the depth at which streambed temperature is measured. Previous studies (Johnson 2004, Moore *et al.*, 2005b) estimated streambed thermal conductivities based on streambed material as

opposed to measuring streambed thermal conductivity. For both reaches, a thermal conductivity of 2.5 W/mK was assumed, corresponding to soil minerals (Campbell and Norman, 1998). Streambed temperature was measured five cm below the streambed surface (Moore *et al.*, 2005b). The above calculations account for the major non-advected energy fluxes acting on stream temperature. Therefore calculation of these fluxes provides quantifiable estimates of the forested riparian canopy's ability to ameliorate stream heating.

Discharge Data

Stage measurements at the climate stations were used to calculate discharge. Quantifying discharge was necessary to estimate the volume of flow through each study reach. For higher values of discharge, a stream will warm less given the same energy fluxes (equation 1.3). To relate stream stage to discharge, a rating curve was established based on measurements of stream discharge for varying stream stages. Rating curves relate stream stage to stream discharge and are generally of the form:

$$Q = a * Z^b \tag{2.31}$$

Where Q is discharge in units volume/time, Z is stream stage in units length, and a and b are coefficients determined by the stream channel morphology within the area of measurement, as well as the location and datum of stage measurements (Dingman, 2002). Past studies have used this general form of a rating curve when estimating discharge from

stage measurements (Dingman and Sharma, 1997; Shiklomanov *et al.*, 2006; Yu, 2000). This form of a rating curve applies to measurements collected at natural controls within a stream, e.g. straight, unobstructed reaches like the gauge locations used for this study (Dingman, 2002). Single stage-discharge relations hold only for a given range of stage; quantifying flow above bankfull stage generally requires establishment of compound rating curves which have different relations for different ranges of stage (Petersen-Øverleir and Reitan, 2005; Shiklomanov *et al.*, 2006). However, accurately quantifying discharge across all stages, including up to and over bankfull stage (which represented only a very small fraction of the water year), was beyond the scope of this work.

Discharge to establish the rating curve was quantified with velocity-area cross sections. This method directly quantifies stream discharge by dividing a stream cross section into multiple vertical sections and integrating the measured discharge within each section across the channel. Ten second average velocity readings are collected at 0.2, 0.6, and 0.8 of the stream's depth within each vertical transect; the stream depth within each vertical is also recorded. Multiple previous studies indicated that the velocity at 0.6 of the stream's depth is a reasonable approximation of the average velocity within the vertical section (Dingman, 1984). For a more accurate approximation, the average of the .8 and .2 depth velocities is used (Carter and Anderson, 1963). When possible, the average of .8 and .2 velocities was used in this work. However, it is not always possible to measure velocity at .8 of the stream depth in shallow (<12cm) sections of the stream. In these cases, the .6 depth velocity method was used. Total discharge (Q) is calculated by multiplying the cross-sectional area of each vertical (A_i) by the average velocity within

the vertical (U_i), according to the following equation (Dingman, 2002), and illustrated in Figure 8 below:

$$Q = \sum_{i=1}^{N} U_i \times A_i \tag{2.32}$$

where N is the number of vertical transects in the cross section. Area of each vertical (A_i) is calculated by multiplying its width by its associated stream depth.

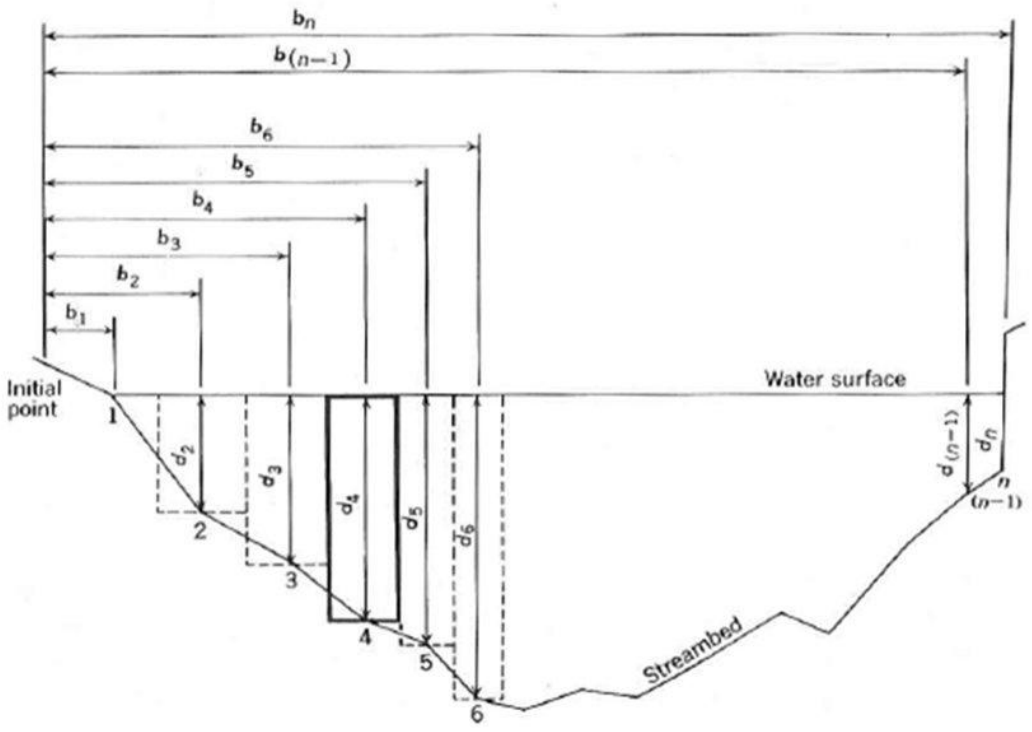

Figure 8: Delineation of a cross section for measurement of discharge by the velocity-area method (Dingman, 2002)

Regular and event based velocity-area stream flow gauging was conducted at each climate station to establish rating curves for water flowing within each study reach.

Event based cross section work focused on measuring discharge at varying stages, resulting in a wider range of data points to which the rating curves were fit (Dingman, 2002).

Identification of Energy Fluxes Driving Stream Temperature

Previous stream energy balance studies focused on identifying the relative contributions of different energy fluxes (i.e. net radiation, sensible and latent heats, substrate, advection) to changes in stream temperature (Cozzetto *et al.*, 2006; Hannah *et al.*, 2008; Moore *et al.*, 2005b; Story *et al.*, 2003; Webb and Zhang, 1997). Comparisons were usually made by examining the magnitude of individual energy sources to the total magnitude of energy sources through a reach. Similar comparisons were made for all measured and estimated energy fluxes in this study. Fluxes with the highest contribution to the total energy gains or losses through a stream reach are the most important in determining stream temperature changes (Webb and Zhang, 1997). Therefore, identification of the most important energy fluxes relative to temperature change within a riparian stream will improve understanding of the role riparian buffers play in ameliorating stream heating. As the current energy balance study was conducted in a deciduous forest of an Ozark border stream of the central U.S. the relative contributions of these fluxes to stream water temperature, as well as how they vary with time, may be different than found in previous studies in different climates and forest types.

Data analysis also focused on comparing stream temperatures upstream and downstream from each climate station, and relating changes in temperature between these

two points to modeled energy fluxes. This approach allowed for characterization of spatial and temporal variation in stream temperature through each reach, as well as the importance of the various energy exchange processes in controlling stream temperature.

Climate variables and energy fluxes were compared between the E-W reach and N-S reach using the ANOVA method previously described (see, Horizontal Attenuation of Energy by a Forest Canopy). This test was conducted to see if stream orientation was statistically significant to processes (i.e. net radiation, sensible, and latent heat exchange) controlling stream heating.

CHAPTER III:

RESULTS AND DISCUSSION

RESULTS

Climate During Study Period

Climate descriptive statistics for the 2010 water year calculated from the above canopy reference flux tower (Figure 1) data are presented in Table 4 and Figure 9 below. The period of study was on average cooler and wetter than the long term average, with an average temperature of 12.8 ˚C and total precipitation of 1446.8 mm relative to averages recorded between 2005-2008 on site from the flux tower of 13.5 ˚C air temperature and 969.8 mm annual precipitation.

Table 4: Summary climate statistics collected at the above canopy reference site (Ameriflux tower, Baskett Wildlife Research Area) central Missouri, USA, water year 2010. *Precipitation is annual total.

	Mean	**Standard Deviation**	**Minimum**	**Maximum**
Air Temperature (˚C)	12.8	11.7	-19.6	36.2
Relative Humidity (%)	71.2	19.0	18.2	98.5
Solar Radiation (W/m^2)	172.6	268.2	0.0	1054.0
Wind Speed (m/s)	2.6	1.2	0.0	9.2
Soil Temperature 16 cm (˚C)	13.3	7.5	1.7	25.8
Precipitation (mm)	1446.8*	-	-	-

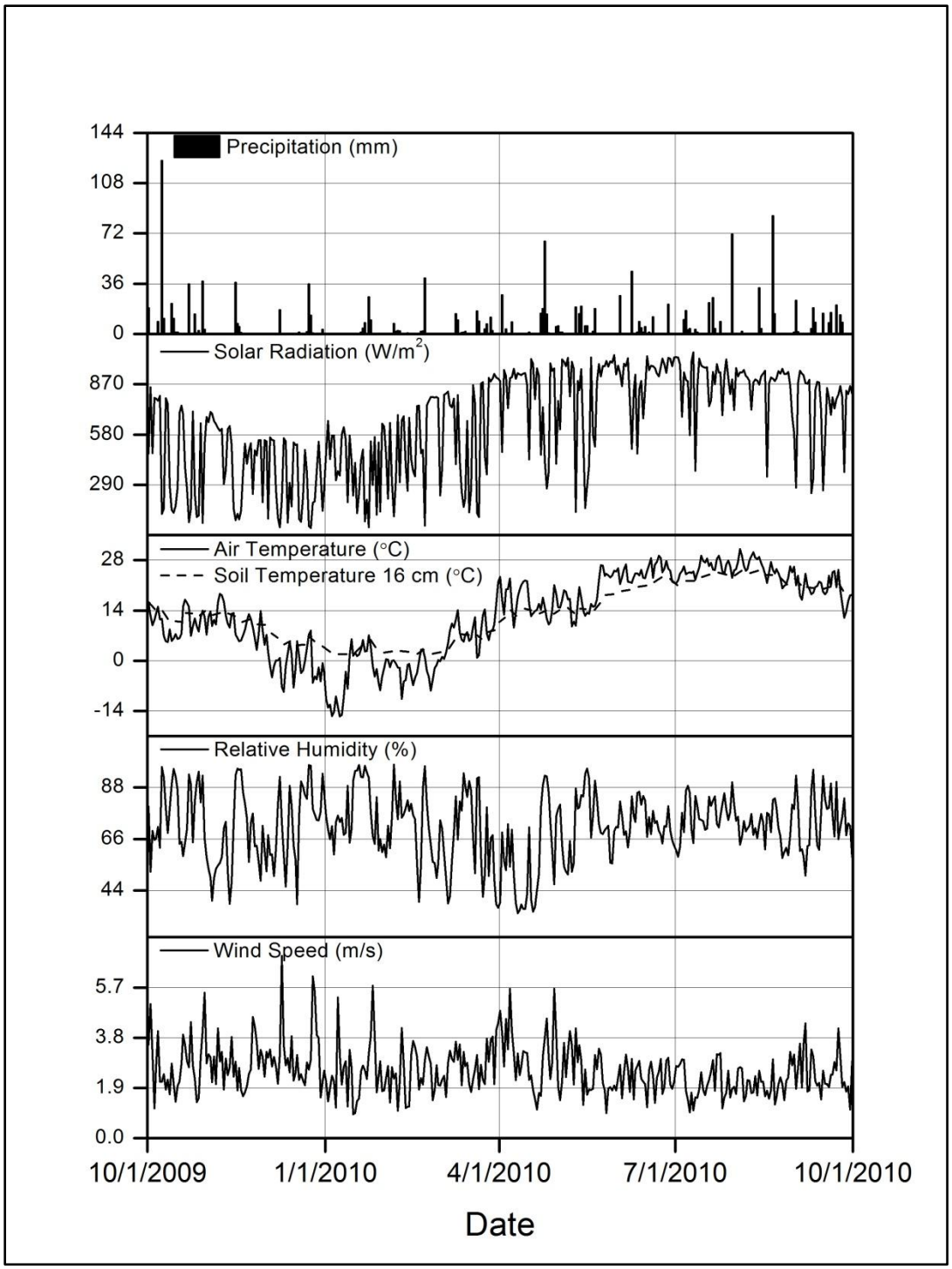

Figure 9: Water year 2010 climate at above canopy reference site: Ameriflux tower, Baskett Research and Education Area, central Missouri USA. Figures are daily averages except solar radiation, which is daily maximum. Precipitation is daily total.

Canopy Attenuation of Light and Energy

LAI values were computed for eight measurement dates following both ceptometer and hemispherical photo methods described previously. Results from ceptometer measurements are presented below in Table 5 and Figure 10. The measurements collected on November 17 are representative of final leaf off; therefore measured values are representative of residual stems and not leaves. In general, leaf area index is not reported during times of leaf off, and no methods for adjusting values during foliation based on these measurements were found. Measurements during leaf off cannot simply be subtracted from the other values as many of the stems are covered by leaves during times of foliation. However, these measurements are reported as they are useful to quantify the amount of light transmitted through the canopy during times of leaf off. Maximum measured LAI was 4.51; this measurement was collected within the riparian zone adjacent to the E-W reach on June 7 2010. The maximum measurements of LAI occurred on June 7 for the E-W stream reach, E-W riparian zone, N-S stream reach, and N-S riparian zone, and declined in all following measurements. The E-W reach in general had higher LAI values both within the stream reach (average 1.97 vs. 1.36 for N-S) and within the adjacent riparian zone (average 2.64 vs. 2.43 for N-S). LAI measured within the stream reaches (average 1.67) was lower than the adjacent riparian zones (average 2.54) for all measurements except for the E-W reach on April 26.

LAI measurements collected with the hemispherical photo method were similar to the ceptometer method. Maximum LAI was measured on July 7 and occurred within the E-W reach's riparian zone at a value of 4.47 (Table 6 and Figure 10) . Unlike the

ceptometer method, maximum LAI for some measurement categories were collected on July 7, while some maximum measurements for other categories were collected on June 5. For all measurement dates, LAI was lower within the study stream reaches (average 1.99) relative to the adjacent riparian zones (average 2.69). As with the ceptometer, hemispherical photo analysis showed that the E-W reach generally had higher LAI values within the stream reach (average 2.18 vs. 1.80 for N-S) and within the adjacent riparian zone (average 2.71 vs. 2.65 for N-S).

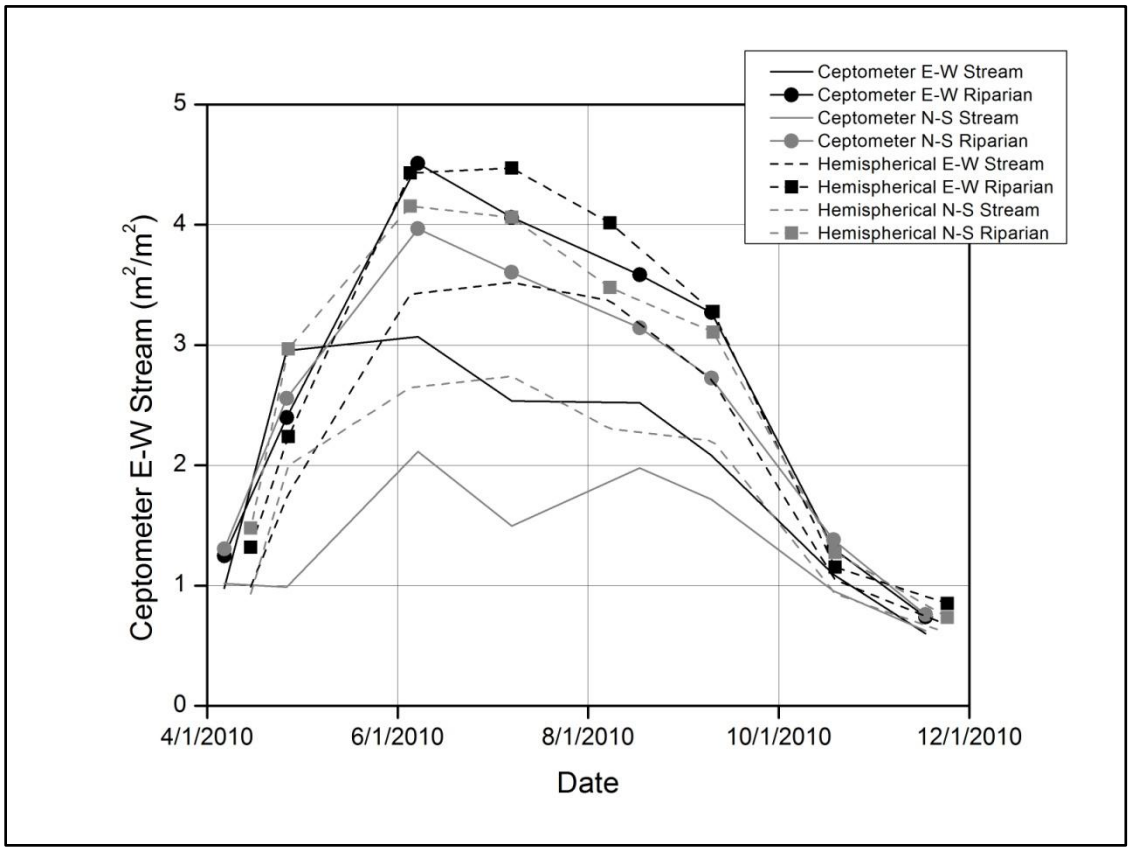

Figure 10: Leaf area index (LAI) values for stream canopy gaps and riparian zones for east-west and north-south oriented study reaches as measured with ceptometer and hemispherical photos during 2010 calendar year, Baskett Research Wildlife and Education Area, Missouri, USA.

Table 5: Leaf area index (LAI) values for stream canopy gaps and riparian zones for east-west and north-south oriented study reaches as measured with ceptometer during 2010 calendar year, Baskett Research Wildlife and Education Area, Missouri, USA.

		Apr 6	Apr 26	Jun 7	Jul 7	Aug 17	Sep 9	Oct 18	Nov 17
E-W	Riparian	1.25	2.40	4.51	4.06	3.58	3.27	1.31	0.74
	Stream	0.98	2.95	3.07	2.54	2.52	2.08	1.09	0.60
N-S	Riparian	1.30	2.56	3.97	3.60	3.14	2.72	1.38	0.76
	Stream	1.02	0.99	2.11	1.50	1.98	1.72	0.95	0.63
Average	Riparian	1.27	2.48	4.24	3.83	3.36	3.00	1.34	0.75
	Stream	1.00	1.97	2.59	2.02	2.25	1.90	1.02	0.62

Table 6: Leaf area index (LAI) values for stream canopy gaps and riparian zones for east-west and north-south oriented study reaches as measured with hemispherical photos during 2010 calendar year, Baskett Research Wildlife and Education Area, Missouri, USA.

		Apr 15	Apr 27	Jun 5	Jul 7	Aug 8	Sep 10	Oct 19	Nov 24
E-W	Riparian	1.32	2.24	4.43	4.47	4.02	3.28	1.15	0.85
	Stream	0.99	1.76	3.42	3.52	3.37	2.70	1.05	0.67
N-S	Riparian	1.48	2.97	4.15	4.06	3.48	3.11	1.28	0.74
	Stream	0.93	2.00	2.65	2.74	2.30	2.20	0.93	0.61
Average	Riparian	1.38	2.52	4.32	4.31	3.81	3.21	1.20	0.80
	Stream	0.96	1.88	3.03	3.13	2.84	2.45	0.99	0.64

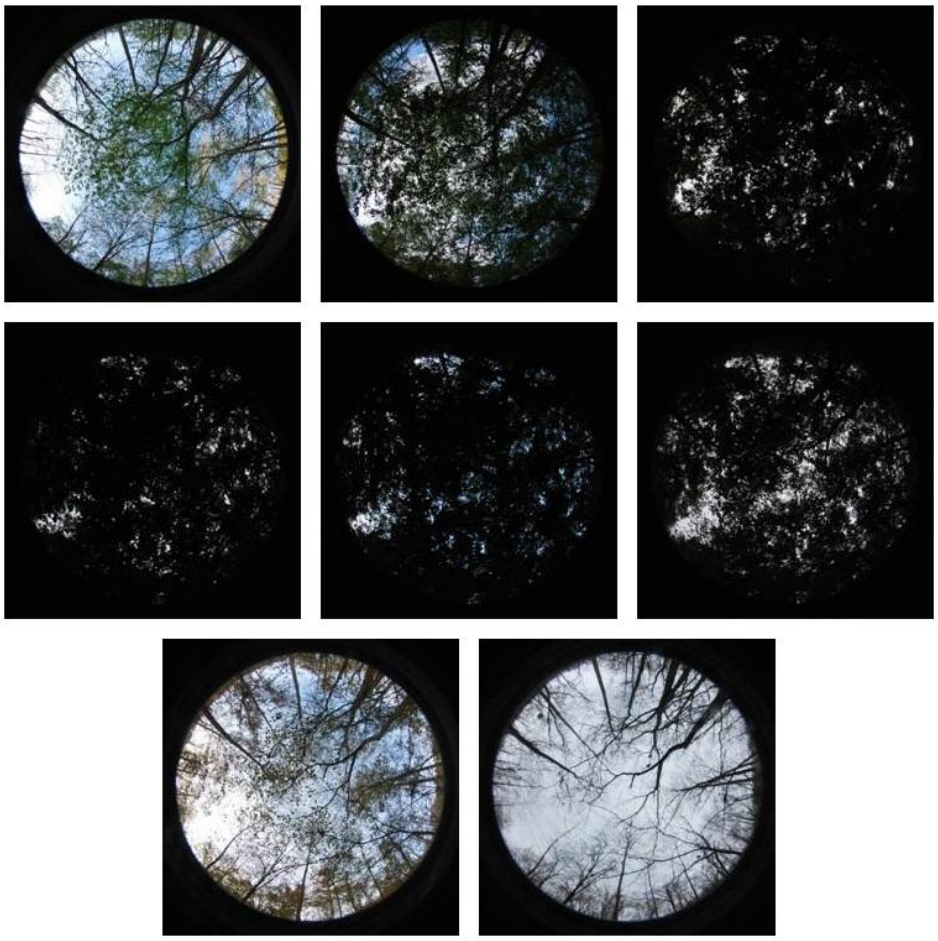

Figure 11: Progression of canopy cover above EW stream reach located in central Missouri, USA. Images collected using hemispherical lens on dSLR camera. Photos progress monthly from April (top left) through November, 2010 (bottom right).

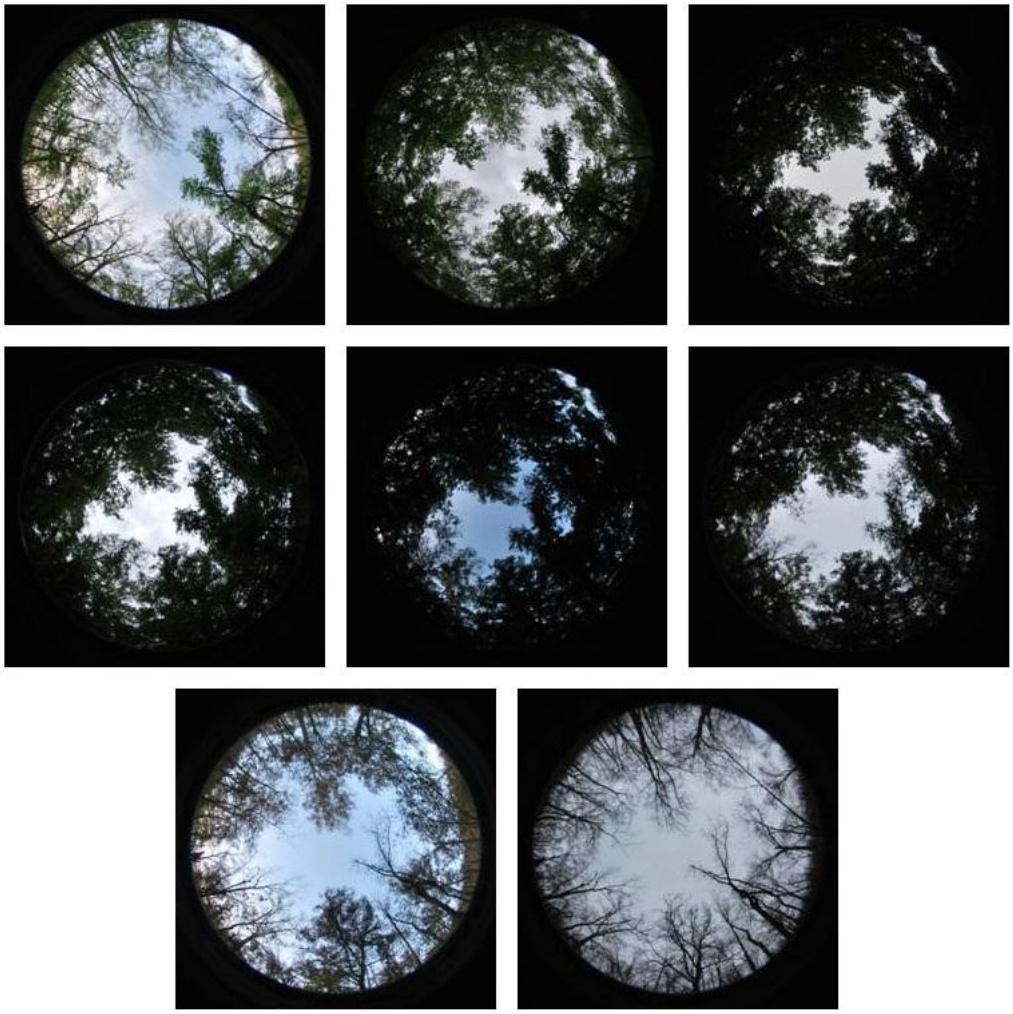

Figure 12: Progression of canopy cover above NS stream reach located in central Missouri, USA. Images collected using hemispherical lens on dSLR camera. Photos progress monthly from April (top left) through November, 2010 (bottom right).

Canopy density is important for this study because it controls total radiation reaching the stream's surface. One of the primary areas of focus in data analysis was to select the best method for quantifying radiation at the stream surface. First, models of shortwave radiation developed for each hydroclimate stations were compared to shortwave radiation measured at each climate station. Table 7 and Table 8 compare

measured and modeled radiation at each climate station for daily averages of shortwave radiation and 15 minute averages of shortwave radiation, respectively. Radiation models developed based on hemispherical photos for the E-W hydroclimate station and the N-S hydroclimate station tended to result in underestimates relative to measured shortwave radiation; mean modeled shortwave radiation was 35.5 W/m^2 and 41.1 W/m^2 versus 44.7 W/m^2 and 46.8 W/m^2 (E-W reach and N-S reach, respectively). Daily average modeled values were better correlated to measured values at daily averages relative to 15 minute averages (R^2=0.76 and 0.87 vs. 0.66 and 0.80 for E-W and N-S reach, respectively). Based on daily averages for the entire year, root mean square error for modeled shortwave radiation at the climate stations relative to measured was 18.2 W/m^2 for the E-W reach and 14.8 W/m^2 for the N-S reach.

Table 7: Comparison of daily average measured shortwave radiation for climate stations along E-W and N-S reach of Brushy Creek, BREA, Central Missouri USA, versus modeled using above canopy radiation and gap fraction from hemispherical photos. All values in W/m^2.

	Mean	Standard Deviation	Minimum	Maximum	RMSE	MBE	R^2
EW Measured	44.7	31.8	3.5	146.2	-	-	-
NS Measured	46.8	37.8	2.4	196.5	-	-	-
EW Modeled	35.5	30.7	2.8	146.6	18.2	-9.2	0.76
NS Modeled	41.1	38.1	2.0	180.8	14.8	-5.7	0.87

RMSE = Root Mean Square Error
MBE = Mean Bias Error
R^2 = Coefficient of Determination

Table 8: Comparison of 15 minute average measured shortwave radiation for climate stations along E-W and N-S reach of Brushy Creek, BREA, Central Missouri USA, versus modeled using above canopy radiation and gap fraction from hemispherical photos. All values in W/m^2.

	Mean	Standard Deviation	Minimum	Maximum	RMSE	MBE	R^2
EW Measured	44.7	94.4	0	854.0	-	-	-
NS Measured	46.8	102.0	0	877.0	-	-	-
EW Modeled	35.5	80.0	0	735.7	56.1	-9.2	0.66
NS Modeled	41.1	94.9	0	776.2	48.9	-5.7	0.80

RMSE = Root Mean Square Error
MBE = Mean Bias Error
R^2 = Coefficient of Determination

Modeled shortwave radiation was closer to climate station measurements from November through May (little foliation) than from June through October (foliation) for the E-W reach (R^2 of 0.82 vs. 0.78, respectively, based on daily averages). However, modeled values of shortwave radiation were closer to measured values at the N-S climate station for June through October than from November through May (R^2 of 0.89 for June through October versus 0.87 for November through May). Error for the climate station shortwave radiation model was large for the E-W reach during the months June through August, when canopy was the most dense (Figure 17); average modeled daily shortwave radiation during this period was 17.7 W/m^2 versus measured E-W climate station shortwave radiation of 40.5 W/m^2. Figure 14 and Figure 15 illustrate modeled versus measured shortwave radiation at an individual hydroclimate station for selected four day periods; stations and dates were selected to show the observed range in fit between measured and modeled values. In general, peaks of modeled incident radiation tend to be of the same magnitude and occur around the same time as those measured in Figure 14,

which shows the E-W hydroclimate station for four days in late April. Figure 15, which shows the N-S hydroclimate station for a four day period in August, illustrates that measured and modeled incident shortwave radiation are sometimes very different. Again, since the canopy is highly variable and hemispherical photos were not collected at the exact location where radiation was measured, some variation is to be expected.

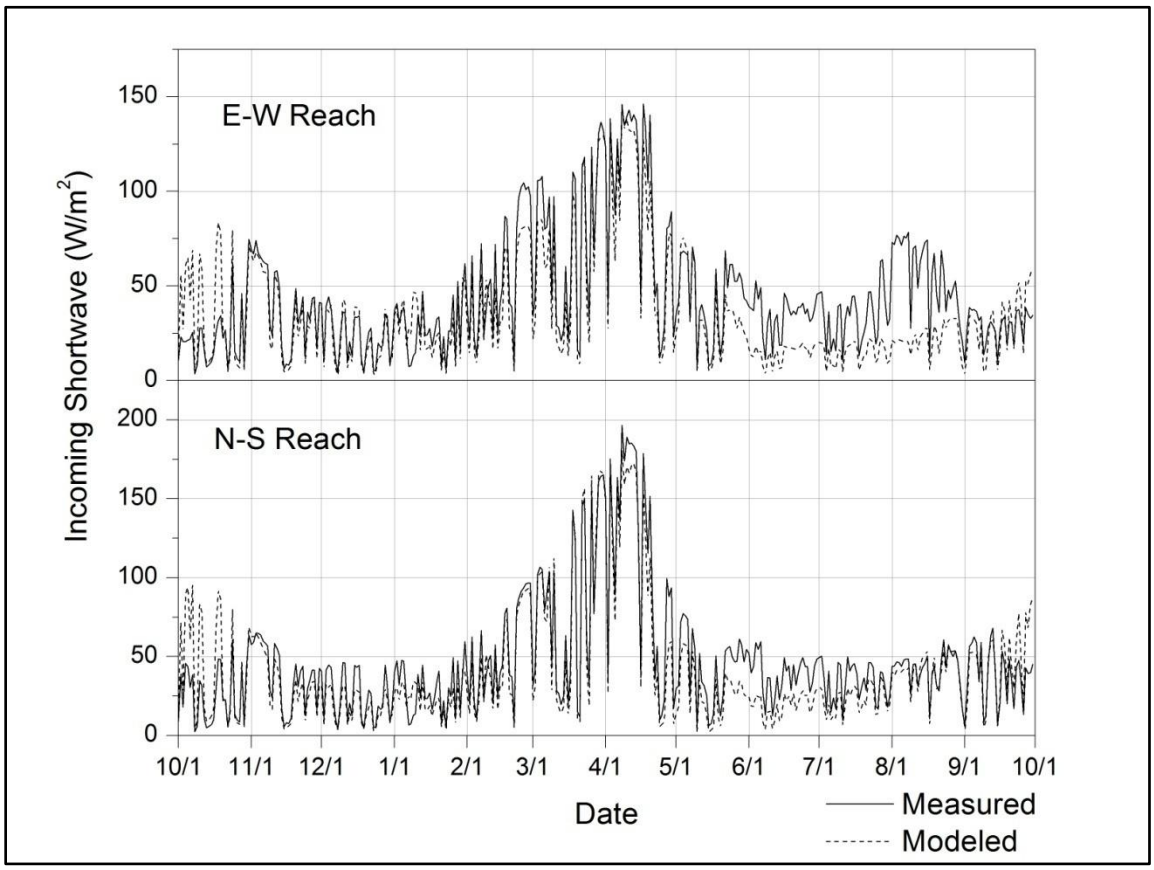

Figure 13: Daily average values of incoming shortwave radiation adjacent to an E-W stream reach and N-S stream reach, Brushy Creek, Baskett Research and Education Area, Central Missouri USA, as measured with a pyranometer versus values modeled via gap fraction analysis of surrounding hemispherical photos and above canopy measurements.

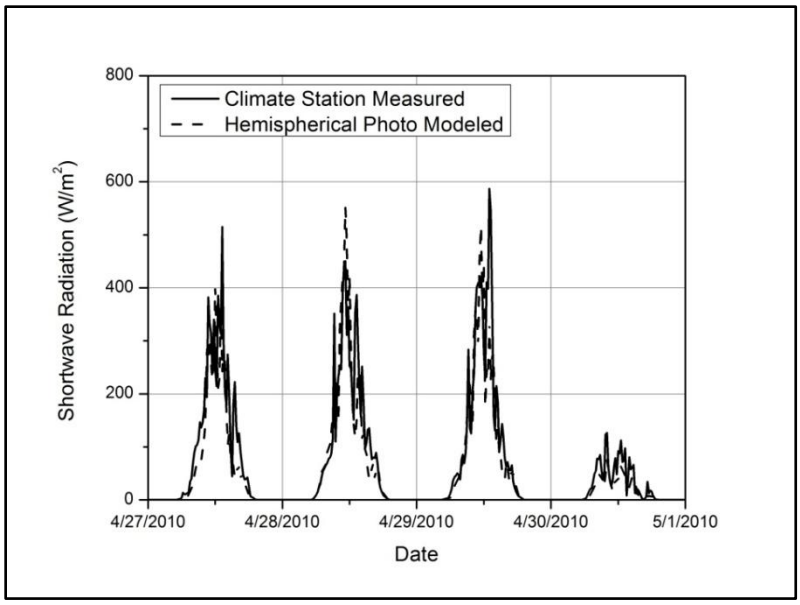

Figure 14: 15 minute averages of measured shortwave radiation at hydroclimate station along E-W oriented riparian reach, Baskett Research and Education Area, Central Missouri USA, compared to values modeled via above canopy measurements and hemispherical photography gap fraction analysis.

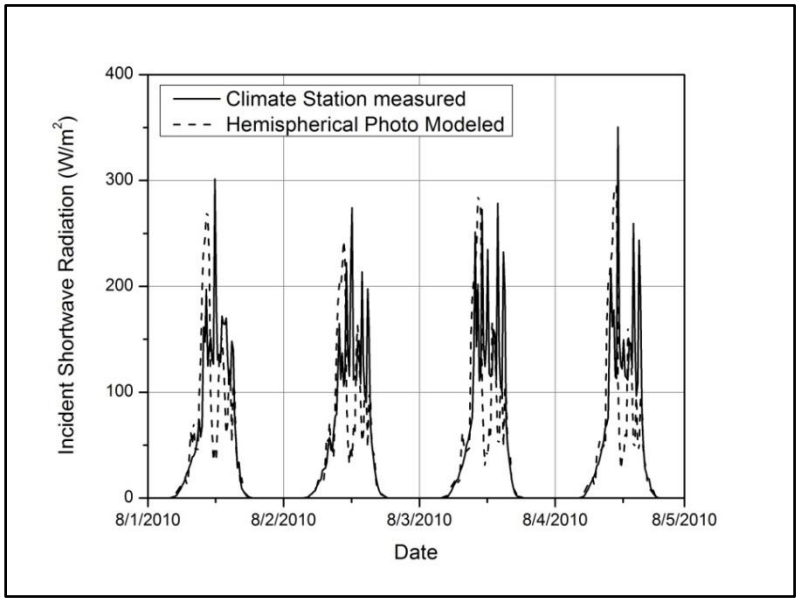

Figure 15: 15 minute averages of measured shortwave radiation at hydroclimate station along N-S oriented riparian reach, Baskett Research and Education Area, Central Missouri USA, compared to values modeled via above canopy measurements and hemispherical photography gap fraction analysis.

Summary statistics for comparisons between described stream shortwave radiation models and values measured in stream from September 2 through September 30 with the Appogee pyranometer are presented in Table 9 below. Methods compared in Table 9 include:

1. Direct measurement of shortwave radiation with above stream pyranometer (Appogee).
2. Direct measurement of shortwave radiation collected at a hydroclimate station (CS) located adjacent to the stream reach.
3. Modeled shortwave radiation using hemispherical photo gap fraction analysis and above canopy measurements (hemi).
4. Modeled shortwave radiation using inversion of leaf area index equation to calculate average shortwave transmissivity and above canopy measurements from ceptometer measurements (LAI).

Hemispherical photo modeled estimates (method 2 in the methods section description) had the lowest root mean square error (RMSE) (46.1 W/m^2 and 52.4 W/m^2) for both the E-W reach and N-S reach. However, the climate station's average was closer to the measured in stream value than the hemispherical model for both the E-W and N-S reach. The ceptometer LAI based inversion values (method 3 in methods section description) were consistently higher than the measured in stream values, with an average of 62.3 W/m^2 and 69.2 W/m^2 versus 31.3 W/m^2 and 31.5 W/m^2 for the E-W and N-S reaches, respectively. Despite this difference in means, LAI-ceptometer based modeled values were most correlated with in stream pyranometer measurements (R^2=0.58 for E-W

reach and 0.66 for N-S reach). Figure 16 shows that the climate station measurements and hemispherical photo model tend to be closest to in-stream pyranometer measurements for daily averages. Methods for quantifying shortwave radiation at the stream surface in Figure 16 are the same as Table 9.

Table 9: Comparison of methods to estimate shortwave radiation at the stream surface for both an E-W stream reach and N-S stream reach (bottom) of a second order stream reach, central Missouri USA. Values are based on 15 minute averages of data collected from September 2-September 30, 2010. All columns are in units W/m^2, with the exception of the R^2 column, which is unitless.

	Mean	S.D.	Minimum	Maximum	RMSE	MBE	R^2
EW Appogee	31.3	66.4	0.0	507.2	-	-	-
NS Appogee	31.5	55.4	0.0	487.1	-	-	-
EW CS	29.5	49.8	0.0	568.4	53.1	-1.8	0.38
NS CS	39.6	80.1	0.0	661.2	52.6	8.1	0.59
EW Hemi	33.5	57.9	0.0	311.7	46.1	2.2	0.54
NS Hemi	43.8	82.3	0.0	525.4	52.4	12.3	0.63
EW LAI	62.3	90.8	0.0	308.9	66.3	31.1	0.58
NS LAI	69.2	100.5	0.0	335.9	74.5	37.6	0.66

RMSE = Root Mean Square Error
MBE = Mean Bias Error
R2 = Coefficient of Determination
CS=Radiation measured at climate station
Hemi=Radiation modeled by hemispherical photos
LAI=Radiation modeled by computation of transmissivity from leaf area index measurements with ceptometer

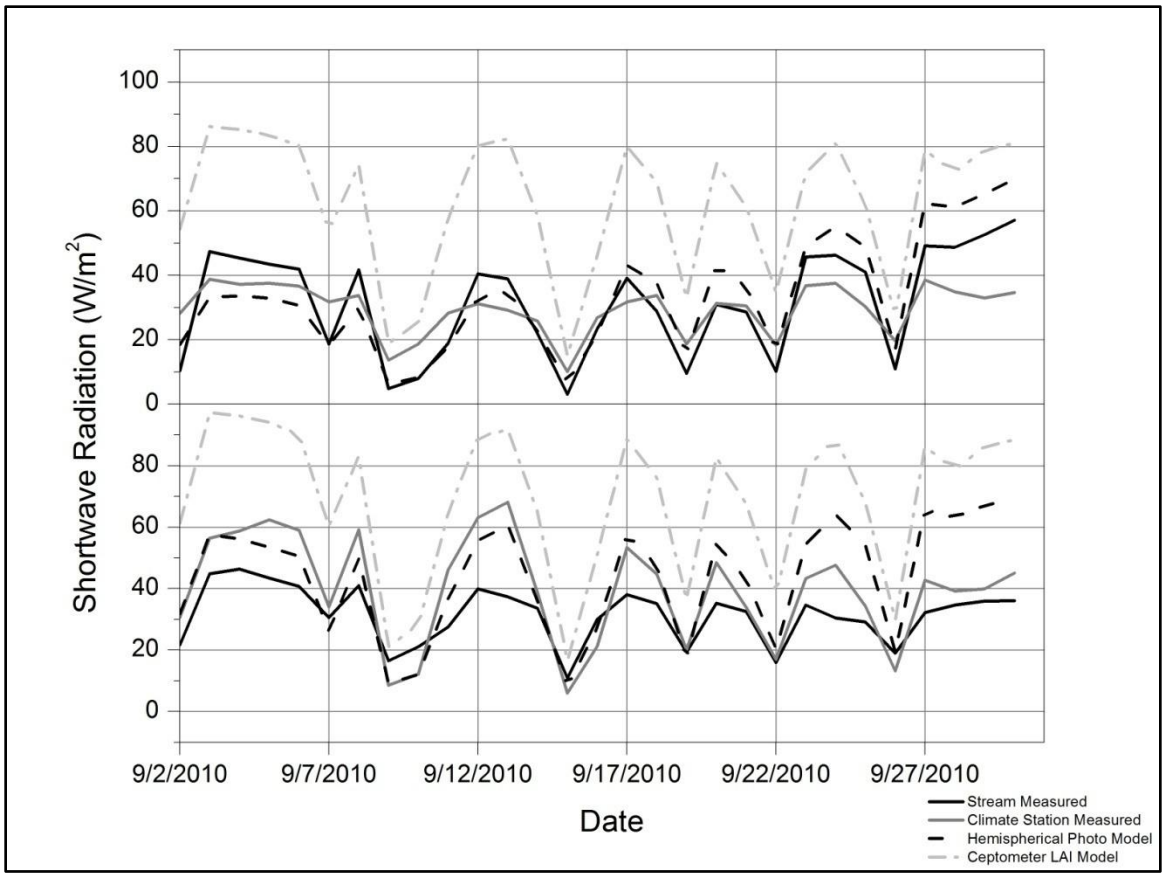

Figure 16: Comparison of results from four methods to quantify incident radiation at stream surface for both an E-W stream reach (top) and N-S stream reach (bottom) along Brushy Creek, Baskett Research and Education Area, Central Missouri USA. Values are daily averages.

Figure 17 below shows relationships between 15 minute averages of the measured and modeled values of shortwave radiation incident at the stream's surface for a four day period, using the same methods listed in Table 9. For most days in the N-S reach, all three methods tended to overestimate incident shortwave radiation. In the E-W reach, the trend is the same with the exception of one peak early in the day for both the first and third days. Near the location of the sensor there was a large gap in the canopy visible from the position of the in-stream pyranometer that was not well characterized by the

hemispherical and LAI models which averaged multiple measurements along the stream reach. It is also possible that bank shading was a factor in the lower relative values of in-stream measured values. Ceptometer measurements and hemispherical photos were collected higher relative to the streambed versus the pyranometer, where bank shading might have been less prominent.

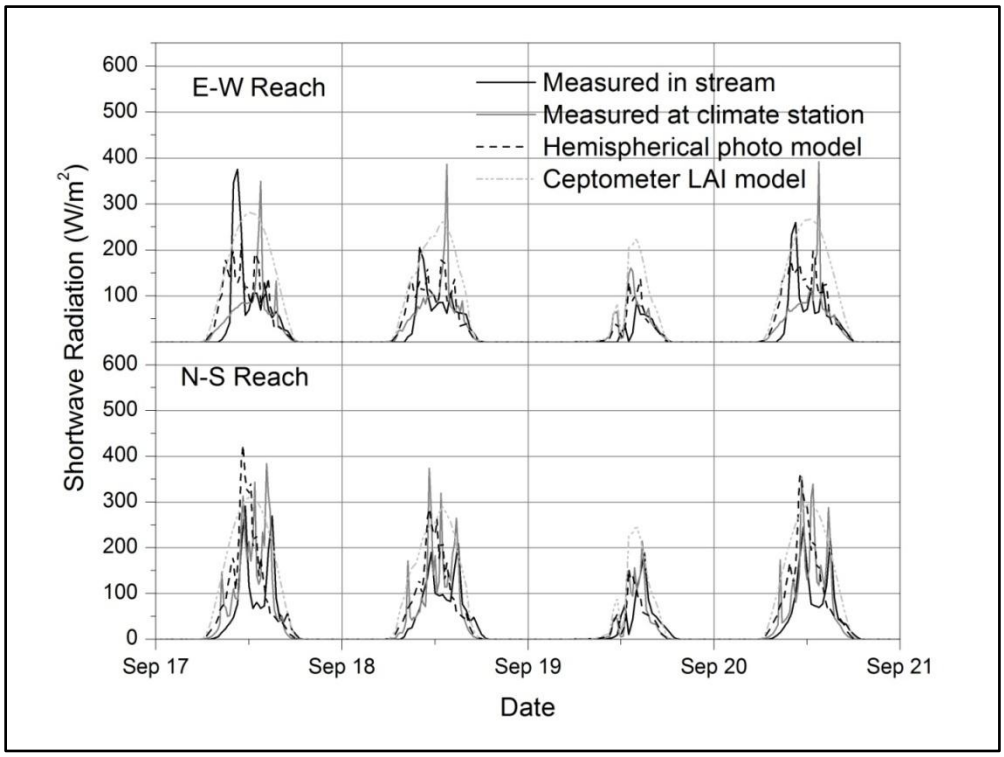

Figure 17: Comparison of shortwave radiation incident on stream surface calculated or measured using four methods for selected time period for both an E-W stream reach (top) and N-S stream reach (bottom) along Brushy Creek, Baskett Research and Education Area, Central Missouri USA. Values are 15 minute averages.

Ultimately, no method exactly replicated an in-stream pyranometer in quantifying incident shortwave radiation at the stream's surface. Quantifying incident shortwave radiation is challenging since canopy attenuation of radiation varies spatially within the

reach, temporally due to changes in canopy foliation, and changes in solar position and above canopy radiation (Ringold *et al.*, 2003). Regardless, based on analysis results, the hemispherical photo model was selected to be used for stream energy balance calculations due to close approximation of observed radiation for the in stream model. This decision is consistent with previous research (Leach and Moore, 2010a; Moore *et al.*, 2005b). The hemispherical photo model had the lowest root mean square error value relative to the in-stream pyranometer (46.1 W/m^2 in E-W reach, 52.4 W/m^2 in N-S reach. Furthermore, the hemispherical photo model is the only method that quantifies the previously discussed variations in canopy attenuation as it characterizes gap fraction as a function of solar position for the direct beam radiation component (Hale and Edwards, 2002; Rich, 1990).

For analysis, data from the iButton temperature and humidity sensors were separated into two groups based on solar zenith angle; one group included measurements collected when the zenith angle was less than 90° (daylight values), and the other group included measurements collected when the zenith angle was greater than 90° (nighttime values). Only daylight values are presented as this research is primarily concerned with stream heating, which generally has been shown to occur during the daytime with incident shortwave solar radiation. Table 10 and Table 11 list summary statistics for measured values of temperature and relative humidity during the 2010 water year for the E-W reach and N-S reach, respectively.

Table 10: Measured values of temperature and relative humidity for Thermochron iButton transect extending north of an east-west flowing stream reach (EW-N) and south of an east-west flowing stream reach (EW-S), BREA, central Missouri USA. Values reflect hourly measurements during the 2010 water year when solar zenith angle < 90°.

	Distance from Stream (m)	Mean	Standard Deviation	Minimum	Maximum
EW-N					
Temp (°C)	0	16.1	10.7	-23.3	35.0
	5	16.0	10.6	-24.0	34.6
	10	16.1	10.7	-24.3	36.9
	25	16.0	10.7	-24.7	35.1
	40	16.0	10.9	-24.6	38.9
RH (%)	0	73.6	23.0	14.7	110.8
	5	72.3	23.4	12.9	107.2
	10	71.3	23.5	11.8	105.7
	25	71.6	24.2	11.6	106.3
	40	70.9	24.1	10.8	106.9
EW-S					
Temp (°C)	0	16.0	10.8	-24.3	34.9
	5	16.2	10.8	-24.4	36.4
	10	16.1	10.7	-24.1	36.5
	25	16.1	10.8	-24.0	38.1
	40	16.4	11.0	-24.4	41.0
RH (%)	0	72.8	23.1	13.8	108
	5	70.7	23.6	11.4	106.5
	10	72.5	23.3	12.8	107.6
	25	70.2	23.8	10.9	105.7
	40	70.4	24.1	10.3	106.5

Table 11: Measured values of temperature and relative humidity for Thermochron iButton transect extending east of a north-south flowing stream reach (NS-E) and west of a north-south flowing stream reach (NS-W), BREA, central Missouri USA. Values are for hourly measurements during entirety of 2010 water year when solar zenith angle < 90°.

	Distance from Stream (m)	Mean	Standard Deviation	Minimum	Maximum
NS-E					
Temp (°C)	0	16.1	11.0	-24.4	36.8
	5	16.1	11.1	-24.6	37.6
	10	16.3	11.2	-24.9	37.3
	25	15.9	10.8	-25.0	36.9
	40	16.1	10.8	-25.0	35.9
RH (%)	0	72.6	22.7	14.5	105.2
	5	70.6	23.8	10.8	107.6
	10	70.4	24.2	9.6	107.0
	25	73.4	26.2	9.5	119.3
	40	73.8	23.8	13.2	108.2
NS-W					
Temp (°C)	0	15.9	10.8	-24.6	35.0
	5	15.8	10.7	-24.9	35.3
	10	15.8	10.8	-25.1	35.1
	25	16.4	11.3	-25.0	40.6
	40	17.0	11.5	-24.7	41.9
RH (%)	0	73.3	23.0	12.7	107.2
	5	73.1	23.4	11.5	107.2
	10	72.3	23.1	12.1	107.6
	25	69.9	23.7	11.0	106.8
	40	69.9	24.1	11.9	106.0

Mean temperature for daytime values over the entire water year did not display a consistent pattern as a function of distance from the stream for any of the temperature transects. For the EW-N transect, the iButtons with highest mean temperatures (16.1 ˚C) were 0 and 10 meters from the stream edge. For the EW-S transect, the iButton with greatest mean temperature (16.4 ˚C) was 40 meters from the stream edge, and the second

greatest (16.2 ˚C) at five meters from the stream edge. In the NS-E transect, the iButton with greatest mean temperature (16.3 ˚C) was ten meters from the stream edge, and in the NS-W transect the iButton with greatest mean temperature was 40 meters from the stream. For all transects except the NS-E transect, the maximum individual temperature measurement occurred 40 meters from the stream; the maximum individual temperature measurement occurred 5 meters from the stream for the NS-W reach.

Pairwise comparison tests were conducted for both temperature and relative humidity measurements. One-way ANOVA showed that for daytime temperature measurements in the EW-N transect, there were no significant differences between iButtons at the α=0.01 level or α=0.05 level. For the EW-S transect, temperature measured at the iButton at 40m was significantly different than the iButton at the stream edge. For the NS-E transect, the iButton at 25 meters was significantly different than the iButton at 10 meters, but not significantly different than the iButton at the stream edge. In the NS-W transect, temperature measured at iButtons 25 and 40 meters from the stream edge was significantly different than temperature measured at the stream edge.

One-way ANOVA showed that for daytime relative humidity measurements in the EW-N transect, relative humidity was significantly different from that measured at the stream edge starting five meters from the stream. This relationship was also true for the EW-S and NS-E transect. In the NS-W transect, measured relative humidity was not significantly different until ten meters from the stream edge.

Stream Discharge Computation

Prior to calculating stream energy flux components, discharge within each reach was quantified. Calculation of discharge was necessary, as the rate of stream heating is dependent on the volume of water flowing through a reach (equation 1.4). Discharge was estimated by fitting a rating curve to velocity area cross sections collected within each reach based on 15 minute averages of stage from each hydroclimate station. Rating curves are shown in Figure 18 and Figure 19 below. R^2 values for rating curves were 0.99 for the E-W reach and 0.98 for the N-S reach. Figure 20 and Figure 21 show channel geometry for the E-W and N-S reaches, respectively. These profiles were constructed based on the velocity area cross sections corresponding to greatest measured discharge. Depth is shown on the Y-axis for each graph and represents distance from the water surface to the streambed measured during the velocity area cross section at 25 points across the stream channel; the Y-axis does not start at zero as these profiles do not represent the channel at bankfull stage, which was not measured and was beyond the scope of this work. For the E-W reach, the channel is split during periods of high flow, overflowing into a secondary channel. While the exact stage at which discharge began to flow through the secondary channel was not quantified, flow was only observed in this channel immediately following large precipitation events and generally receded within one to two days; four cross sections quantified secondary channel flow. As the two channels were close together (approximately 10 m), and were in the same canopy gap with canopy density measurements were taken in between the channels, this divergence did not impact study findings.

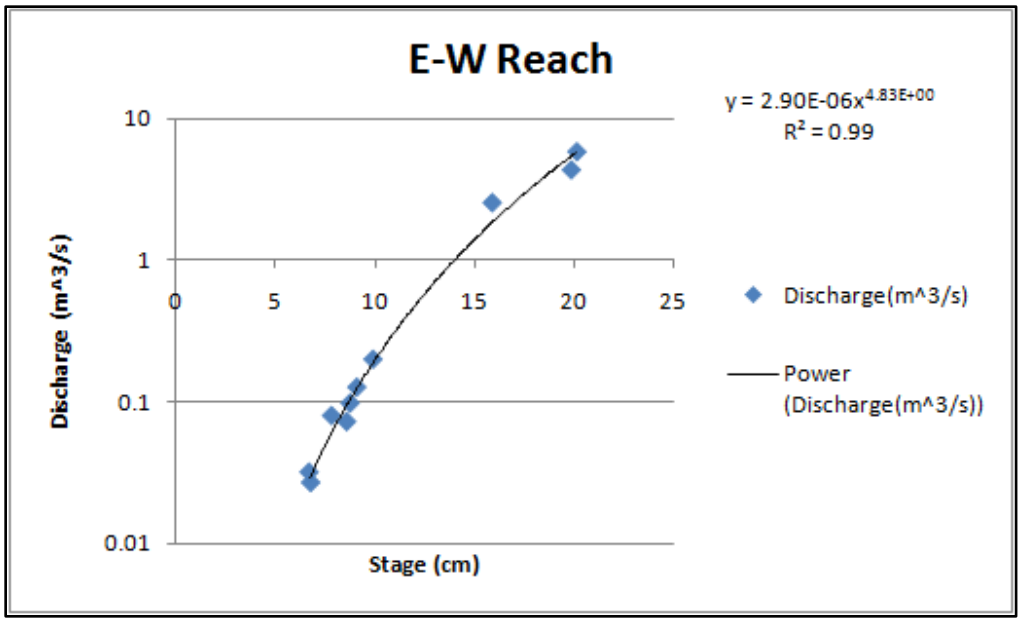

Figure 18: Rating curve fit for E-W flowing second order stream reach (Brushy Creek), Baskett Wildlife Research and Education Area, central Missouri USA during the 2010 water year.

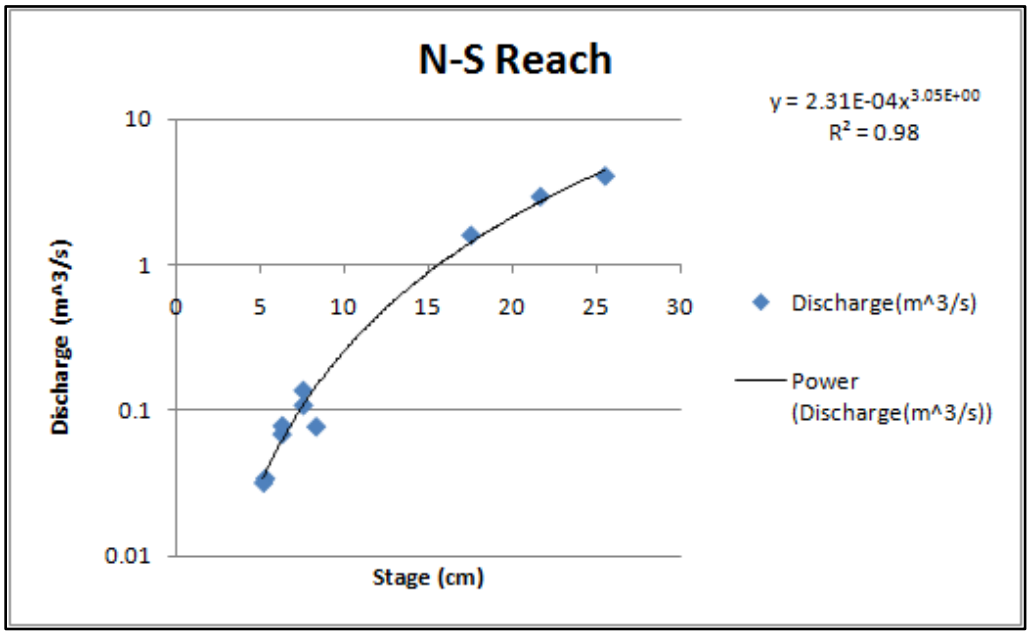

Figure 19: Rating curve for a N-S flowing second order stream reach (Brushy Creek), Baskett Wildlife Research and Education Area, central Missouri USA, during the 2010 water year.

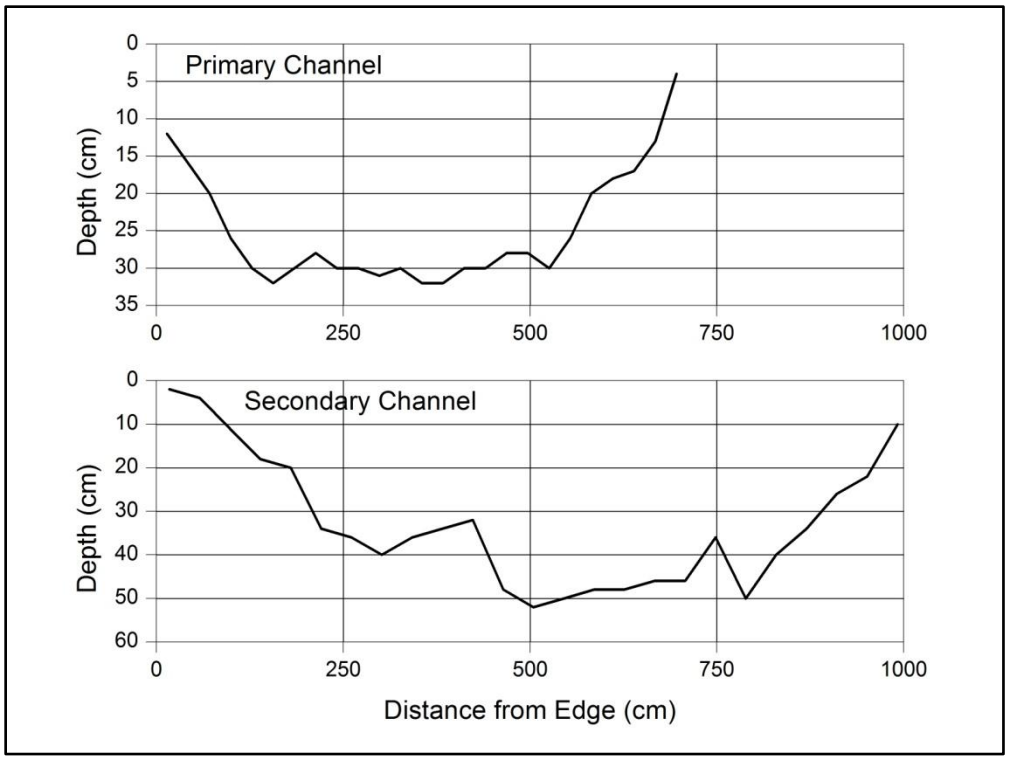

Figure 20: Channel geometry for E-W flowing second order stream reach (Brushy Creek), Baskett Wildlife Research and Education Area, central Missouri USA. The secondary channel only receives flow during periods of very high discharge.

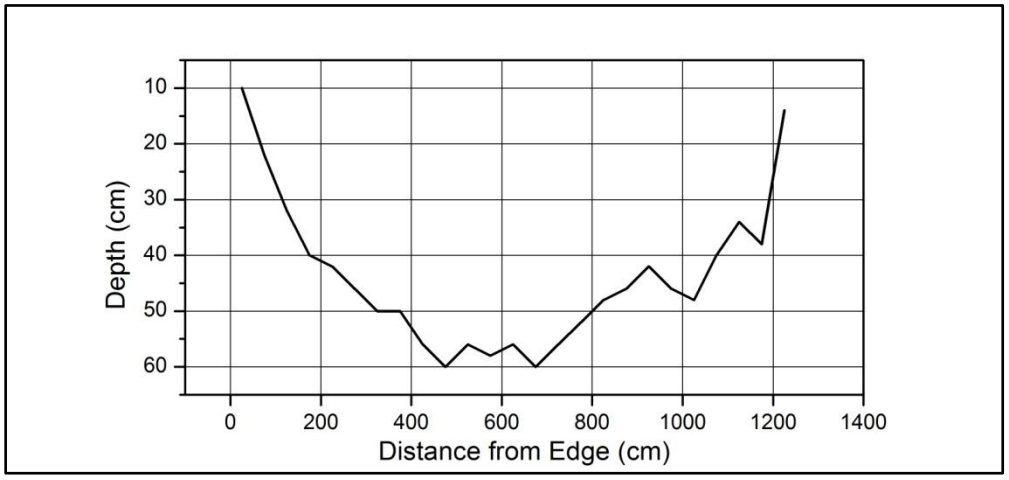

Figure 21: Channel morphology for E-W flowing second order stream reach (Brushy Creek), Baskett Wildlife Research and Education Area, central Missouri USA.

Stream Energy Fluxes

Average air temperature within the riparian zone for the 2010 water year was 11.6 °C along the E-W reach and 11.7 °C within the N-S reach. The E-W reach received 1253.5 mm of precipitation, while the N-S reach received 1477.2 mm, compared to 1446.8 mm measured at the flux tower. On average, the E-W reach received less solar radiation than the N-S reach and was cooler and more humid (Table 12). Both riparian zones received less solar radiation, and were cooler and more humid than the above canopy reference. The average of all 15 minute solar radiation measurements, including night hours, was 44.7 W/m^2 at the E-W climate station and 46.8 W/m^2 at the N-S climate station versus 172.6 W/m^2 at the above canopy reference. Average temperature was 11.6 ˚C (E-W) and 11.7 ˚C (N-S) versus 12.8 ˚C (ref). Average relative humidity was 82.5% (E-W) and 81.2% (N-S) versus 71.2% (ref). Figure 22 compares measured microclimate variables between the two hydroclimate stations during the 2010 water year.

Consistent with analyses conducted by other researchers (Brosofske *et al.*, 1997; Rambo and North, 2009), one-way ANOVA at the $\alpha=0.01$ level was conducted to compare air temperature, wind speed, relative humidity, and shortwave radiation between the E-W and N-S climate stations. Air temperature measured at the E-W climate station was not significantly different ($P=0.16$) than that measured at the N-S climate station. Relative humidity ($P=0.087$) was also not significantly different between the climate stations. Wind speed ($P<0.001$), and shortwave radiation ($P<0.001$) were both significantly different between the E-W climate station and N-S climate station.

Table 12: Summary climate statistics for E-W and N-S study reaches (WY 2010) at the BREA in central Missouri, USA. *Precipitation value is annual sum. % Refers to percent difference of E-W reach value relative to N-S value. Ref refers to values measured at above canopy reference flux tower.

Climate Variable		**Mean**	**Standard Deviation**	**Minimum**	**Maximum**
Air Temperature (˚C)	EW	11.6	11.4	-26.1	34.5
	NS	11.7	11.4	-25.8	35.1
	%	-0.9	0	1.2	-1.7
	Ref	12.8	11.7	-19.6	36.2
Relative Humidity (%)	EW	82.5	18.5	17.0	100.0
	NS	81.2	18.0	16.0	100.0
	%	1.6	2.8	6.3	0
	Ref	71.2	19.0	18.2	98.5
Solar Radiation (W/m^2)	EW	44.7	94.4	0.0	854.0
	NS	46.8	102.0	0.0	877.0
	%	-4.5	-7.5	0	-2.6
	Ref	172.6	268.2	0.0	1054.0
Wind Speed (m/s)	EW	0.4	1.2	0.0	2.5
	NS	0.4	0.4	0.0	2.7
	%	0.0	200.0	0.0	-7.4
	Ref	2.6	1.2	0.0	9.2
Soil Temperature 15 cm (˚C)	EW	12.6	8.2	0.3	26.7
	NS	13.0	8.0	0.5	27.1
	%	-3.1	2.5	0.0	-1.5
	Ref	13.3	7.5	1.7	25.8
Precipitation (mm)	EW	1477.2*	-	-	-
	NS	1253.5*	-	-	-
	%	17.8	-	-	-
	Ref	1446.8*			

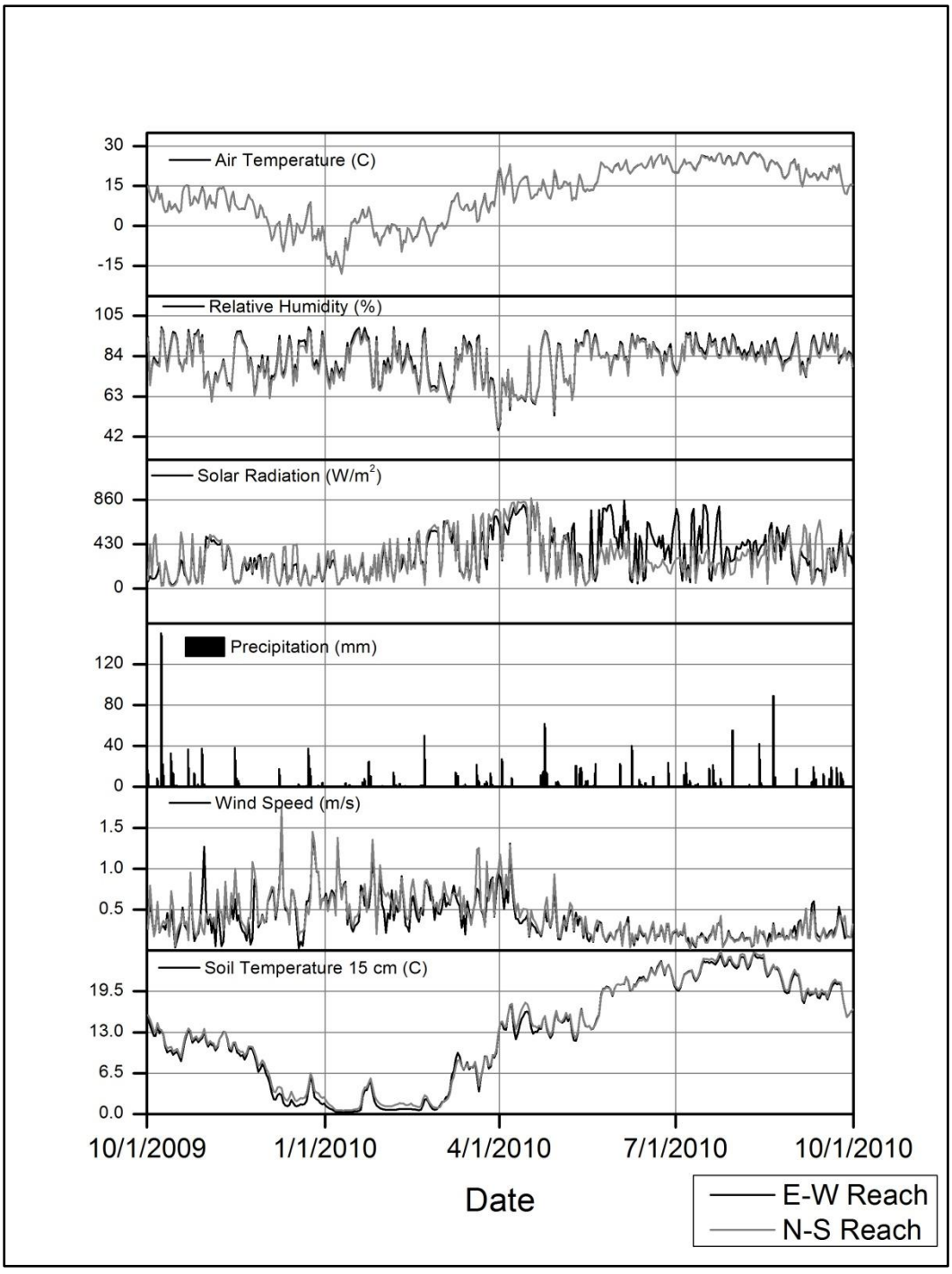

Figure 22: Climate comparison for E-W and N-S study reaches along Brushy Creek, Baskett Research and Education Area, Central Missouri USA during 2010 water year. Air temperature, relative humidity, wind speed, and soil temperature are daily averages; solar radiation is daily maximum of 30 minute logged averages; and precipitation is daily total.

Energy fluxes affecting each stream reach were quantified as detailed in Materials and Methods. Incoming shortwave and incoming longwave radiation were modeled based on hemispherical photo gap fraction analysis. Friction with the streambed was negligible (average 2.0 W/m^2 for the E-W reach and 3.5 W/m^2 for the N-S reach), consistent with previous studies (Hannah *et al.* 2008). Given this result, streambed friction is not included in comparison tables. Summary statistics of energy flux components for the entire water year are provided in Table 13. Net shortwave radiation was, on average, the largest contributor of energy to both reaches. Average net shortwave radiation was 42.9 W/m^2 for the E-W reach and 49.9 W/m^2 for the N-S reach. Net radiation (combined net shortwave and net longwave) on average warmed the stream for the entire year. Latent heat and sensible heat were on average about an order of magnitude smaller than net radiation when net radiation was at its maximum. Average latent heat flux was -17.2 W/m^2 for the E-W reach and -18.8 W/m^2 for the N-S reach; latent heat therefore had on average a cooling effect on both reaches for the entire year. Sensible heat cooled both reaches during the first half of the water year, and warmed both reaches during the second half of the water year. Average sensible heat flux during the first half of the water year was -8.4 W/m^2 for E-W and -9.6 W/m^2 for N-S. Average sensible heat flux during the second half of the water year was 1.5 W/m^2 for E-W and 1.4 W/m^2 for N-S. Heat conducted to and from the stream water by the stream bed warmed the stream on average, except for the E-W reach during the second half of the water year.

Table 13: Summary statistics for energy fluxes affecting E-W and N-S stream reaches, in the BREA central Missouri, USA, 2010. Values computed from 15 minute averages. Table includes first half of WY, second half, as well as total WY.

Energy Flux			Mean	SD	Min	Max
Net Shortwave	EW	Oct-Mar	41.6	89.4	0.0	598.6
(W/m^2)		Apr-Sep	44.2	85.8	0.0	626.7
		Total	42.9	87.6	0.0	626.7
	NS	Oct-Mar	43.9	95.1	0.0	721.0
		Apr-Sep	55.9	108.1	0.0	741.4
		Total	49.9	102.0	0.0	741.4
Net Longwave	EW	Oct-Mar	-28.4	27.0	-109.9	42.8
(W/m^2)		Apr-Sep	-9.4	21.1	-89.1	48.9
		Total	-18.9	26.0	-109.9	48.9
	NS	Oct-Mar	-30.8	27.8	-114.9	39.0
		Apr-Sep	-10.2	20.1	-85.4	51.1
		Total	-20.5	26.3	-114.9	51.1
Latent Heat	EW	Oct-Mar	-16.2	13.5	-103.6	29.0
(W/m^2)		Apr-Sep	-18.1	19.0	-132.6	32.3
		Total	-17.2	16.5	-132.6	32.3
	NS	Oct-Mar	-17.7	13.2	-110.4	48.6
		Apr-Sep	-19.9	23.8	-292.4	37.4
		Total	-18.8	19.3	-292.4	48.6
Sensible Heat	EW	Oct-Mar	-8.4	18.0	-86.2	73.2
(W/m^2)		Apr-Sep	1.5	12.3	-32.9	80.6
		Total	-3.4	16.2	-86.2	80.6
	NS	Oct-Mar	-9.6	18.3	-93.9	73.0
		Apr-Sep	1.4	11.6	-36.1	64.8
		Total	-4.1	16.3	-93.9	73.0
Streambed Heat	EW	Oct-Mar	34.6	13.7	-0.7	64.3
(W/m^2)		Apr-Sep	-5.4	32.2	-346.4	150.7
		Total	14.6	31.8	-346.4	150.7
	NS	Oct-Mar	68.6	21.8	15.3	98.2
		Apr-Sep	2.0	55.1	-786.0	319.8
		Total	35.2	53.5	-786.0	319.8

To examine variability in individual energy fluxes over the course of the year, and to quantify attenuation of energy by the temporally variable riparian canopy LAI, energy fluxes were also analyzed by monthly averages. This analysis was conducted for calculated energy fluxes using the above methods with hydroclimate data, as well as for energy fluxes calculated using climate data from the reference site in place of the hydroclimate data. Energy fluxes calculated using the above canopy (reference) climate variables theoretically represent what energy exchange with the stream would be if the riparian canopy was not present (i.e., the riparian zone was clearcut). Results from this analysis are split into two tables, corresponding to the first and second half of the water year, Table 14 and Table 15. The sum term in each table refers to the total of calculated energy fluxes, and is considered the residual. In this study, the only primary source of energy not considered is advected exchange (groundwater and hyporheic exchange). Therefore, in this study, the residual term refers to the sum of advected energy flux and energy stored or released by the stream as thermal energy (change in stream temperature). Notably, advected sources of heat from groundwater exchange can either warm or cool the stream. The percent column shows percent difference comparing the percent difference (residual) between below and above canopy microclimate and energy fluxes. Note that it is possible for energy fluxes not quantified to be greater in magnitude than the residual term, therefore resulting in, for example, cooling of the stream through a reach when the sum of calculated energy fluxes is positive, which would suggest stream heating (Johnson, 2004; Story *et al.*, 2003). When percent difference (%) is positive, the total computed energy flux is greater for below canopy variables than above canopy; a

negative % means stream energy flux calculated with above canopy variables is greater and energy is therefore attenuated by the canopy.

Table 14: Mean monthly (Oct-Mar, 2010 WY) energy fluxes calculated for study reaches at Brushy Creek, BREA central Missouri, USA. Sum is the total of the computed energy fluxes. % is relative difference in available stream energy from the EW or NS value to the respective reference value immediately below; negative values mean available energy is lower underneath the canopy (energy is attenuated).

Month		Net Shortwave (W/m^2)	Net Longwave (W/m^2)	Latent Heat (W/m^2)	Sensible Heat (W/m^2)	Streambed Heat (W/m^2)	Sum (W/m^2)	%
October	EW	37.4	-22.5	-17.3	-5.3	17	9.3	400.0
	Ref	98.3	-51.9	-55.9	-10.6	17	-3.1	
	NS	39	-24.2	-19.4	-5.8	39.2	28.8	185.1
	Ref	98.3	-53.6	-60.3	-13.5	39.2	10.1	
November	EW	37.8	-25.7	-18.7	-2.2	22.4	13.6	525.0
	Ref	91.6	-59.1	-61.6	3.5	22.4	-3.2	
	NS	38.1	-27.4	-20	-3.3	48.5	35.9	169.9
	Ref	91.6	-60.9	-66.1	0.2	48.5	13.3	
December	EW	20.3	-32.6	-14.9	-13.7	43.2	2.3	105.5
	Ref	57.9	-58.6	-47.2	-36.8	43.2	-41.5	
	NS	22.7	-36.2	-17.4	-16	82	35.1	263.3
	Ref	57.9	-62.5	-54.2	-44.7	82	-21.5	
January	EW	27.9	-35.9	-13.5	-19.2	48	7.3	150.7
	Ref	74.9	-59.1	-34.7	-43.5	48	-14.4	
	NS	30.1	-38.7	-15.5	-21.1	91	45.8	188.1
	Ref	74.9	-62.2	-38.8	-49	91	15.9	
February	EW	52.7	-33.6	-14.1	-11.1	47.3	41.2	27.6
	Ref	114.9	-63	-37.9	-29	47.3	32.3	
	NS	57.7	-36.9	-15.6	-12.6	89.3	81.9	38.1
	Ref	114.9	-66.6	-42.9	-35.4	89.3	59.3	
March	EW	74.5	-20.6	-18.4	1.2	30.8	67.5	-12.3
	Ref	143.1	-53.1	-52.3	8.5	30.8	77	
	NS	77.2	-21.9	-18.2	0.9	62.8	100.8	-3.4
	Ref	143.1	-54.7	-52.9	6.1	62.8	104.4	

Table 15: Mean monthly (Apr-Sep, 2010 WY) energy fluxes calculated for study reaches of Brushy Creek, BREA central Missouri, USA. Sum is the total of the computed energy fluxes. % is relative difference in available stream energy from the EW or NS value to the respective reference value immediately below; negative values mean available energy is lower underneath the canopy (energy is attenuated).

		Net Shortwave (W/m^2)	Net Longwave (W/m^2)	Latent Heat (W/m^2)	Sensible Heat (W/m^2)	Streambed Heat (W/m^2)	Sum (W/m^2)	%
April	EW	93.2	-21.5	-31.7	5.1	3	48.1	-24.3
	Ref	205.5	-63	-101.7	19.7	3	63.5	
	NS	98.8	-19.4	-28.4	4.8	10.1	65.9	-17.7
	Ref	205.5	-61.4	-96.8	22.7	10.1	80.1	
May	EW	46.6	-8.2	-14.2	1.1	1.7	27	-79.2
	Ref	219.2	-47.6	-50.2	6.7	1.7	129.8	
	NS	49.7	-6.4	-12.5	2.1	1.4	34.3	-75.4
	Ref	219.2	-45.6	-44.7	9.4	1.4	139.7	
June	EW	36.4	-3.2	-13.3	2.3	-2.8	19.4	-88.9
	Ref	259.3	-43.3	-49.7	12	-2.8	175.5	
	NS	52.1	-3.2	-12.9	2.9	-1.3	37.6	-79.5
	Ref	259.3	-42.1	-46.1	13.6	-1.3	183.4	
July	EW	26.4	-2.4	-11.6	2.1	-8.2	6.3	-96.1
	Ref	237.4	-36	-44.7	11.2	-8.2	159.7	
	NS	46.2	-7.8	-21.2	0.04	14.1	31.34	-78.6
	Ref	237.4	-41.1	-68.1	4.3	14.1	146.6	
August	EW	32.5	-6	-17.9	0.9	-20.8	-11.3	-108.6
	Ref	254.6	-49.4	-63.4	11.1	-20.8	132.1	
	NS	49	-8.6	-23.3	0.3	-20.6	-3.2	-102.8
	Ref	254.6	-51.8	-75.6	7.9	-20.6	114.5	
September	EW	30.8	-15.3	-20.4	-2.1	-4.9	-11.9	-123.5
	Ref	184	-57.2	-70.2	-1.1	-4.9	50.6	
	NS	40.3	-16.1	-21.2	-1.8	8.8	10	-84.5
	Ref	184	-57.2	-70.1	-1.1	8.8	64.4	

Average net shortwave radiation was highest for below canopy computations in April for both the EW and NS reaches, at 93.2 and 98.8 W/m^2, respectively. Highest values for average unattenuated net radiation occurred in June (259.3 W/m^2). For all

months, for both reaches, and for both above and below canopy energy flux calculations, net longwave radiation and latent heat were negative and therefore cooled the stream; average net longwave radiation was -18.9 W/m^2 for the E-W reach and -20.5 W/m^2 for the N-S reach, while latent heat was on average -17.2 W/m^2 for the E-W reach and -18.8 W/m^2 for the N-S reach..

Percent difference between beneath canopy energy flux computations and reference above canopy computations was mostly positive for the first half of the water year (ranging from -3.4% to 525%), and negative for the entirety of the second half (ranging from -17.7% to -123.5%). The stream was losing less energy to net longwave radiation and latent heat exchange relative to the reference site (a theoretical clearcut scenario). In November when the calculated percent difference of energy fluxes is largest the E-W reach lost 18.7 W/m^2 to latent heat exchange and the N-S reach loses 20.0 W/m^2 to latent heat exchange relative to 66.1 W/m^2 lost using the reference site data. In the second half of the water year, while latent heat flux remained higher for the reference calculations, the percent difference between EW/NS values and the reference site become smaller due to decreased net shortwave radiation. Net shortwave radiation at the stream surface was 41.3% and 41.6% (E-W and N-S reach, respectively) of reference values in November when the canopy was leafless. However, values of shortwave radiation at the stream surface were only 12.8% and 19.2 % (E-W and N-S reach, respectively) of those measured at the reference site in August during full canopy foliation.

Stream Temperature Dynamics

Average stream temperature for the 2010 water year was 12.9 °C for the E-W reach and 13.2 °C for the N-S reach. Highest monthly average stream temperature occurred in August for the E-W reach (23.6 ˚C) and July for the N-S reach (24.4 ˚C) (Table 16). The terms "temperature gradient" will hereafter refer to difference between temperature measurements at the downstream and upstream temperature sensors within each study reach. By this convention, negative gradients indicate that water is cooling as it flows downstream through a reach (losing energy), and positive gradients indicate that water is warming as it flows downstream through a reach. The gradient within the EW reach was generally negative during the first half of the year (average -0.27 ˚C), turning positive in May through September (average 0.16 ˚C). The temperature gradient through the NS reach was mostly negative during the second half of the water year (average -0.17 ˚C), which is the time when streams reach maximum temperature. The computed energy balance residual term is positive for both reaches for most of the year (average 20.2 W/m^2 for E-W reach and 45.8 W/m^2 for N-S reach), suggesting the stream should be warming as it flows through both reaches assuming no influence from groundwater.

Table 16: Comparison of stream discharge, temperature within stream reach, difference between upstream and downstream temperature, and sum of calculated energy flux terms for an E-W reach and N-S reach of a second order stream (Brushy Creek), central Missouri USA.

	Discharge (m^3/s)		**Temperature (°C)**		**Temperature Gradient (°C)**		**Sum (W/m^2)**	
	EW	NS	EW	NS	EW	NS	EW	NS
October	0.55	0.94	12	12.4	-0.17	-0.02	9.3	28.8
November	0.03	0.11	10.1	10.4	-0.2	0.41	13.6	35.9
December	0.06	0.21	1.6	1.5	-0.48	0.96	2.3	35.1
January	0.06	0.26	0.8	1.5	-0.5	0.68	7.3	45.8
February	0.08	0.32	1.0	1.8	-0.31	0.22	41.2	81.9
March	0.04	0.16	7.0	7.4	-0.01	-0.03	67.5	100.8
April	0.5	0.62	14.9	14.5	-0.14	-0.13	48.1	65.9
May	0.15	0.15	16.8	16.4	0.03	-0.04	27.0	34.3
June	0.02	0.02	22.5	22.3	0.33	0.07	19.4	37.6
July	0.04	0.03	23.5	24.4	0.41	-0.72	6.3	31.3
August	0.13	0.13	23.6	24	0.17	-0.2	-11.8	-3.2
September	0.1	0.08	19.6	19.6	0.16	0	-11.9	10

DISCUSSION

Canopy Attenuation of Energy

Leaf area index values characterized canopy density both above each stream reach as well as within the riparian zone adjacent to each reach. This measurement was important as canopies with higher densities transmit less light (Stenberg *et al.*, 1994). Leaf area index values measured within the riparian zones of this study were slightly higher than those measured near the reference site (Figure 23), with peak measured LAI of 4.5 for the study riparian zones versus 3.75 for the reference site. In June 2006 an LAI of 4.2 was estimated for the reference site based on leaf litter weights and specific leaf

area (Gu *et al.*, 2007). Compared to this estimate, LAI measured in the study riparian zone was in June 2010 was 1.0% greater as measured with ceptometer and 2.8% greater based on hemispherical photos (LAI values used for comparison from Table 5 and Table 6. We are aware of no other work that directly compared ceptometer and hemispherical photo measurements of leaf area index. Values slightly below one prior to day of year 100 and after day of year 300 of Figure 23 are consistent with those in Table 5 and Table 6 (LAI=0.75 for ceptometer and LAI=0.80 for hemispherical photos). However, unlike the riparian zones, conifers, which have leaves year-round, make up part of the forest around the reference site (Gu *et al.*, 2006). Therefore, stem density at the reference site is different than the riparian study sites, and observed variation in canopy density between the reference site and study sites may be attributable to differences in species composition.

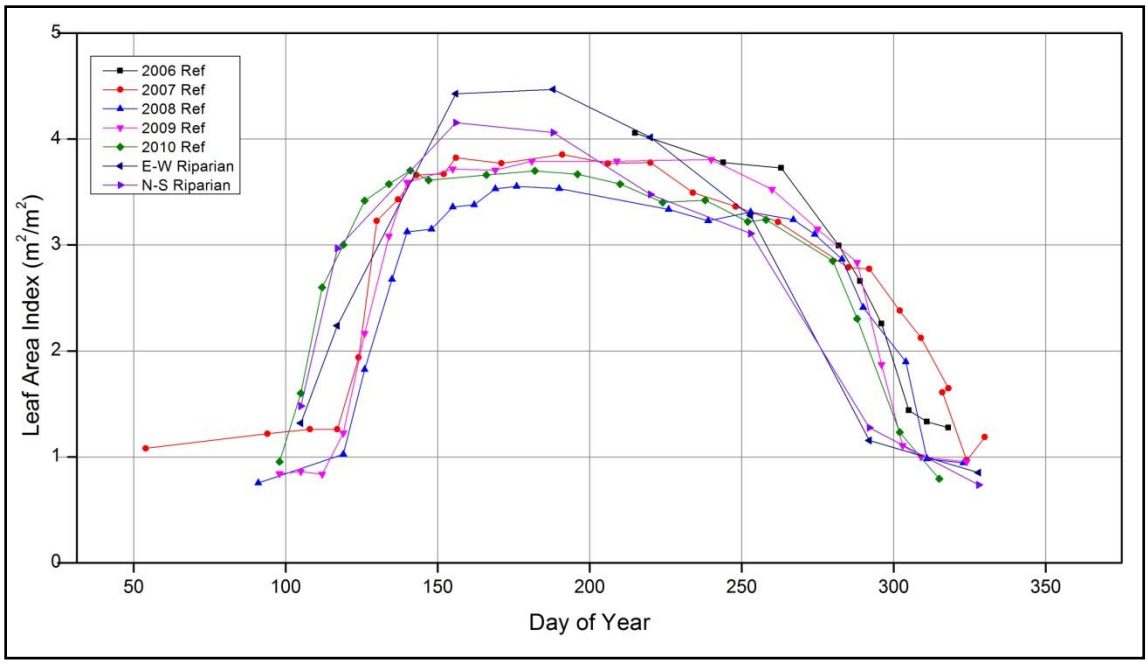

Figure 23: Leaf area index values measured for area around reference flux tower from 2006-2010 compared to measurements from riparian zone along two stream reaches, BREA central Missouri, USA. (Pallardy and Hosman, unpublished data).

PAR measurements collected with the ceptometer were better correlated to LAI measurements collected with hemispherical photography for the riparian zone (R^2=0.98) than for in stream measurements (R^2=0.67). We are aware of no other studies that used LAI as a metric for the difference in canopy density above a stream relative to the adjacent riparian zone. As above stream LAI values are lower, it is possible one or both methods had larger errors relative to actual LAI when there is a gap in the canopy (canopy density is lower). However, previous studies showed no significant decrease in accuracy for measurements collected in lower canopy densities; rather, hemispherical photos are known to be in error for high densities when shortwave radiative transmittance is less than 10% (Hale and Edwards, 2002).

Hemispherical photo based estimates of LAI were higher than those collected with the ceptometer. Average riparian zone LAI for all measurements was 2.69 estimated with hemispherical photos, 6.3% greater than the average of 2.53 estimated with ceptometer. While no previous study was found that directly compared ceptometer and hemispherical photo measurements collected from the same study site, one study did measure identical LAI of 1.7 for a study site of 14 year old ponderosa pines in central Oregon, USA with both a ceptometer and LAI-2000, which used a hemispherical lens to gather light (Law *et al.*, 2001). This close correlation between methods suggests that our LAI measurements are reliable.

Net radiation was the primary component of the stream energy balance for each reach, consistent with previous studies (Evans *et al.*, 1998; Leach and Moore, 2010a; Webb and Zhang, 1997). Quantifying net radiation at the stream surface through the study reaches was crucial to understanding stream thermal dynamics. In this study, as in previous work (Leach and Moore, 2010a; Webb and Nobilis, 1997), instrument availability precluded the use of multiple sensors located directly above the stream to quantify the spatial and temporal variations in net radiation. The chosen alternative to in stream measurement was hemispherical photography based modeling.

Average modeled shortwave radiation at the E-W climate station based on hemispherical photos for the study period was 20.5% lower than measured values. For the N-S climate station, modeled values were 12.2% lower than measured values. Maximum 15 minute average modeled shortwave radiation at the E-W climate station was 735.7 W/m^2 versus a measured maximum of 854 W/m^2. For the N-S climate station,

maximum modeled shortwave radiation was 776.2 W/m^2 versus a measured maximum of 877 W/m^2. Previous work did indicate absolute differences in summary statistics for measured and modeled radiation, but focused on RMSE and MBE (Leach and Moore, 2010a; Moore *et al.*, 2005b). Leach and Moore (2010a) reported a positive MBE, suggesting their model overestimated net radiation, compared to the negative values (underestimation) found in this study. Differences in model predictions may be attributable to differences in canopy species composition; however differences between modeled and measured values are generally small, which agrees with previous research (Leach and Moore, 2010a).

Previous studies that used hemispherical photos to quantify stream net radiation did so only for periods up to 6 months, and did so in more homogeneous (spatially and temporally) coniferous forest canopies (Leach and Moore, 2010a; Moore *et al.*, 2005b). The RMSE compared to measured net radiation reported in one previous study was 46 W/m^2 for 10 minute averages of net radiation, similar to 56.1 W/m^2 and 48.9 W/m^2 found in this study for the E-W and N-S climate station radiation models (Leach and Moore, 2010a). When compared with in stream pyranometer measurements, the hemispherical photo based stream radiation model's RMSE of 46.1 W/m^2 and 52.4 W/m^2 was similar to previous computations of RMSE of 46 W/m^2 (Leach and Moore, 2010a). Therefore, error between measured and modeled values is consistent with previous work, and modeled values of net shortwave radiation are good approximations of actual net shortwave radiation across the stream reach.

In Figure 17, which compared modeled values of shortwave radiation to an in-stream pyranometer, large variations observed in the measured curve suggest incident radiation was high only for momentary periods. Spikes in incident radiation are attributable to either the sun passing over small gaps in the canopy where beam transmissivity was high, or the result of clouds temporarily obscuring beam radiation. Additionally, comparison to the values from the in stream pyranometer may be useful, but should not be considered the best reference for accuracy for modeled values. The pyranometer measured radiation only at a single point, and is therefore not necessarily representative of average radiation across the entire reach, which may be better quantified by a method that takes into account measurements at multiple locations (e.g. hemispherical photo model) (Rich, 1990). The low R^2 values seen in Table 9 could therefore result from comparing reach-scale averages to measurements at a single point, which should not necessarily be identical. Hemispherical models, such as those used in this work, are one way to quantify spatial and temporal variation in net shortwave radiation across the reach, and were therefore used to quantify net shortwave radiation for energy balance calculations.

Results from pairwise ANOVA analysis indicated significant ($P = 0.01$) differences between measurements of temperature and relative humidity collected at the stream edge and measurements collected within the riparian zone. Temperature was significantly different at either 25 or 40 meters from the stream edge in three of the four transects. For the NS-W transect average temperature was 3.1% (˚C) greater 25 meters from the stream edge, and for the EW-S transect temperature was 2.5% (˚C) greater 40

meters from the stream edge. Relative humidity was significantly ($\alpha = 0.01$) different than the stream edge five meters away from the stream for 3 of 4 transects, and significantly different at 10 meters for the remaining transect. Averaging all 4 transects, relative humidity was 2% lower ten meters away from the stream edge. Few studies have examined microclimate within riparian buffers (Moore *et al.*, 2005a). However, one study did examine change in multiple microclimate variables as a function of distance from stream. Brosofske (1997) found all climate variables approached interior forest values within 31- 62m from the stream, which is consistent with findings from this study for air temperature.

In addition to proximity to the stream, iButton temperature was influenced by incident solar radiation; due to the heterogeneous nature of the canopy within the riparian zone the stream is not the only gap in the canopy through which direct beam radiation may be incident on the iButton transects. To attempt to better observe patterns in iButton measured temperatures, three clear-sky days were randomly selected for further analysis. These days were April 10, June 16, and August 16.

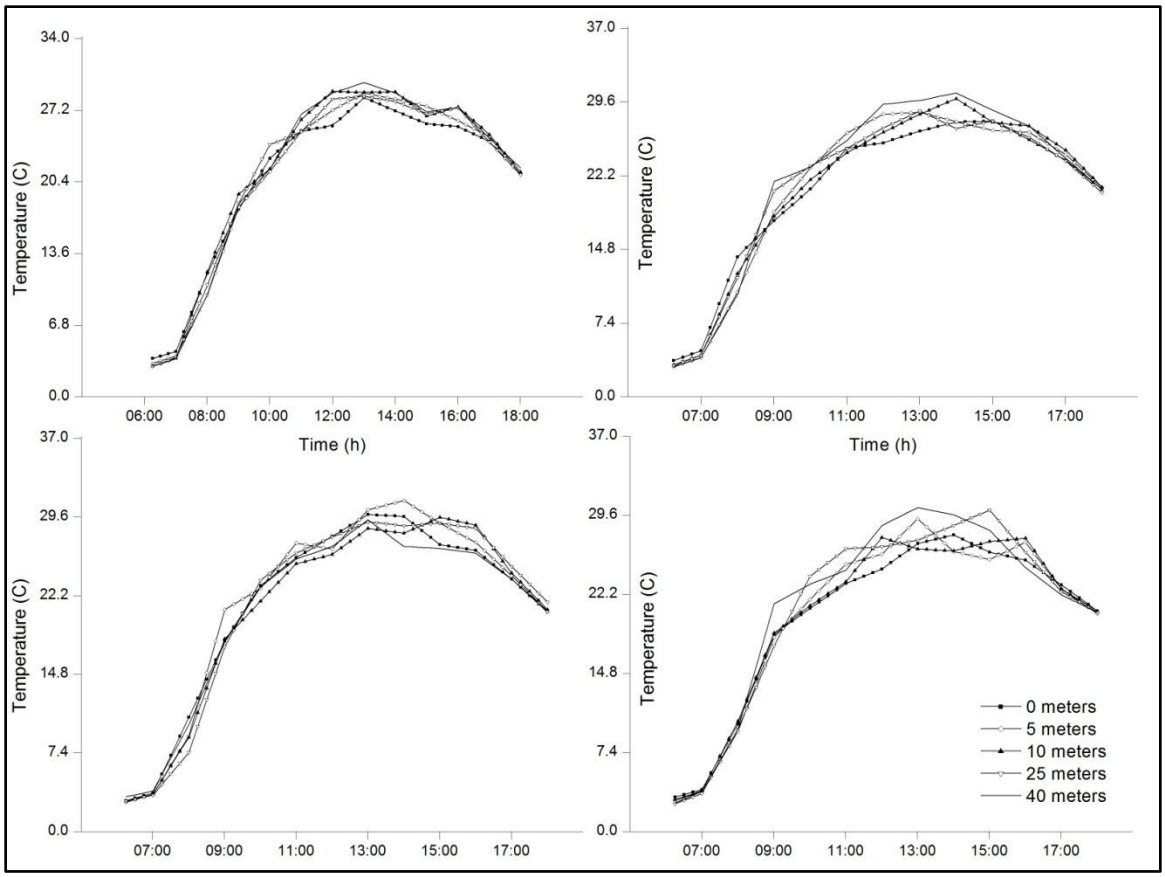

Figure 24: Comparison of (clockwise from top left) EW-N, EW-S, NS-E, and NS-W riparian iButton temperature measurements along transect extending away from stream edge (Brushy Creek, Baskett Research and Education Area, Central Missouri USA) over the course of April 10, 2010.

Figure 24 above illustrates iButton temperature along the riparian transect for April 10, 2010. For this date, air temperature is highest 40 meters away from the stream for at least a portion of the day for three of the four transects (maximum temperatures were 29.8 ˚C 40 meters from the stream versus 28.4 ˚C measured simultaneously at the stream edge for the EW-N transect, 30.3 ˚C versus 27.3 ˚C for the EW-S transect, and 30.3 ˚C versus 26.9 ˚C for the NS-W transect), supporting the hypothesis that the stream

creates a distinct microclimate which keeps the surrounding air cooler (Moore *et al.*, 2005a).

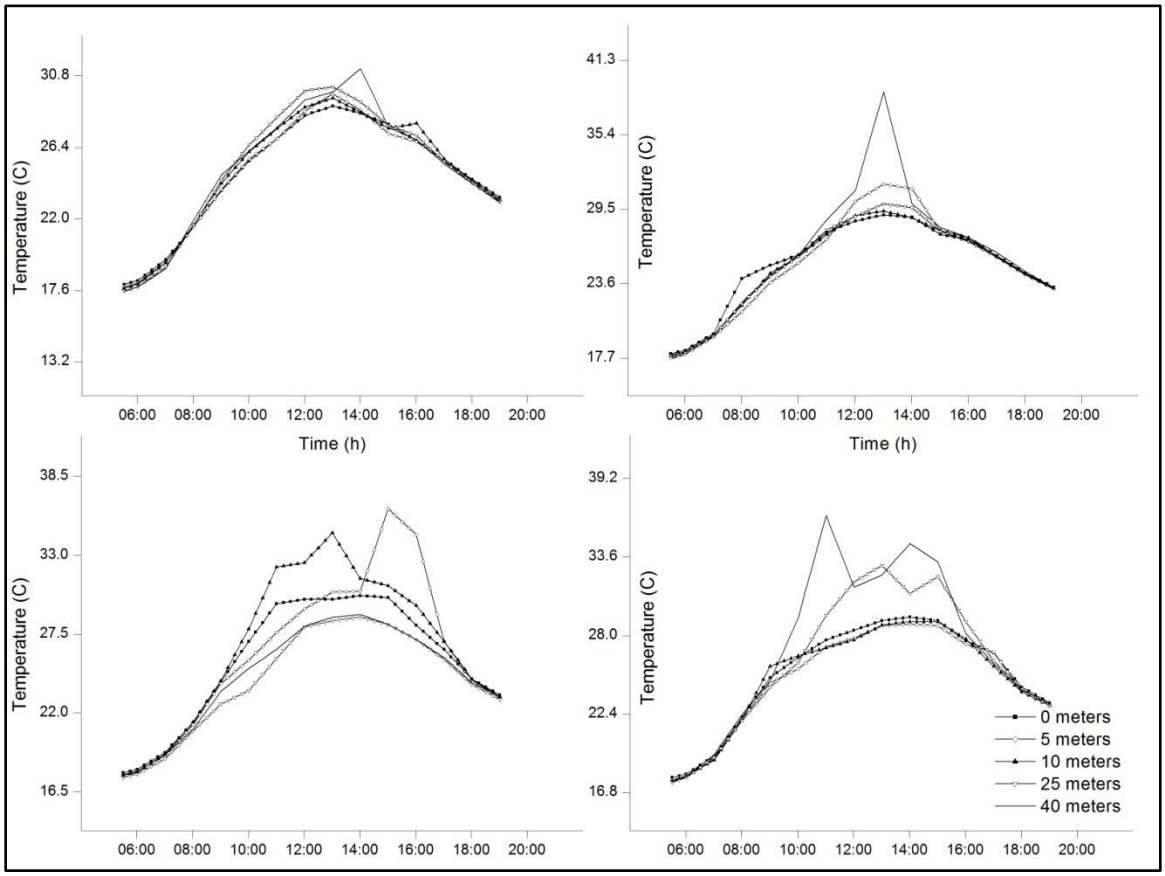

Figure 25: Comparison of (clockwise from top left) EW-N, EW-S, NS-E, and NS-W riparian iButton temperature measurements along transect extending away from stream edge (Brushy Creek, Baskett Research and Education Area, Central Missouri USA) over the course of June 16, 2010.

Figure 25 above illustrates iButton temperature along the riparian transect for June 16, 2010. For this date, air temperature is highest furthest away from the stream for at least a portion of the day for two of the four transects. Maximum temperature was 31.3 ˚C for the EW-N transect and occurred at 14:00 at 40 meters from the stream edge, while maximum temperature was 38.8 ˚C for the EW-S transect and occurred at 13:00 40

meters from the stream edge. Maximum temperatures occurring farthest from the stream edge indicates a possible cooling effect from the stream. Large peaks in temperature at different times and locations over the course of a day at various locations within the riparian buffer were not seen in previous work (Brosofske *et al.*, 1997). Such peaks may be attributable to lower canopy density and different canopy structure (riparian versus upland deciduous).

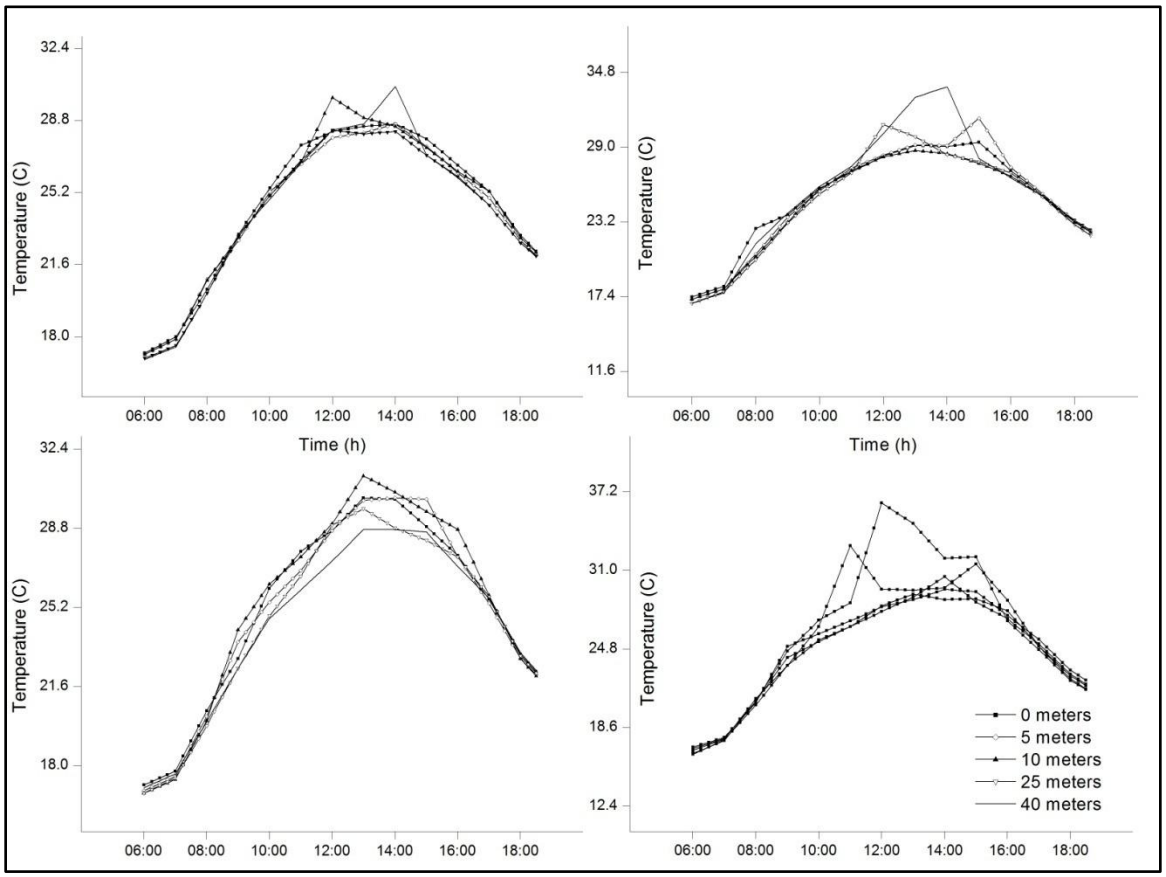

Figure 26: Comparison of (clockwise from top left) EW-N, EW-S, NS-E, and NS-W riparian iButton temperature measurements along transect extending away from stream edge (Brushy Creek, Baskett Research and Education Area, Central Missouri USA) over the course of August 16, 2010.

For August 16 (Figure 26), maximum temperature in the EW-S and NS-E transects occurred 40 meters away from the stream edge (33.5 ˚C and 36.3˚C, respectively). Overall, Figure 24, Figure 25, and Figure 26 and the summary data presented previously indicate that for the iButton temperature/humidity transects, there is a large degree of variability in measured temperature between iButtons within each transect. The largest within transect difference occurred in the EW-N transect in the June graph, when maximum temperature was 33.3% (˚C) greater (38.8 ˚C vs. 29.1 ˚C). As an alternative to air temperature, sky view factor as measured via hemispherical photos at each sensor was considered an alternative to quantify light penetration into the riparian zone, characterized for a single measurement date in Table 17 below.

Table 17: Sky view factor measured with hemispherical photos and gap light analyzer software at locations of iButton temperature/RH sensors along transects within riparian zone extending away from Brushy Creek, Baskett Wildlife Research Area, Central Missouri USA. Photos were collected on June 5, 2010.

	Distance from Stream	Sky View Factor (%)
EW-N	0	4.18
	5	2.16
	10	1.73
	25	2.01
	40	1.46
EW-S	0	3.46
	5	2.18
	10	1.75
	25	3.97
	40	3.67
NS-E	0	7.06
	5	3.93
	10	2.16
	25	2.67
	40	1.9
NS-W	0	3.82
	5	4.56
	10	2.7
	25	11.23
	40	22.18

The above table shows decreasing sky view factors for the first ten meters away from the stream edge for the EW-N, EW-S, and NS-E transects. This trend does not continue past ten meters for any transect, suggesting influences from gaps in the canopy created by the stream may be restrained to within ten meters of the streambank. A previous investigation of light penetration into a forest edge using hemispherical photographs in a deciduous ash forest in Australia found light penetration was attenuated

rapidly over the first ten to 30 meters from a forest edge. The large increase in sky view factor 25 and 40 meters away from the stream along the NS-W transect shows the heterogeneous nature of the canopy density measured within the riparian zone.

Stream Discharge Computation

We are aware of no studies in the region which have reported values for rating curve coefficients in streams with similar stream geomorphology. Comparisons to such studies may be of limited use regardless, as differences in stream morphology between channels would lead to different values (Dingman, 2002). In this study, cross sections did not cover the entire range of stage measured at each climate station; there were several instances when discharge exceeded the highest amount measured with a cross section. The rating curves were still used for these times as they did not occur very often and were generally small in duration (less than half of one day). Accurately quantifying discharge at all stages was beyond the scope of this work, which focused on energy fluxes and their interaction with non-peak flows. Furthermore, sample size (eleven cross sections per reach) was adequate compared to past work, for which four to twelve cross sections have been used to construct rating curves for a given year (McMillan *et al.*, 2010). Rating curves should therefore be accurate for the majority of observed levels of stage. Future work in the stream might better quantify discharge up to bank-full stage.

Stream Energy Fluxes

Wind speed, air temperature, relative humidity, and shortwave radiation were closer between the two hydroclimate stations than between either of the hydroclimate sites versus the reference site (see table 11). However, there were still statistically significant differences (α=0.01) between the two climate stations for shortwave radiation ($P<0.001$), and wind speed ($P<0.001$). Average relative humidity was 1.6% greater at the E-W climate station than the N-S climate station. Shortwave radiation was 4.5% lower at the E-W climate station than the N-S climate station. This difference is in part be explained by greater average values for LAI measured in the E-W riparian zone versus the N-S riparian zone (2.71 versus 2.65). Average wind speed was statistically different ($P<0.001$) between the E-W and N-S climate stations despite similar means (0.4 m/s at each); wind speed was more variable at the E-W climate station resulting in individual measurements which differed between the stations even though each measurement series averaged to nearly the same value. Standard deviation for the E-W climate station was ±1.2 m/s versus ±0.4 m/s for the N-S climate station. Notably, these differences are generally within the error for instruments listed in Table 2. It is therefore possible that observed differences between climate stations are due to instrument error. Other potential sources of variation include differences in canopy cover, topographic shading and thus below canopy turbulence. Canopy cover may have been a factor as LAI was on average higher within the E-W riparian zone (2.71) relative to the N-S riparian zone (2.65). Notably, this difference is not consistent with precipitation data; total precipitation was 17.8% greater at the E-W climate station than the N-S station despite increased canopy

cover at the E-W station. Though on average canopy density was higher within the E-W riparian zone was higher, it is possible that canopy density directly above the precipitation gauge was lower than at the N-S site. Study sites were selected such that topographic shading would not be different between the reaches. Generally, the shape of the valley in which the study sites were located was such that there were hills directly east and west of each reach, and topographic shading likely therefore did not result in detectable differences in radiation and temperature between the climate stations, but may have influenced differences in wind speed.

Larger differences were observed for climate variables between the study reaches and the reference site. Average air temperature at the E-W climate station was 9.4% (˚C) lower than the above canopy reference, and the N-S climate station was 8.6% (˚C) lower than the reference. Topographic shading may have played a role in the differences between the climate stations (similar topographic shading) and flux tower (different topographic shading than climate stations); the location of the climate stations within a valley leads to more shading from direct radiation over the course of the day relative to the reference site, which was on a ridge. Due to the low elevation of the hydroclimate stations relative to the reference site, cold air drainage may explain some of the differences. Air temperature may also be cooler at the hydroclimate stations as a result of shelter from incident radiation provided by the riparian canopy, resulting in less surface heating during the day and less surface re-emittance during the night. Brosofske (1997) found air temperature to be approximately one degree Celsius lower within riparian zones near streams than upland clearings. Average reference air temperature was also

approximately one degree Celsius lower at each climate station relative to the above canopy reference for this study (averages of 11.6 ˚C and 11.7 ˚C for climate stations versus 12.8 ˚C for the reference). Wind speed was significantly higher above the canopy relative to the below canopy hydroclimate stations. Average wind speed was reduced by 84.6% for both climate stations relative to the above canopy reference. This finding is consistent with previous studies that reported wind speeds underneath riparian canopies that are 10-20% of those measured in forest openings (Davies-Colley *et al.*, 2000; Moore *et al.*, 2005a). Average incident solar radiation at the E-W climate station was 74.1% lower than the reference, and the N-S climate station was 72.8% lower than the reference. This reduction is at the low end of the range 75-90% reduction for shortwave radiation specified in a review paper of riparian microclimate (Moore *et al.*, 2005a). Reduction in radiation was likely lower than other studies because many previous energy balance studies have been conducted in coniferous forests with greater canopy densities, particularly during times of leaf off in deciduous forests (Hannah *et al.*, 2008). Differences in climate measurements between climate stations and the reference site discussed below are greater than the instruments' error. Measurement differences between climate stations and the reference site are therefore likely due to differences in climate rather than instrument error.

Energy balance calculations indicated that net shortwave radiation was the largest average positive flux for the entire water year (42.9 W/m^2 E-W, 49.9 W/m^2 N-S), while latent heat and net longwave radiation were the largest average negative fluxes of energy (-18.9 & -17.2 E-W, -20.5 &-18.8 N-S). Only one other stream energy balance study has

observed streams within a deciduous forest; Hannah (2008) also found shortwave radiation to be the largest positive flux of energy, and latent heat and net longwave radiation on average to be the largest negative fluxes for a forested stream reach in Scotland (averages over two years, 2003-2004). However, for this system, as shown in Table 16, the sum of modeled energy fluxes is not always an accurate indicator of stream thermal regime. There are numerous months during which a negative residual term was calculated, but water warmed through the modeled reach, and other months in which a positive residual term was calculated, but water cooled through the modeled reach. One problematic area is the hydrologic regime for the study stream. Brushy creek is located over semi-karst terrain, which is characterized by flashy flow, and there could be quick drainage to an underlying aquifer (Young *et al.*, 2001). If this quick drainage exists, it could explain in part why discharge within the study stream was often very low, sometimes resulting in a dry streambed around the stream temperature sensors during base-flow conditions. Low discharge can also be attributed to the presence of the upstream dam and lake. Periods of low discharge could play a large role in confounding stream temperature dynamics-modeled surface energy exchanges could be balanced out or exceeded by increased groundwater interaction (O'Driscoll and DeWalle, 2006). This interaction was explored in previous studies that identified that groundwater played a large role in determining changes in stream temperature (O'Driscoll and DeWalle, 2006; Story *et al.*, 2003; Webb *et al.*, 2003). Quantification of groundwater influence on stream temperature is beyond the scope of this project, but supplies impetus for future studies.

To better characterize contributions of energy fluxes to stream heating and/or cooling, several time periods were selected during which stage within the creek was high enough for all temperature sensors two be submerged. Figure 27 and Figure 28 illustrate two periods which follow peak discharge events by several days.

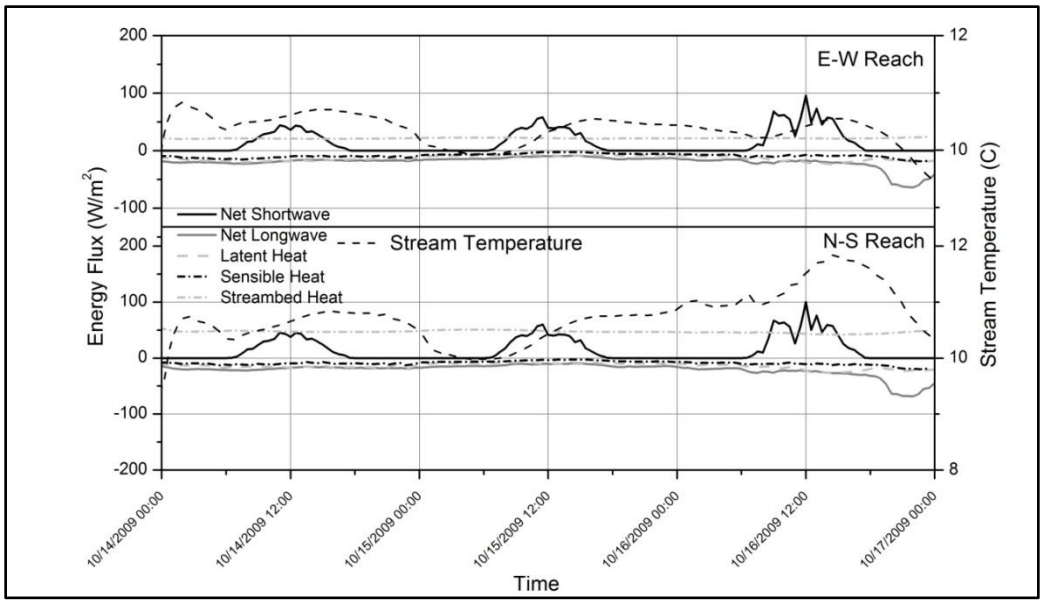

Figure 27: Modeled energy fluxes and measured stream temperature for an E-W oriented and N-S oriented stream reach, BREA central Missouri, USA, October 14 2009-October 17 2009.

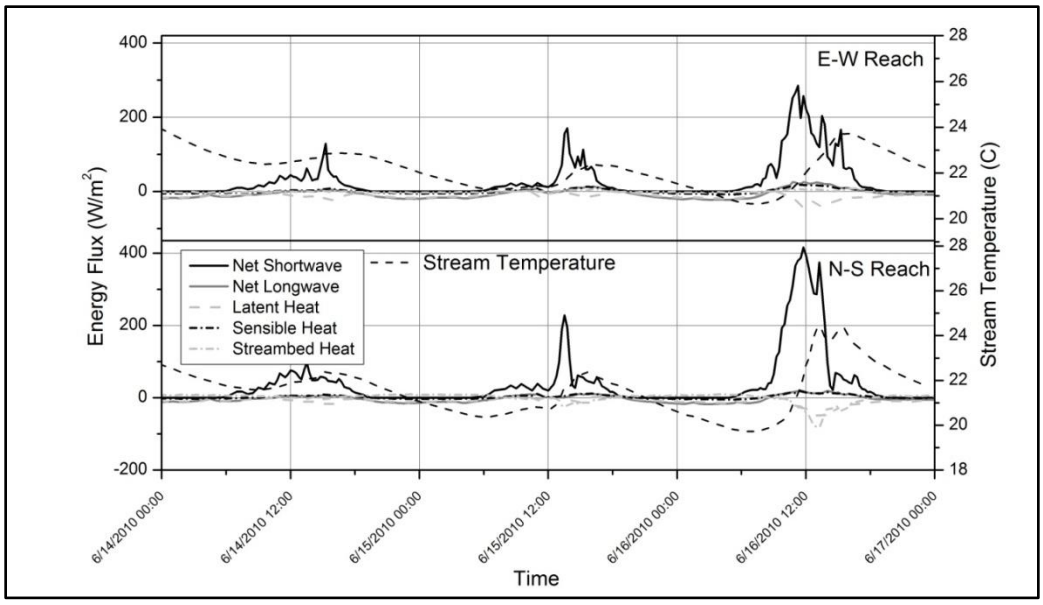

Figure 28: Modeled energy fluxes and measured stream temperature for an E-W oriented and N-S oriented stream reach, BREA central Missouri, USA, June 14 2010-June 17 2010.

Figure 27 and Figure 28 illustrate several key points. The average magnitude of net shortwave radiation across the entire water year is 150% greater in magnitude than the next largest flux for the E-W reach and 42.0% greater than the next largest flux for the N-S reach (notably, large values of shortwave radiation during the day are balanced by times during the night when net shortwave radiation is 0 W/m^2), differences between daily maximum values of net shortwave radiation and other fluxes are even greater by approximately an order of magnitude. Peaks in shortwave radiation are closely followed by peaks in stream temperature. Second, in Figure 28, latent heat flux increases to partially balance out the increased net radiation and sensible heat exchange (dependent on air temperature) during the day (Edinger *et al.*, 1968). Increases in stream temperature from increased incident radiation are therefore balanced partially, but not completely, by

increased cooling from latent heat loss with latent cooling increasing as a function of stream temperature.

The residual term (described in the results section under *Stream Energy Fluxes*) for the stream energy balance was calculated for energy fluxes influencing stream temperature. This calculation was conducted using both microclimate variables adjacent to each stream reach, as well as above canopy reference data. The residual term was not always a good predictor of stream thermal regime. Generally, a residual term is not calculated as studies either do not attempt to close the energy balance (Leach and Moore, 2010a; Moore *et al.*, 2005b) or rely on previous investigations of groundwater dynamics for their study systems (Hannah *et al.*, 2008; O'Driscoll and DeWalle, 2006; Story *et al.*, 2003). However, comparison of residual terms calculated from above and below canopy microclimate variables is useful as it allows for closure of the energy balance and quantification of the canopy's ability to ameliorate stream heating. During months of maximum stream temperature, July and August, the riparian canopy (average hemispherical LAI was 4.31 July 7 and 3.81 August 8) reduced energy exchange with the stream by up to 124%.

Stream Temperature Dynamics

Average daily stream temperature varied from approximately 0 to 25 °C. The largest value for average daily temperature was 26.5 ˚C for the E-W reach and occurred on July 21, while the largest value for the N-S reach was 27.6 ˚C and occurred on August 13 in agreement with a previous study that estimated a mean upper boundary for stream

temperature of 27.6 °C with a standard deviation of 5.0 °C based on temperature data from 720 USGS gauging stations (Bogan *et al.*, 2006). Maximum stream temperatures ocurred in late July and early August. Several factors likely account for this. First, discharge during this period was on average low-averaging 0.087 m^3/s for the E-W reach and 0.080 m^3/s for the N-S reach. The stream was warmer during periods of low discharge as water moved more slowly and had more time to reach a state of thermal equilibrium with the overlying air and underlying streambed. Figure 29 shows that during winter, higher discharge was associated with higher stream temperature, and during summer higher discharge is generally associated with lower stream temperature. Differences in the source of water at different stages (upstream lake versus groundwater) may explain some observed differences in temperature. Webb *et al.* (2003) also observed that water temperature was inversely related to discharge for a range of stream sizes, spanning catchments from 2.1 to 601 km^2 in the U.K. Webb *et al.* (2003) also reported that air temperature-water temperature correlations were stronger for flows below the median discharge (R^2 between air temperature and water temperature 0.88 for smallest stream hourly values when discharge less than median versus 0.82 when discharge above median). While correlations between air temperature and water temperature were not made in this study, sensitivity of stream temperature to discharge is evident in Figure 29 as higher temepratures are observed when discharge is at its minimum.

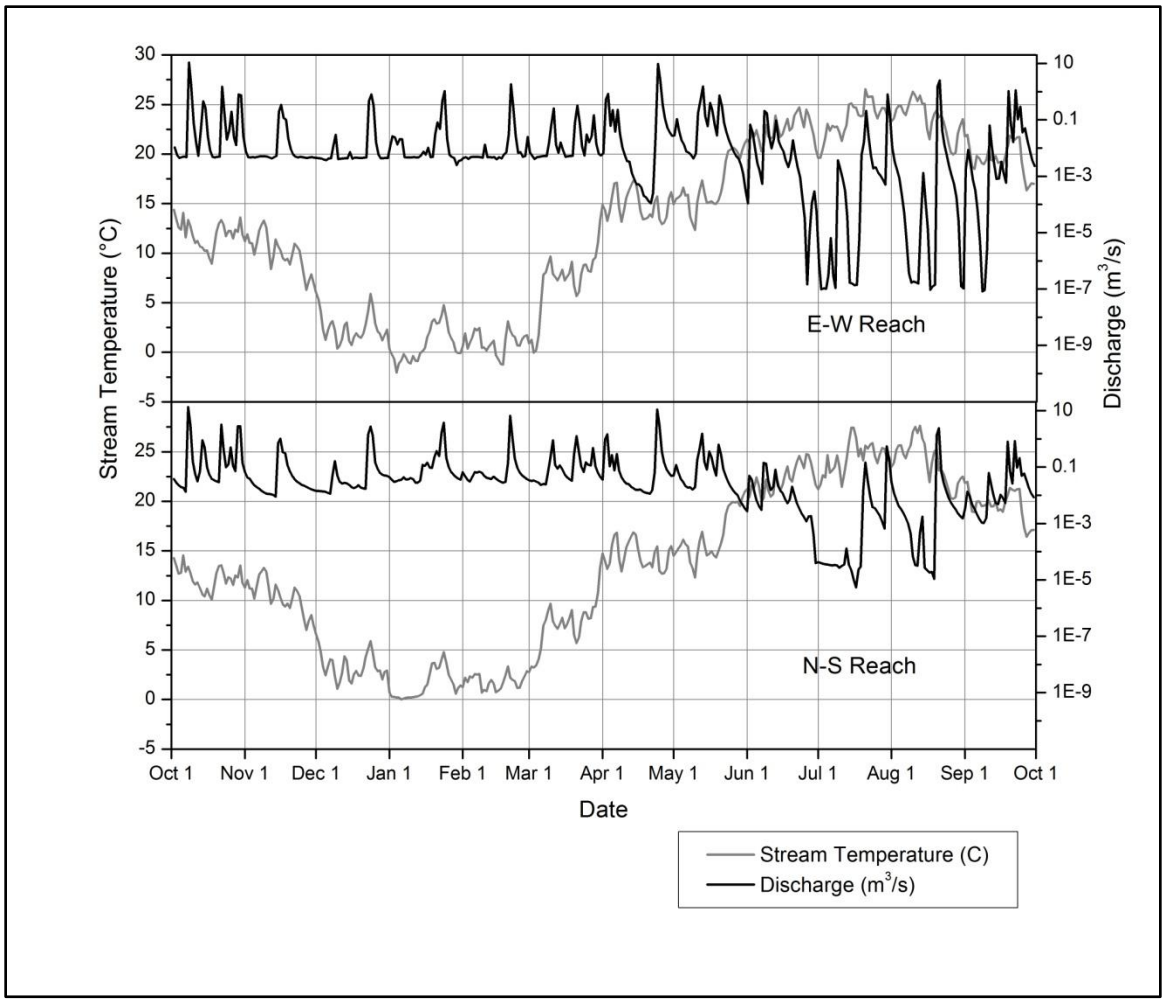

Figure 29: Comparison of estimated discharge and measured stream temperature during 2010 WY for E-W stream reach and N-S stream reach, Brushy Creek, BREA central Missouri, USA.

CHAPTER IV:

CONCLUSIONS AND SYNTHESIS

The overall goals of this project were two-fold. First, the project was designed to better understand riparian canopy attenuation of energy and, by extension, amelioration of stream heating by providing quantitative results. Second, it was hoped that by providing these data, management of forested riparian ecosystems within the state of Missouri would be improved by more informed science-based decision processes.

This work is the first known study quantifying the role of energy attenuation by a riparian forest canopy and effects on stream water temperature in the ecologically and climatologically distinct Ozark border region of the central U.S. Canopy density was quantified via ceptometer and hemispherical photography. Maximum measured leaf area index was in June and was 4.51 in the E-W riparian zone, 3.07 above the E-W stream reach, 3.97 in the N-S riparian zone, and 2.11 above the N-S stream reach (ceptometer measurements). The E-W reach in general had higher LAI values both within the stream reach (average 1.97 vs. 1.36 for N-S) and within the adjacent riparian zone (average 2.64 vs. 2.43 for N-S), with the range in values illustrating the spatial heterogeneity of the canopy. It was important to account for this spatial heterogeneity when quantifying energy attenuated by the canopy versus that reaching the stream surface, because point measurements of microclimate variables (particularly net radiation) are not always representative of an entire reach (Leach and Moore, 2010a; Rich, 1990; Ringold *et al.*, 2003). Methods that take into account measurements of radiation attenuation at multiple

points in space and time are better able to characterize average energy attenuation across a spatially and temporally changing riparian canopy, which is why multiple studies have used hemispherical photography to characterize exposure of streams to solar radiation (Leach and Moore, 2010a; Moore *et al.*, 2005b; Ringold *et al.*, 2003).

Unsurprisingly, and consistent with numerous previous studies, shortwave radiation was shown to be the primary energy input to both reaches (Webb *et al.*, 2008). Average net shortwave radiation was 150% greater in magnitude than the next largest flux (streambed heat) for the E-W reach and 42.0% greater than the next largest flux (streambed heat) for the N-S reach, and maximum values of net shortwave radiation were one order of magnitude greater than other energy fluxes. On average, net shortwave radiation accounted for 74.6% of positive energy fluxes within the E-W reach and 58.6% within the N-S reach. Net longwave radiation accounted for 47.8% of negative energy fluxes within the E-W reach and 47.2% within the N-S reach, with the rest primarily accounted for by latent heat loss (43.5% in the E-W reach and 43.3% in the N-S reach). The sum of energy fluxes (residual term) was on average positive (20.2 W/m^2 for E-W reach and 45.5 W/m^2 for N-S reach). Use of hemispherical photographs to model radiation through each reach was selected as the primary alternative, based on previous published studies (Moore *et al.*, 2005a; Leach and Moore, 2010a), to direct above stream measurement of net radiation, which would have been difficult given the flashy discharge (estimated discharge increased more than 10 m^3/s in less than one hour for large precipitation events) in this system.

Large differences in climate were observed between the study sites and above canopy reference. Average air temperature at the E-W climate station was 9.4% (˚C) lower than the above canopy reference, and the N-S climate station was 8.6% (˚C) lower than the reference. Modeled net shortwave radiation incident on the E-W stream reach was 75.1% lower than that measured at the reference site, while N-S reach incident radiation was 71.1% lower. Differences are primarily attributed to the presence of the riparian canopy. Topographic shading may also be important. Future studies and/or improvements to the radiation model used in this study might investigate the relationship between topographic shading and stream orientation. Streams flowing perpendicular to a topographic feature might receive spatially variable radiation as part of the stream remains shaded while another part remains exposed to solar radiation as the sun rises or sets. Radiation measurements at multiple points along the reach would be necessary to quantify this effect.

Highest stream temperatures occurred in July and August for both reaches. Mean stream temperature was 23.5 ˚C in July and 23.6 ˚C in August for the E-W reach, and 24.4 ˚C in July and 24.0 ˚C in August for the N-S reach. The observation that highest stream temperature was associated with times of lowest discharge was consistent with previous work (Webb *et al.*, 2003). Future investigations into ameliorating stream heating in this area might focus on management practices to maintain pre-development discharge levels in headwater systems. Obstructions to flow, such as the dam upstream from the study sites in this work, may lower downstream discharge, particularly baseflow, resulting in increased stream temeprature regime.

Currently, the minimum recommended buffer width within the state of Missouri is 50 ft, which applies for slopes from 0-20% and does not specify stream order. Comparison of climate measurements collected with iButtons along transects extending from the stream showed that, for Brushy Creek, the stream examined in this study, there is an influence on microclimate extending to on average 25-40m from the stream edge at four transect locations. Similar work found stream influenced microclimate extended from between 31-62 meters from the stream's center into the adjacent riparian zone (Brosofske *et al.*, 1997). Brosofske (1997) concluded that the stream influenced microclimate needs to be protected from outside climate effects to avoid stream heating. The width of riparian zone where climate is influenced by the stream should be added to the distance which outside climate extends into forest interior from edges to calculate necessary buffer width to protect stream thermal regime (Brosofske *et al.*, 1997). Unfortunately, there are no data currently available detailing penetration of outside climate variables and edge effects for Ozark forests; however, research in other regions has shown outside climate generally extends into forest interior anywhere from 15m-60m. Taking conservative values of a 25m zone of microclimate extending from the stream and 15m for edge effects, this study suggests riparian buffers should be a minimum of 40m (131ft) wide to sustain Ozark border climate and vegetation given the stand density from this study (see below). Note this value is more than twice the current recommended buffer width.

Current management practices for riparian zones within the state of Missouri also allow for thinning of the riparian zone. Recommendations include a minimum of one-

third, and preferably one-half to three-quarters of "typical size trees" be left unharvested. Recommended basal area is 40 ft^2/acre. Basal area was not measured in this study, but values of 95.7 ft^2/acre are reported for the reference site, which has a similar leaf area index (peak measured value=3.75). A recent dissertation also quantified a basal area of 125.5 ft^2/acre for an average of six study sites in both riparian zones and uplands within the Baskett Research Area (Reed, 2010). Removal of two-thirds of trees within the riparian zones studied in this research would result in a basal area of approximately 40 ft^2/acre based on these nearby basal area measurements, and an average above stream LAI of approximately 0.99 for June, 1.03 for July, and 0.94 for August, assuming leaves are equally distributed between those trees that are removed and those left unharvested. This reduction in leaf area index corresponds to an increase in shortwave transmissivity through the canopy from 6.5% to 41.2% for June, 6.0% to 39.6% for July, and 7.8% to 42.9% in August (based on equation 2.4). Keeping other energy fluxes the same, an increase in radiative transmissivity for August to 42.9% would increase net shortwave radiation at the stream surface from an average of 40.8 W/m^2 (average of values from hemispherical photo models for August) to 109.2 W/m^2. The exact water temperature increase this change would correspond to depends on the discharge and stream surface area through each reach and is thus dependent on individual streams. However, based on the findings of this work, stream water temperature could be dramatically affected (i.e. warmed) by thinning to 40 ft^2/acre. This observation holds important implications for current forest biomass BMP's in the state of Missouri, and riparian forest harvest practices in other deciduous forests.

It should be noted that during July and August, stream temperatures were already very high at the BREA compared to other U.S. streams. Bogan *et al.* (2006) reported average upper observed bounds for stream temperature in the U.S. of 27.6 ˚C. Mean daily stream temperature was 23.5 ˚C in July and 23.6 ˚C in August for the E-W reach, and 24.4 ˚C in July and 24.0 ˚C in August for the N-S reach. Given these water temperatures and other findings of this study, thinning is not recommended within forest riparian zones if forest managers are primarily concerned with stream temperature. This work indicates that any thinning could conceivably result in stream water heating. Stream temperature is already very warm given the low volume of discharge characteristic of the study stream system. Streams with pre-development levels of discharge might be able to better support thinning of the riparian zone, and management of streams and riparian zones to this end would be a potential area for further research.

LITERATURE CITED

Allan JD, Castillo MM. 2007. *Stream ecology: structure and function of running waters*. Springer Verlag: Dordrecht, Netherlands.

Amaranthus M, Jubas H, Arthur D. 1989. Stream Shading, Summer Streamflow and Maximum Water Temperature Following Intense Wildfire In Headwater Streams In *Proceedings of the Symposium On Fire and Watershed Management, USDA Forest Service General Technical Report,* N. B ed. Pacific Southwest Forest and Range Experiment Station: Berkley, California;75-78.

Anderson P, Larson D, Chan S. 2007.Riparian buffer and density management influences on microclimate of young headwater forests of western Oregon. *Forest Science* **53**: 254-269.

Baird K, Maddock T. 2005.Simulating riparian evapotranspiration: a new methodology and application for groundwater models. *Journal of Hydrology* **312**: 176-190.

Belden A, Pallardy S. 2009.Successional trends and apparent Acer saccharum regeneration failure in an oak-hickory forest in central Missouri, USA. *Plant Ecology* **204**: 305-322.

Beschta R. 1997.Riparian shade and stream temperature: an alternative perspective. *Rangelands* **19**: 25-28.

Bogan T, Othmer J, Mohseni O, Stefan H. 2006.Estimating extreme stream temperatures by the standard deviate method. *Journal of Hydrology* **317**: 173-189.

Bourque C, Pomeroy J. 2001.Effects of forest harvesting on summer stream temperatures in New Brunswick, Canada: an inter-catchment, multiple-year comparison. *Hydrology and Earth System Sciences* **5**: 599-614.

Bowen I. 1926.The ratio of heat losses by conduction and by evaporation from any water surface. *Physical Review* **27**: 779-787.

Bravo H, Krajewski W, Holly F. 1993.State space model for river temperature prediction. *Water Resources Research* **29**: 1457-1466.

Breda N. 2003.Ground-based measurements of leaf area index: a review of methods, instruments and current controversies. *Journal of Experimental Botany* **54**: 2403-2417.

Broadmeadow S, Nisbet T. 2004.The effects of riparian forest management on the freshwater environment: a literature review of best management practice. *Hydrology and Earth System Sciences* **8**: 286-305.

Brooks K. 2003. *Hydrology and the Management of Watersheds*. Wiley.

Brosofske K, Chen J, Naiman R, Franklin J. 1997.Harvesting effects on microclimatic gradients from small streams to uplands in western Washington. *Ecological Applications* **7**: 1188-1200.

Brown G. 1969.Predicting temperatures of small streams. *Water Resources Research* **5**: 68-75.

Brown G, Krygier J. 1970.Effects of clear-cutting on stream temperature. *Water Resources Research* **6**: 1133-1139.

Brown L, Hannah D. 2008.Spatial heterogeneity of water temperature across an alpine river basin. *Hydrological Processes* **22**: 954-967.

Bunn S, Davies P, Mosisch T. 1999.Ecosystem measures of river health and their response to riparian and catchment degradation. *Freshwater Biology* **41**: 333-345.

Caissie D. 2006.The thermal regime of rivers: a review. *Freshwater Biology* **51**: 1389-1406.

Campbell GS, Norman JM. 1998. *An Introduction to Environmental Biophysics*. Springer Science+Buisness Media, LLC: New York.

Carter R, Anderson I. 1963.Accuracy of current meter measurements. *J. Hydraul. Div. Am. Sot. Civil Eng* **89**: 105-115.

Chen J, Franklin J. 1997.Growing-season microclimate variability within an old-growth Douglas-fir forest. *Clim Res* **8**: 21-34.

Chen J, Saunders S, Crow T, Naiman R, Brosofske K, Mroz G, Brookshire B, Franklin J. 1999.Microclimate in forest ecosystem and landscape ecology. *BioScience* **49**: 288-297.

Cooter E, Cooter W. 1990.Impacts of greenhouse warming on water temperature and water quality in the southern United States. *Climate Res* **1**: 1-12.

Cozzetto K, McKnight D, Nylen T, Fountain A. 2006.Experimental investigations into processes controlling stream and hyporheic temperatures, Fryxell Basin, Antarctica. *Advances in Water Resources* **29**: 130-153.

Crisp D, Howson G. 1982.Effect of Air Temperature upon Mean Water Temperature in Streams in the North Pennines and English Lake District. *Freshwater biology. Oxford* **12**: 359-367.

Danehy R, Colson C, Parrett K, Duke S. 2005.Patterns and sources of thermal heterogeneity in small mountain streams within a forested setting. *Forest Ecology and Management* **208**: 287-302.

Danehy R, Kirpes B. 2000.Relative humidity gradients across riparian areas in eastern Oregon and Washington forests. *Northwest Science* **74**: 224-233.

Davies-Colley R, Payne G, Van Elswijk M. 2000.Microclimate gradients across a forest edge. *New Zealand Journal of Ecology* **24**: 111-121.

Decagon Devices. 2006. AccuPAR PAR/LAI ceptometer, model LP-80. Operator's manual. Decagon Devices: Pullman, WA.

Dechert T, Woodruff L. 2003. *South Fork Clearwater River Subbasin Assessment and TMDLs*. Idaho Department of Environmental Quality: Lewiston, Idaho.

Devore J. 2000. *Probability and Statistics for Engineering and the Sciences*. Duxbury Pacific Grove: Belmont, CA.

Dignan P, Bren L. 2003.Modelling light penetration edge effects for stream buffer design in mountain ash forest in southeastern Australia. *Forest Ecology and Management* **179**: 95-106.

Dingman S. 1984. *Fluvial hydrology*. WH Freeman and Company, New York.

Dingman S. 2002. Physical Hydrology, 646 pp. Prentice-Hall, Upper Saddle River, NJ.

Dingman SL, Sharma KP. 1997.Statistical development and validation of discharge equations for natural channels. *Journal of Hydrology* **199**: 13-35.

Dong J, Chen J, Brosofske K, Naiman R. 1998.Modelling air temperature gradients across managed small streams in western Washington. *Journal of environmental management* **53**: 309-321.

DuCharme C. 2001. Wetland Hydrology: determination of the hydrology of Missouri riparian wetlands In *Wetland Program Development Grant*. Missouri Department of Natural Resources.

Dunham J, Rosenberger A, Luce C, Rieman B. 2007.Influences of wildfire and channel reorganization on spatial and temporal variation in stream temperature and the distribution of fish and amphibians. *Ecosystems* **10**: 335-346.

Edinger J, Duttweiler D, Geyer J. 1968.The response of water temperatures to meteorological conditions. *Water Resources Research* **4**: 1137-1143.

Erbs D, Klein S, Duffie J. 1982.Estimation of the diffuse radiation fraction for hourly, daily and monthly-average global radiation. *Solar Energy* **28**: 293-302.

Evans E, McGregor G, Petts G. 1998.River energy budgets with special reference to river bed processes. *Hydrological Processes* **12**: 575-595.

Fischer R, Martin C, Ratti J, Guidice J. 2000.Riparian terminology: Confusion and clarification. *EMRRP Technical Note Series, EMRRP-SI-. US Army Engineer Research and Development Center, Vicksburg, MS, in prep*.

Frazer G, Canham C, Lertzman K. 1999. Gap Light Analyzer (GLA), Version 2.0: Imaging software to extract canopy structure and gap light transmission indices from true-colour fisheye photographs, users manual and program documentation. Copyright.

Gower S, Kucharik C, Norman J. 1999.Direct and indirect estimation of leaf area index, f (APAR), and net primary production of terrestrial ecosystems. *Remote Sensing of Environment* **70**: 29-51.

Gregory S, Swanson F, McKee W, Cummins K. 1991.An ecosystem perspective of riparian zones. *BioScience* **41**: 540-551.

Gu L, Meyers T, Pallardy S, Hanson P, Yang B, Heuer M, Hosman K, Liu Q, Riggs J, Sluss D. 2007.Influences of biomass heat and biochemical energy storages on the land surface fluxes and radiative temperature. *Journal of Geophysical Research* **112**: D02107.

Gu L, Meyers T, Pallardy S, Hanson P, Yang B, Heuer M, Hosman K, Riggs J, Sluss D, Wullschleger S. 2006.Direct and indirect effects of atmospheric conditions and soil moisture on surface energy partitioning revealed by a prolonged drought at a temperate forest site. *Journal of Geophysical Research* **11**: D16102.

Hagan J, Whitman A. 2000.Microclimate changes across upland and riparian clearcut forest boundaries in Maine. *Manomet Center for Conservation Studies, Mosaic Science Notes* **4**: 1-6.

Hale S, Edwards C. 2002.Comparison of film and digital hemispherical photography across a wide range of canopy densities. *Agricultural and Forest Meteorology* **112**: 51-56.

Hannah D, Malcolm I, Soulsby C, Youngson A. 2004.Heat exchanges and temperatures within a salmon spawning stream in the Cairngorms, Scotland: seasonal and sub-seasonal dynamics. *River Research and Applications* **20**: 635-652.

Hannah D, Malcolm I, Soulsby C, Youngson A. 2008.A comparison of forest and moorland stream microclimate, heat exchanges and thermal dynamics. *Hydrological Processes* **22**: 919-940.

Heithecker T, Halpern C. 2007.Edge-related gradients in microclimate in forest aggregates following structural retention harvests in western Washington. *Forest Ecology and Management* **248**: 163-173.

Hitt N. 2003.Immediate effects of wildfire on stream temperature. *Journal of Freshwater Ecology* **18**: 171.

Hubbart J, Link T, Campbell C, Cobos D. 2005.Evaluation of a low-cost temperature measurement system for environmental applications. *Hydrological Processes* **19**: 1517-1523.

Ice G. 2001. How direct solar radiation and shade influences temperature in forest streams and relaxation of changes in stream temperature In *National Council for Air and Stream Improvement*.

Ice G, Light J, Reiter M. 2004.Use of natural temperature patterns to identify achievable stream temperature criteria for forest streams. *Western Journal of Applied Forestry* **19**: 252-259.

Jeppesen E, Iversen T. 1987.Two simple models for estimating daily mean water temperatures and diel variations in a Danish low gradient stream. *Oikos* **49**: 149-155.

Johnson F. 1971.Stream temperatures in an alpine area. *Journal of Hydrology* **14**: 322-366.

Johnson S. 2003.Stream temperature: scaling of observations and issues for modelling. *Hydrological Processes* **17**: 497-499.

Johnson S. 2004.Factors influencing stream temperatures in small streams: substrate effects and a shading experiment. *Canadian Journal of Fisheries and Aquatic Sciences* **61**: 913-923.

Johnson S, Jones J. 2000.Stream temperature responses to forest harvest and debris flows in western Cascades, Oregon. *Canadian Journal of Fisheries and Aquatic Sciences* **57**: 30-39.

Lane E, Carlson E, Hanson O. 1949.Low temperature increases sediment transportation in Colorado River. *Civil engineering* **19**: 619-620.

Larson L, Larson P. 2002.Perspectives on Water Flow and the Interpretations of FLIR Images. *Journal of Range Management* **55**: 100-101.

Larson L, Larson S. 1996.Riparian shade and stream temperature: a perspective. *Rangelands* **18**: 149-152.

Law B, Van Tuyl S, Cescatti A, Baldocchi D. 2001.Estimation of leaf area index in open-canopy ponderosa pine forests at different successional stages and management regimes in Oregon. *Agricultural and Forest Meteorology* **108**: 1-14.

Leach J, Moore R. 2008.Stream temperature response to wildfire disturbance: lessons from Fishtrap Creek. *Streamline Watershed Management Bulletin* **12**: 11-16.

Leach J, Moore R. 2010a.Above-stream microclimate and stream surface energy exchanges in a wildfire-disturbed riparian zone. *Hydrological Processes* **24**: 2369-2381.

Leach J, Moore R. 2010b.Stream temperature dynamics in two hydrogeomorphically distinct reaches. *Hydrological Processes* **25**: 679-690.

LeBosquet Jr M, Tsivoglou E. 1950.Simplified dissolved oxygen computations. *Sewage and Industrial Wastes* **22**: 1054-1061.

Ledwith T. 1996. The effects of buffer strip width on air temperature and relative humidity in a stream riparian zone. The Watershed Management Council.

Lerch R, Wicks C, Moss P, USDA A. 2005.Hydrologic characterization of two karst recharge areas in Boone County, Missouri. *Journal of Cave and Karst Studies* **67**: 158-173.

Macdonald J, MacIsaac E, Herunter H. 2003.The effect of variable-retention riparian buffer zones on water temperatures in small headwater streams in sub-boreal forest ecosystems of British Columbia. *Canadian Journal of Forest Research* **33**: 1371-1382.

Mackey A, Berrie A. 1991.The prediction of water temperatures in chalk streams from air temperatures. *Hydrobiologia* **210**: 183-189.

Malcolm I, Hannah D, Donaghy M, Soulsby C, Youngson A. 2004.The influence of riparian woodland on the spatial and temporal variability of stream water temperatures in an upland salmon stream. *Hydrology and Earth System Sciences* **8**: 449-459.

Malcolm I, Soulsby C, Hannah D, Bacon P, Youngson A, Tetzlaff D. 2008.The influence of riparian woodland on stream temperatures: implications for the performance of juvenile salmonids. *Hydrological Processes* **22**: 968-979.

MCAF. 2005.Establishing and Managing Riparian Forest Buffers. *Agroforestry in Action* **1009**.

MCC. 2006. *Missouri Watershed Protection Practice: 2006 Management Guidelines for Maintaining Forested Watersheds to Protect Streams*. Missouri Department of Conservation.

McMillan H, Freer J, Pappenberger F, Krueger T, Clark M. 2010.Impacts of uncertain river flow data on rainfall runoff model calibration and discharge predictions. *Hydrological Processes* **24**: 1270-1284.

Mohseni O, Erickson T, Stefan H. 1999.Sensitivity of stream temperatures in the United States to air temperatures projected under a global warming scenario. *Water Resources Research* **35**: 3723-3733.

Mohseni O, Stefan H, Eaton J. 2003.Global warming and potential changes in fish habitat in US streams. *Climatic change* **59**: 389-409.

Mohseni O, Stefan H, Erickson T. 1998.A nonlinear regression model for weekly stream temperatures. *Water Resources Research* **34**: 2685-2692.

Moore J, Miner J. 1997.Stream temperatures: some basic considerations. *Oregon State University Extension Service, Corvallis, Oregon*.

Moore R, Spittlehouse D, Story A. 2005a.Riparian microclimate and stream temperature response to forest harvesting: a review. *Journal of the American Water Resources Association* **41**: 813-834.

Moore R, Sutherland P, Gomi T, Dhakal A. 2005b.Thermal regime of a headwater stream within a clear-cut, coastal British Columbia, Canada. *Hydrological Processes* **19**: 2591-2608.

MoRAP. 2009. Missouri Resource Assesment Partnership Project: Land Cover.

Naiman R, Decamps H. 1997.The ecology of interfaces: riparian zones. *Annual Review of Ecology and Systematics* **28**: 621-658.

Neumann D, Rajagopalan B, Zagona E. 2003.Regression model for daily maximum stream temperature. *Journal of Environmental Engineering* **129**: 667-674.

O'Driscoll M, DeWalle D. 2006.Stream–air temperature relations to classify stream–ground water interactions in a karst setting, central Pennsylvania, USA. *Journal of Hydrology* **329**: 140-153.

Pallardy S, Nigh T, Garrett H. 1988.Changes in forest composition in central Missouri: 1968-1982. *American Midland Naturalist* **120**: 380-390.

Petersen-Øverleir A, Reitan T. 2005.Objective segmentation in compound rating curves. *Journal of Hydrology* **311**: 188-201.

Pluhowski E. 1972.Clear-cutting and its effect on the water temperature of a small stream in northern Virginia. *U.S. Geological Survey Professional Paper 800-C*: C257-C262.

Pluttowski E. 1970.Urbanization and its effects on the temperature of the streams on Long Island, New York. *Washington, DC; US Government Printing Office, 1970, 110 p. Ilus, tablas (Geological Survey professional paper, 627-D).*

Polehn R, Kinsel W. 2000.Transient temperature solution for a river with distributed inflows. *Water Resources Research* **36**: 787-791.

Poole G, Berman C. 2001.An Ecological Perspective on In-Stream Temperature: Natural Heat Dynamics and Mechanisms of Human-CausedThermal Degradation. *Environmental Management* **27**: 787-802.

Rambo T, North M. 2009.Canopy microclimate response to pattern and density of thinning in a Sierra Nevada forest. *Forest Ecology and Management* **257**: 435-442.

Reed SE. 2010. Ambrosia Beetle Habitat Use, Host Use, and Influence on Early Wood Colonizing Microbes in an Oak-Hickory Forest In *Forestry*. University of Missouri: Columbia, Missouri.

Rich P. 1990.Characterizing plant canopies with hemispherical photographs. *Remote sensing reviews* **5**: 13-29.

Richards C, Johnson L, Host G. 1996.Landscape-scale influences on stream habitats and biota. *Canadian Journal of Fisheries and Aquatic Sciences* **53**: 295-311.

Richardson J, Danehy R. 2007.A synthesis of the ecology of headwater streams and their riparian zones in temperate forests. *Forest Science* **53**: 131-147.

Ringold P, Sickle J, Rasar K, Schacher J. 2003.Use of Hemispheric Imagery for Estimating Stream Solar Exposure. *JAWRA Journal of the American Water Resources Association* **39**: 1373-1384.

Rios S, Bailey R. 2006.Relationship between riparian vegetation and stream benthic communities at three spatial scales. *Hydrobiologia* **553**: 153-160.

Schultz R, Collettil J, Isenhart T, Simpkins W, Mize C, Thompson M. 1995.Design and placement of a multi-species riparian buffer strip system. *Agroforestry Systems* **29**: 201-226.

Shiklomanov AI, Yakovleva TI, Lammers RB, Karasev IP, Vörösmarty C. 2006.Cold region river discharge uncertainty--estimates from large Russian rivers. *Journal of Hydrology* **326**: 231-256.

Smith K. 1981.The prediction of river water temperatures. *Hydrological Sciences Bulletin* **26**: 19-32.

Sridhar V, Sansone A, LaMarche J, Dubin T, Lettenmaier D. 2004.Prediction of stream temperature in forested watersheds. *Journal of the American Water Resources Association* **40**: 197-213.

Stenberg P, Linder S, Smolander H, Flower-Ellis J. 1994.Performance of the LAI-2000 plant canopy analyzer in estimating leaf area index of some Scots pine stands. *Tree physiology* **14**: 981-995.

Story A, Moore R, Macdonald J. 2003.Stream temperatures in two shaded reaches below cutblocks and logging roads: downstream cooling linked to subsurface hydrology. *Canadian Journal of Forest Research* **33**: 1383-1396.

Strahler A. 1952.Hypsometric (area-altitude) analysis of erosional topography. *Geological Society of America Bulletin* **63**: 1117-1142.

Sugimoto S, Nakamura F, Ito A. 1997.Heat budget and statistical analysis of the relationship between stream temperature and riparian forest in the Toikanbetsu River Basin, northern Japan. *Journal of Forest Research* **2**: 103-107.

Theurer F, Voos K, Miller W. 1984.Instream water temperature model. Instream flow information paper 16. *US Fish and Wildlife Service. FWS/OBS-84/15*.

Thom R, Wilson J. 1980.The natural divisions of Missouri. *Transactions of the Missouri Academy of Science* **14**: 9-23.

Thompson J. 2005.Keeping it cool: unraveling the influences on stream temperature. *Science Findings* **73**: 1-5.

US ACOE. 1987. Corps of Engineers Wetlands Delineation Manual. Technical Report Y-87-1. Department of the Army, Washington DC, USA.

Wallace JB, Eggert SL. 2009. Benthic Invertebrate Fauna, Small Streams. In *Encyclopedia of Inland Waters*, Likens GE (ed). Elsevier Ltd.: Oxford, New York.

Webb B, Clack P, Walling D. 2003.Water–air temperature relationships in a Devon river system and the role of flow. *Hydrological Processes* **17**: 3069-3084.

Webb B, Hannah D, Moore R, Brown L, Nobilis F. 2008.Recent advances in stream and river temperature research. *Hydrological Processes* **22**: 902-918.

Webb B, Nobilis F. 1997.Long-term perspective on the nature of the air-water temperature relationship: a case study. *Hydrological Processes* **11**: 137-147.

Webb B, Walsh A. 2004.Changing UK river temperatures and their impact on fish populations. *Hydrology: Science & Practice for the 21st Century, II*: 177-191.

Webb B, Zhang Y. 1997.Spatial and seasonal variability in the components of the river heat budget. *Hydrological Processes* **11**: 79-101.

Webb B, Zhang Y. 1999.Water temperatures and heat budgets in Dorset chalk water courses. *Hydrological Processes* **13**: 309-321.

Whitledge G, Rabeni C, Annis G, Sowa S. 2006.Riparian shading and groundwater enhance growth potential for smallmouth bass in Ozark streams. *Ecological Applications* **16**: 1461-1473.

Young F, Radatz C, Marshall C. 2001. Soil survey for Boone County, Missouri In *NRCS, Washington, DC*.

Yu B. 2000.A systematic over-estimation of flows. *Journal of Hydrology* **233**: 258-262.

Zhang Y, Chen J, Miller J. 2005.Determining digital hemispherical photograph exposure for leaf area index estimation. *Agricultural and Forest Meteorology* **133**: 166-181.

APPENDIX A

ASSESMENT OF IBUTTON RADIATION SHIELD PERFORMANCE

(This work was conducted by Jason Hubbart, publication in prep.)

Seven iButtons were placed in a greenhouse to assess and compare the efficacy of different solar radiation shields relative to an unshielded iButton sensor. The radiation shield experiment was designed to subject the sensors to a worst-case scenario (e.g. with negligible ventilation). Three Gill model 41002, six-plate radiation shields (R. M. Young Co.), one Spectrum (Spectrum Technologies), and two home built alternative radiation shields were used for the radiation shield experiment. One of the Gill shields was aspirated with a 12v (1.6W), 5 cm^2, computer processor cooling fan as a reference shield. The cost of each of these shields is approximately 160.00, 45.00, and 4.00 USD for the Gill, Spectrum, and home-built shield, respectively.

All seven data loggers and respective shields (one without a radiation shield) were installed in a greenhouse for a 24-hour period under cloudless conditions to assess thermal response variation between differing types of shields. All windows and doors were closed and no fans operated in the greenhouse during the experiment. The radiation shields were oriented approximately two meters above the ground on Poly Vinyl Chloride (PVC) scaffolding created for this experiment. The shields were held in a nearly concentric ring around the center of the scaffold with a distance of at least 40 cm from

each other. In this manner, all shields were occupying similar space, without altering the microclimate of a neighboring shield. Data acquired using the two un-aspirated Gill shields and the two home-built shields were each averaged for subsequent analysis.

Descriptive statistics for the solar radiation data (Table 1) revealed that mean temperatures recorded by the Thermochron iButton shielded by the aspirated Gill radiation shield were lower and less variable than all other radiation shields, with a mean temperature of 18.26 ºC collected at 1-minute resolution. The unshielded iButton recorded the highest mean daily temperature of 23.42 ºC during the same time period. The un-aspirated Gill, Spectrum, and Alternative (home-built) radiation shields exhibited mean daily temperatures of 20.46 ºC, 20.59 ºC, and 21.10 ºC respectively during the same time period.

Table A 1: Summary table of descriptive statistics for solar radiation data collected by Thermochron iButtons held in various radiation shields (one iButton unshielded), where the control is the aspirated Gill shield. *Represents results of two shields with corresponding data averaged.

Shield Type	**N**	**Mean Temp (˚C)**	**Min Temp (˚C)**	**Max Temp (˚C)**
Gill Aspirated	1440	18.26	7	35
Gill Un-Aspirated	1440	20.46	8	40.25
Spectrum	1440	20.59	8	40.5
Alternate*	1440	21.10	8	41.5
No Shield	1440	23.42	7.5	51.5

The diurnal temperature ranges recorded by the temperature data loggers were 28 ºC, 32.25 ºC, 32.5 ºC, 33.5 ºC, and 44 ºC, for the aspirated Gill, un-aspirated Gill, Spectrum, alternative, and unshielded loggers respectively (Figure 1). The maximum

temperature difference observed was 16.5 ºC between the aspirated Gill shield and the unshielded temperature logger. Other temperature differences between shields at the time of maximum temperature ranged from 5.25 ºC to 6.5 ºC, relative to the 35 ºC maximum temperature recorded by the sensor in the aspirated Gill shield.

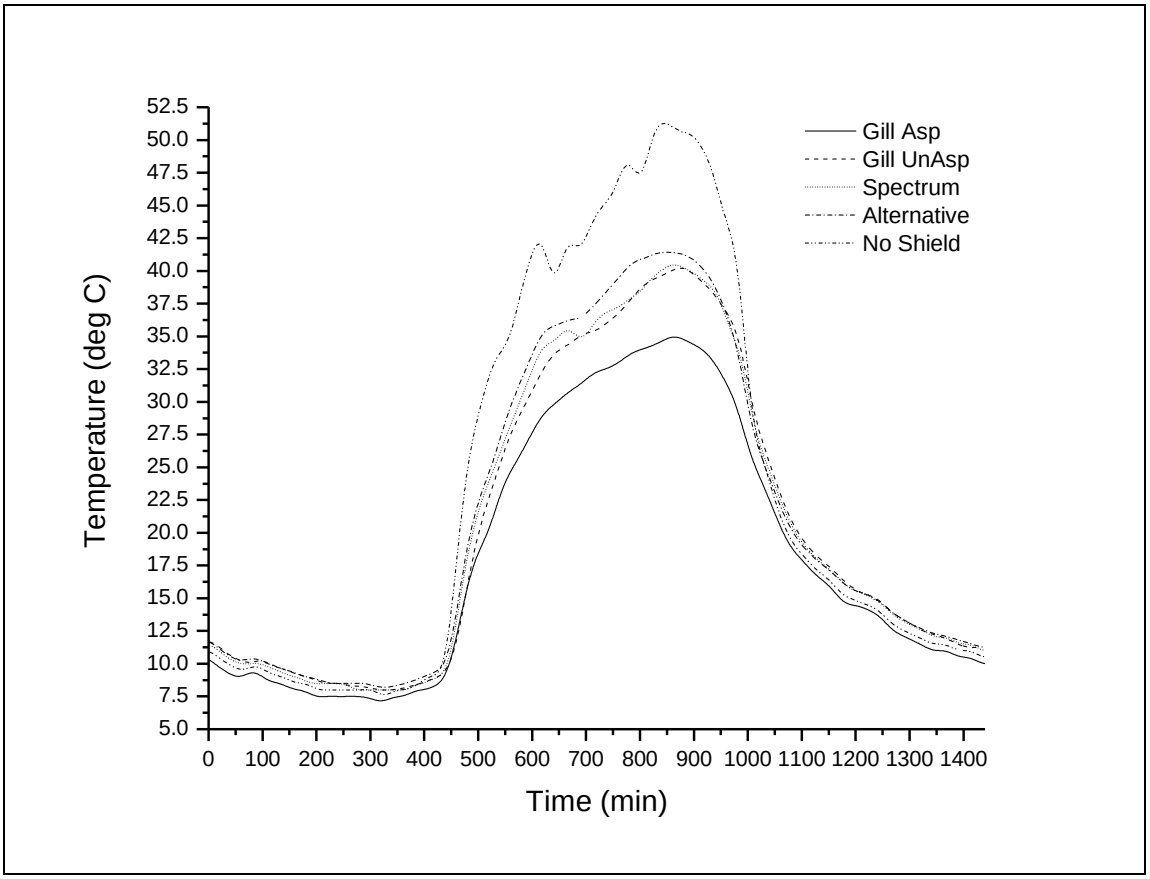

Figure A 1: Temperature responses of Thermochron iButtons placed in a greenhouse setting employing various solar radiation shields (one without shielding). Graphs presented with 25 point smoothing.

The solar radiation shield experiment showed a relatively close relationship between the control (aspirated Gill shield) and the other shields employed, indicating that the type of radiation shield may not be as important as whether or not it is aspirated.

APPENDIX B

HEMISPHERICAL PHOTO ANALYSIS CODE

```
% streamgapfractions.m An m-file to calculate diffuse sky view factors
as well as gap fraction for beam radiation as functions of time.
% Values of diffuse sky view factors and gap fraction for 5 degree
intervals of both zenith and azimuth angles are defined on given
measurement days.
% For each time step, diffuse sky view factor is linearly interpolated
between nearest measurement dates. Solar position (altitude and zenith
angle)
% determine which gap fraction cell should be used for that time step.
Value for this gap fraction cell is then linearly interpolated between
two nearest
% known timesteps.
% Requires input arrays:

%initialize arrays
ewgapdiffuse=zeros(35040,1);
nsgapdiffuse=zeros(35040,1);
ewgapbeam=zeros(35040,1);
nsgapbeam=zeros(35040,1);


%convert gap fraction vectors to matrices
for jj=1:1296
      x=altitude_index(jj);
      y=azimuth_index(jj);

      AE1m(x,y)=AE1(jj);
      AE2m(x,y)=AE2(jj);
      AE3m(x,y)=AE3(jj);
      AE4m(x,y)=AE4(jj);
      AE5m(x,y)=AE5(jj);
      BE1m(x,y)=BE1(jj);
      BE2m(x,y)=BE2(jj);
      BE3m(x,y)=BE3(jj);
      BE4m(x,y)=BE4(jj);
      BE5m(x,y)=BE5(jj);
      CE1m(x,y)=CE1(jj);
      CE2m(x,y)=CE2(jj);
      CE3m(x,y)=CE3(jj);
      CE4m(x,y)=CE4(jj);
      CE5m(x,y)=CE5(jj);
      DE1m(x,y)=DE1(jj);
      DE2m(x,y)=DE2(jj);
```

```
DE3m(x,y)=DE3(jj);
DE4m(x,y)=DE4(jj);
DE5m(x,y)=DE5(jj);
EE1m(x,y)=EE1(jj);
EE2m(x,y)=EE2(jj);
EE3m(x,y)=EE3(jj);
EE4m(x,y)=EE4(jj);
EE5m(x,y)=EE5(jj);
FE1m(x,y)=FE1(jj);
FE2m(x,y)=FE2(jj);
FE3m(x,y)=FE3(jj);
FE4m(x,y)=FE4(jj);
FE5m(x,y)=FE5(jj);
GE1m(x,y)=GE1(jj);
GE2m(x,y)=GE2(jj);
GE3m(x,y)=GE3(jj);
GE4m(x,y)=GE4(jj);
GE5m(x,y)=GE5(jj);
HE1m(x,y)=HE1(jj);
HE2m(x,y)=HE2(jj);
HE3m(x,y)=HE3(jj);
HE4m(x,y)=HE4(jj);
HE5m(x,y)=HE5(jj);

AN1m(x,y)=AN1(jj);
AN2m(x,y)=AN2(jj);
AN3m(x,y)=AN3(jj);
AN4m(x,y)=AN4(jj);
AN5m(x,y)=AN5(jj);
BN1m(x,y)=BN1(jj);
BN2m(x,y)=BN2(jj);
BN3m(x,y)=BN3(jj);
BN4m(x,y)=BN4(jj);
BN5m(x,y)=BN5(jj);
CN1m(x,y)=CN1(jj);
CN2m(x,y)=CN2(jj);
CN3m(x,y)=CN3(jj);
CN4m(x,y)=CN4(jj);
CN5m(x,y)=CN5(jj);
DN1m(x,y)=DN1(jj);
DN2m(x,y)=DN2(jj);
DN3m(x,y)=DN3(jj);
DN4m(x,y)=DN4(jj);
DN5m(x,y)=DN5(jj);
EN1m(x,y)=EN1(jj);
EN2m(x,y)=EN2(jj);
EN3m(x,y)=EN3(jj);
EN4m(x,y)=EN4(jj);
EN5m(x,y)=EN5(jj);
FN1m(x,y)=FN1(jj);
FN2m(x,y)=FN2(jj);
FN3m(x,y)=FN3(jj);
FN4m(x,y)=FN4(jj);
```

```
      FN5m(x,y)=FN5(jj);
      GN1m(x,y)=GN1(jj);
      GN2m(x,y)=GN2(jj);
      GN3m(x,y)=GN3(jj);
      GN4m(x,y)=GN4(jj);
      GN5m(x,y)=GN5(jj);
      HN1m(x,y)=HN1(jj);
      HN2m(x,y)=HN2(jj);
      HN3m(x,y)=HN3(jj);
      HN4m(x,y)=HN4(jj);
      HN5m(x,y)=HN5(jj);

      jj=jj+1;

end

%specify  diffuse gap fractions for known timesteps

%Oct. 19
ewgapdiffuse(1776)=(E1diffusesky(7)+E2diffusesky(7)+E3diffusesky(7)+E4d
iffusesky(7)+E5diffusesky(7))/5;
nsgapdiffuse(1776)=(N1diffusesky(7)+N2diffusesky(7)+N3diffusesky(7)+N4d
iffusesky(7)+N5diffusesky(7))/5;
%Nov. 24
ewgapdiffuse(5232)=(E1diffusesky(8)+E2diffusesky(8)+E3diffusesky(8)+E4d
iffusesky(8)+E5diffusesky(8))/5;
nsgapdiffuse(5232)=(N1diffusesky(8)+N2diffusesky(8)+N3diffusesky(8)+N4d
iffusesky(8)+N5diffusesky(8))/5;
%April 1 (estimated start of foliation, period between Nov. 15
measurement and here will be kept constant)
ewgapdiffuse(17520)=(E1diffusesky(8)+E2diffusesky(8)+E3diffusesky(8)+E4
diffusesky(8)+E5diffusesky(8))/5;
nsgapdiffuse(17520)=(N1diffusesky(8)+N2diffusesky(8)+N3diffusesky(8)+N4
diffusesky(8)+N5diffusesky(8))/5;
%April 15
ewgapdiffuse(18864)=(E1diffusesky(1)+E2diffusesky(1)+E3diffusesky(1)+E4
diffusesky(1)+E5diffusesky(1))/5;
nsgapdiffuse(18864)=(N1diffusesky(1)+N2diffusesky(1)+N3diffusesky(1)+N4
diffusesky(1)+N5diffusesky(1))/5;
%April 27
ewgapdiffuse(20016)=(E1diffusesky(2)+E2diffusesky(2)+E3diffusesky(2)+E4
diffusesky(2)+E5diffusesky(2))/5;
nsgapdiffuse(20016)=(N1diffusesky(2)+N2diffusesky(2)+N3diffusesky(2)+N4
diffusesky(2)+N5diffusesky(2))/5;
%June 5
ewgapdiffuse(23760)=(E1diffusesky(3)+E2diffusesky(3)+E3diffusesky(3)+E4
diffusesky(3)+E5diffusesky(3))/5;
nsgapdiffuse(23760)=(N1diffusesky(3)+N2diffusesky(3)+N3diffusesky(3)+N4
diffusesky(3)+N5diffusesky(3))/5;
%July 7
ewgapdiffuse(26832)=(E1diffusesky(4)+E2diffusesky(4)+E3diffusesky(4)+E4
diffusesky(4)+E5diffusesky(4))/5;
```

```
nsgapdiffuse(26832)=(N1diffusesky(4)+N2diffusesky(4)+N3diffusesky(4)+N4
diffusesky(4)+N5diffusesky(4))/5;
%August 8
ewgapdiffuse(29904)=(E1diffusesky(5)+E2diffusesky(5)+E3diffusesky(5)+E4
diffusesky(5)+E5diffusesky(5))/5;
nsgapdiffuse(29904)=(N1diffusesky(5)+N2diffusesky(5)+N3diffusesky(5)+N4
diffusesky(5)+N5diffusesky(5))/5;
%Sept 10
ewgapdiffuse(33072)=(E1diffusesky(6)+E2diffusesky(6)+E3diffusesky(6)+E4
diffusesky(6)+E5diffusesky(6))/5;
nsgapdiffuse(33072)=(N1diffusesky(6)+N2diffusesky(6)+N3diffusesky(6)+N4
diffusesky(6)+N5diffusesky(6))/5;

% compute beam radiation gap fraction for known time steps
x=realaltitude(1776);
y=realazimuth(1776);
ewgapbeam(1776)=(GE1m(x,y)+GE2m(x,y)+GE3m(x,y)+GE4m(x,y)+GE5m(x,y))/5;
nsgapbeam(1776)=(GN1m(x,y)+GN2m(x,y)+GN3m(x,y)+GN4m(x,y)+GN5m(x,y))/5;

x=realaltitude(5232);
y=realazimuth(5232);
ewgapbeam(5232)=(HE1m(x,y)+HE2m(x,y)+HE3m(x,y)+HE4m(x,y)+HE5m(x,y))/5;
nsgapbeam(5232)=(HN1m(x,y)+HN2m(x,y)+HN3m(x,y)+HN4m(x,y)+HN5m(x,y))/5;

x=realaltitude(17520);
y=realazimuth(17520);
ewgapbeam(17520)=(HE1m(x,y)+HE2m(x,y)+HE3m(x,y)+HE4m(x,y)+HE5m(x,y))/5;
nsgapbeam(17520)=(HN1m(x,y)+HN2m(x,y)+HN3m(x,y)+HN4m(x,y)+HN5m(x,y))/5;

x=realaltitude(18864);
y=realazimuth(18864);
ewgapbeam(18864)=(AE1m(x,y)+AE2m(x,y)+AE3m(x,y)+AE4m(x,y)+AE5m(x,y))/5;
nsgapbeam(18864)=(AN1m(x,y)+AN2m(x,y)+AN3m(x,y)+AN4m(x,y)+AN5m(x,y))/5;

x=realaltitude(20016);
y=realazimuth(20016);
ewgapbeam(20016)=(BE1m(x,y)+BE2m(x,y)+BE3m(x,y)+BE4m(x,y)+BE5m(x,y))/5;
nsgapbeam(20016)=(BN1m(x,y)+BN2m(x,y)+BN3m(x,y)+BN4m(x,y)+BN5m(x,y))/5;

x=realaltitude(23760);
y=realazimuth(23760);
ewgapbeam(23760)=(CE1m(x,y)+CE2m(x,y)+CE3m(x,y)+CE4m(x,y)+CE5m(x,y))/5;
nsgapbeam(23760)=(CN1m(x,y)+CN2m(x,y)+CN3m(x,y)+CN4m(x,y)+CN5m(x,y))/5;

x=realaltitude(26832);
y=realazimuth(26832);
ewgapbeam(26832)=(DE1m(x,y)+DE2m(x,y)+DE3m(x,y)+DE4m(x,y)+DE5m(x,y))/5;
nsgapbeam(26832)=(DN1m(x,y)+DN2m(x,y)+DN3m(x,y)+DN4m(x,y)+DN5m(x,y))/5;

x=realaltitude(29904);
y=realazimuth(29904);
ewgapbeam(29904)=(EE1m(x,y)+EE2m(x,y)+EE3m(x,y)+EE4m(x,y)+EE5m(x,y))/5;
nsgapbeam(29904)=(EN1m(x,y)+EN2m(x,y)+EN3m(x,y)+EN4m(x,y)+EN5m(x,y))/5;
```

```
x=realaltitude(33072);
y=realazimuth(33072);
ewgapbeam(33072)=(FE1m(x,y)+FE2m(x,y)+FE3m(x,y)+FE4m(x,y)+FE5m(x,y))/5;
nsgapbeam(33072)=(FN1m(x,y)+FN2m(x,y)+FN3m(x,y)+FN4m(x,y)+FN5m(x,y))/5;


% interpolate end points for time series; record 9 refers to start and
end of time series. Assumes that value for diffuse fraction does
% not change significantly over one time step (first and last time step
use identical values even though technically separated by 15 minutes).

E1diffusesky(9)=(35041-33072)*(E1diffusesky(7)-E1diffusesky(6))/(36816-
33072)+E1diffusesky(6);
E2diffusesky(9)=(35041-33072)*(E2diffusesky(7)-E2diffusesky(6))/(36816-
33072)+E2diffusesky(6);
E3diffusesky(9)=(35041-33072)*(E3diffusesky(7)-E3diffusesky(6))/(36816-
33072)+E3diffusesky(6);
E4diffusesky(9)=(35041-33072)*(E4diffusesky(7)-E4diffusesky(6))/(36816-
33072)+E4diffusesky(6);
E5diffusesky(9)=(35041-33072)*(E5diffusesky(7)-E5diffusesky(6))/(36816-
33072)+E5diffusesky(6);

N1diffusesky(9)=(35041-33072)*(N1diffusesky(7)-N1diffusesky(6))/(36816-
33072)+N1diffusesky(6);
N2diffusesky(9)=(35041-33072)*(N2diffusesky(7)-N2diffusesky(6))/(36816-
33072)+N2diffusesky(6);
N3diffusesky(9)=(35041-33072)*(N3diffusesky(7)-N3diffusesky(6))/(36816-
33072)+N3diffusesky(6);
N4diffusesky(9)=(35041-33072)*(N4diffusesky(7)-N4diffusesky(6))/(36816-
33072)+N4diffusesky(6);
N5diffusesky(9)=(35041-33072)*(N5diffusesky(7)-N5diffusesky(6))/(36816-
33072)+N5diffusesky(6);

ewgapdiffuse(1)=(E1diffusesky(9)+E2diffusesky(9)+E3diffusesky(9)+E4diff
usesky(9)+E5diffusesky(9))/5;
ewgapdiffuse(35040)=(E1diffusesky(9)+E2diffusesky(9)+E3diffusesky(9)+E4
diffusesky(9)+E5diffusesky(9))/5;
nsgapdiffuse(1)=(N1diffusesky(9)+N2diffusesky(9)+N3diffusesky(9)+N4diff
usesky(9)+N5diffusesky(9))/5;
nsgapdiffuse(35040)=(N1diffusesky(9)+N2diffusesky(9)+N3diffusesky(9)+N4
diffusesky(9)+N5diffusesky(9))/5;

for jj=1:1296
      x=altitude_index(jj);
      y=azimuth_index(jj);

      XE1m(x,y)=(35041-33072)*(GE1m(x,y)-FE1m(x,y))/(36816-
33072)+FE1m(x,y);
      XE2m(x,y)=(35041-33072)*(GE2m(x,y)-FE2m(x,y))/(36816-
33072)+FE2m(x,y);
      XE3m(x,y)=(35041-33072)*(GE3m(x,y)-FE3m(x,y))/(36816-
33072)+FE3m(x,y);
```

```
      XE4m(x,y)=(35041-33072)*(GE4m(x,y)-FE4m(x,y))/(36816-
33072)+FE4m(x,y);
      XE5m(x,y)=(35041-33072)*(GE5m(x,y)-FE5m(x,y))/(36816-
33072)+FE5m(x,y);
      XN1m(x,y)=(35041-33072)*(GN1m(x,y)-FN1m(x,y))/(36816-
33072)+FN1m(x,y);
      XN2m(x,y)=(35041-33072)*(GN2m(x,y)-FN2m(x,y))/(36816-
33072)+FN2m(x,y);
      XN3m(x,y)=(35041-33072)*(GN3m(x,y)-FN3m(x,y))/(36816-
33072)+FN3m(x,y);
      XN4m(x,y)=(35041-33072)*(GN4m(x,y)-FN4m(x,y))/(36816-
33072)+FN4m(x,y);
      XN5m(x,y)=(35041-33072)*(GN5m(x,y)-FN5m(x,y))/(36816-
33072)+FN5m(x,y);

jj=jj+1

end


x=realaltitude(1);
y=realazimuth(1);
ewgapbeam(1)=(XE1m(x,y)+XE2m(x,y)+XE3m(x,y)+XE4m(x,y)+XE5m(x,y))/5;
nsgapbeam(1)=(XN1m(x,y)+XN2m(x,y)+XN3m(x,y)+XN4m(x,y)+XN5m(x,y))/5;


for ii=2:1775
      A=1;
      B=1776;
      x=realaltitude(ii);
      y=realazimuth(ii);
      Egap1=(ii-A)*(GE1m(x,y)-XE1m(x,y))/(B-A)+XE1m(x,y);
      Egap2=(ii-A)*(GE2m(x,y)-XE2m(x,y))/(B-A)+XE2m(x,y);
      Egap3=(ii-A)*(GE3m(x,y)-XE3m(x,y))/(B-A)+XE3m(x,y);
      Egap4=(ii-A)*(GE4m(x,y)-XE4m(x,y))/(B-A)+XE4m(x,y);
      Egap5=(ii-A)*(GE5m(x,y)-XE5m(x,y))/(B-A)+XE5m(x,y);
      Ngap1=(ii-A)*(GN1m(x,y)-XN1m(x,y))/(B-A)+XN1m(x,y);
      Ngap2=(ii-A)*(GN2m(x,y)-XN2m(x,y))/(B-A)+XN2m(x,y);
      Ngap3=(ii-A)*(GN3m(x,y)-XN3m(x,y))/(B-A)+XN3m(x,y);
      Ngap4=(ii-A)*(GN4m(x,y)-XN1m(x,y))/(B-A)+XN4m(x,y);
      Ngap5=(ii-A)*(GN5m(x,y)-XN5m(x,y))/(B-A)+XN5m(x,y);
      ewgapbeam(ii)=(Egap1+Egap2+Egap3+Egap4+Egap5)/5;
      nsgapbeam(ii)=(Ngap1+Ngap2+Ngap3+Ngap4+Ngap5)/5;

      Egapd1=(ii-A)*(E1diffusesky(7)-E1diffusesky(9))/(B-
A)+E1diffusesky(9);
      Egapd2=(ii-A)*(E2diffusesky(7)-E2diffusesky(9))/(B-
A)+E2diffusesky(9);
      Egapd3=(ii-A)*(E3diffusesky(7)-E3diffusesky(9))/(B-
A)+E3diffusesky(9);
      Egapd4=(ii-A)*(E4diffusesky(7)-E4diffusesky(9))/(B-
A)+E4diffusesky(9);
```

```
      Egapd5=(ii-A)*(E5diffusesky(7)-E5diffusesky(9))/(B-
A)+E5diffusesky(9);
      Ngapd1=(ii-A)*(N1diffusesky(7)-N1diffusesky(9))/(B-
A)+N1diffusesky(9);
      Ngapd2=(ii-A)*(N2diffusesky(7)-N2diffusesky(9))/(B-
A)+N2diffusesky(9);
      Ngapd3=(ii-A)*(N3diffusesky(7)-N3diffusesky(9))/(B-
A)+N3diffusesky(9);
      Ngapd4=(ii-A)*(N4diffusesky(7)-N4diffusesky(9))/(B-
A)+N4diffusesky(9);
      Ngapd5=(ii-A)*(N5diffusesky(7)-N5diffusesky(9))/(B-
A)+N5diffusesky(9);
      ewgapdiffuse(ii)=(Egapd1+Egapd2+Egapd3+Egapd4+Egapd5)/5;
      nsgapdiffuse(ii)=(Ngapd1+Ngapd2+Ngapd3+Ngapd4+Ngapd5)/5;

      ii=ii+1;
end

x=realaltitude(1776);
y=realazimuth(1776);
ewgapbeam(1776)=(GE1m(x,y)+GE2m(x,y)+GE3m(x,y)+GE4m(x,y)+GE5m(x,y))/5;
nsgapbeam(1776)=(GN1m(x,y)+GN2m(x,y)+GN3m(x,y)+GN4m(x,y)+GN5m(x,y))/5;

for ii=1777:5231
      A=1776;
      B=5232;
      x=realaltitude(ii);
      y=realazimuth(ii);
      Egap1=(ii-A)*(HE1m(x,y)-GE1m(x,y))/(B-A)+GE1m(x,y);
      Egap2=(ii-A)*(HE2m(x,y)-GE2m(x,y))/(B-A)+GE2m(x,y);
      Egap3=(ii-A)*(HE3m(x,y)-GE3m(x,y))/(B-A)+GE3m(x,y);
      Egap4=(ii-A)*(HE4m(x,y)-GE4m(x,y))/(B-A)+GE4m(x,y);
      Egap5=(ii-A)*(HE5m(x,y)-GE5m(x,y))/(B-A)+GE5m(x,y);
      Ngap1=(ii-A)*(HN1m(x,y)-GN1m(x,y))/(B-A)+GN1m(x,y);
      Ngap2=(ii-A)*(HN2m(x,y)-GN2m(x,y))/(B-A)+GN2m(x,y);
      Ngap3=(ii-A)*(HN3m(x,y)-GN3m(x,y))/(B-A)+GN3m(x,y);
      Ngap4=(ii-A)*(HN4m(x,y)-GN1m(x,y))/(B-A)+GN4m(x,y);
      Ngap5=(ii-A)*(HN5m(x,y)-GN5m(x,y))/(B-A)+GN5m(x,y);
      ewgapbeam(ii)=(Egap1+Egap2+Egap3+Egap4+Egap5)/5;
      nsgapbeam(ii)=(Ngap1+Ngap2+Ngap3+Ngap4+Ngap5)/5;

      Egapd1=(ii-A)*(E1diffusesky(8)-E1diffusesky(7))/(B-
A)+E1diffusesky(7);
      Egapd2=(ii-A)*(E2diffusesky(8)-E2diffusesky(7))/(B-
A)+E2diffusesky(7);
      Egapd3=(ii-A)*(E3diffusesky(8)-E3diffusesky(7))/(B-
A)+E3diffusesky(7);
      Egapd4=(ii-A)*(E4diffusesky(8)-E4diffusesky(7))/(B-
A)+E4diffusesky(7);
      Egapd5=(ii-A)*(E5diffusesky(8)-E5diffusesky(7))/(B-
A)+E5diffusesky(7);
      Ngapd1=(ii-A)*(N1diffusesky(8)-N1diffusesky(7))/(B-
A)+N1diffusesky(7);
```

```
      Ngapd2=(ii-A)*(N2diffusesky(8)-N2diffusesky(7))/(B-
A)+N2diffusesky(7);
      Ngapd3=(ii-A)*(N3diffusesky(8)-N3diffusesky(7))/(B-
A)+N3diffusesky(7);
      Ngapd4=(ii-A)*(N4diffusesky(8)-N4diffusesky(7))/(B-
A)+N4diffusesky(7);
      Ngapd5=(ii-A)*(N5diffusesky(8)-N5diffusesky(7))/(B-
A)+N5diffusesky(7);
      ewgapdiffuse(ii)=(Egapd1+Egapd2+Egapd3+Egapd4+Egapd5)/5;
      nsgapdiffuse(ii)=(Ngapd1+Ngapd2+Ngapd3+Ngapd4+Ngapd5)/5;

      ii=ii+1;
end

x=realaltitude(5232);
y=realazimuth(5232);
ewgapbeam(5232)=(HE1m(x,y)+HE2m(x,y)+HE3m(x,y)+HE4m(x,y)+HE5m(x,y))/5;
nsgapbeam(5232)=(HN1m(x,y)+HN2m(x,y)+HN3m(x,y)+HN4m(x,y)+HN5m(x,y))/5;


for ii=5233:17519
      A=5232;
      B=17520;
      x=realaltitude(ii);
      y=realazimuth(ii);
      Egap1=(ii-A)*(HE1m(x,y)-HE1m(x,y))/(B-A)+HE1m(x,y);
      Egap2=(ii-A)*(HE2m(x,y)-HE2m(x,y))/(B-A)+HE2m(x,y);
      Egap3=(ii-A)*(HE3m(x,y)-HE3m(x,y))/(B-A)+HE3m(x,y);
      Egap4=(ii-A)*(HE4m(x,y)-HE4m(x,y))/(B-A)+HE4m(x,y);
      Egap5=(ii-A)*(HE5m(x,y)-HE5m(x,y))/(B-A)+HE5m(x,y);
      Ngap1=(ii-A)*(HN1m(x,y)-HN1m(x,y))/(B-A)+HN1m(x,y);
      Ngap2=(ii-A)*(HN2m(x,y)-HN2m(x,y))/(B-A)+HN2m(x,y);
      Ngap3=(ii-A)*(HN3m(x,y)-HN3m(x,y))/(B-A)+HN3m(x,y);
      Ngap4=(ii-A)*(HN4m(x,y)-HN1m(x,y))/(B-A)+HN4m(x,y);
      Ngap5=(ii-A)*(HN5m(x,y)-HN5m(x,y))/(B-A)+HN5m(x,y);
      ewgapbeam(ii)=(Egap1+Egap2+Egap3+Egap4+Egap5)/5;
      nsgapbeam(ii)=(Ngap1+Ngap2+Ngap3+Ngap4+Ngap5)/5;

      Egapd1=(ii-A)*(E1diffusesky(8)-E1diffusesky(8))/(B-
A)+E1diffusesky(8);
      Egapd2=(ii-A)*(E2diffusesky(8)-E2diffusesky(8))/(B-
A)+E2diffusesky(8);
      Egapd3=(ii-A)*(E3diffusesky(8)-E3diffusesky(8))/(B-
A)+E3diffusesky(8);
      Egapd4=(ii-A)*(E4diffusesky(8)-E4diffusesky(8))/(B-
A)+E4diffusesky(8);
      Egapd5=(ii-A)*(E5diffusesky(8)-E5diffusesky(8))/(B-
A)+E5diffusesky(8);
      Ngapd1=(ii-A)*(N1diffusesky(8)-N1diffusesky(8))/(B-
A)+N1diffusesky(8);
      Ngapd2=(ii-A)*(N2diffusesky(8)-N2diffusesky(8))/(B-
A)+N2diffusesky(8);
```

```
      Ngapd3=(ii-A)*(N3diffusesky(8)-N3diffusesky(8))/(B-
A)+N3diffusesky(8);
      Ngapd4=(ii-A)*(N4diffusesky(8)-N4diffusesky(8))/(B-
A)+N4diffusesky(8);
      Ngapd5=(ii-A)*(N5diffusesky(8)-N5diffusesky(8))/(B-
A)+N5diffusesky(8);
      ewgapdiffuse(ii)=(Egapd1+Egapd2+Egapd3+Egapd4+Egapd5)/5;
      nsgapdiffuse(ii)=(Ngapd1+Ngapd2+Ngapd3+Ngapd4+Ngapd5)/5;

      ii=ii+1;
end

x=realaltitude(17520);
y=realazimuth(17520);
ewgapbeam(17520)=(HE1m(x,y)+HE2m(x,y)+HE3m(x,y)+HE4m(x,y)+HE5m(x,y))/5;
nsgapbeam(17520)=(HN1m(x,y)+HN2m(x,y)+HN3m(x,y)+HN4m(x,y)+HN5m(x,y))/5;

for ii=17521:18863
      A=17520;
      B=18864;
      x=realaltitude(ii);
      y=realazimuth(ii);
      Egap1=(ii-A)*(AE1m(x,y)-HE1m(x,y))/(B-A)+HE1m(x,y);
      Egap2=(ii-A)*(AE2m(x,y)-HE2m(x,y))/(B-A)+HE2m(x,y);
      Egap3=(ii-A)*(AE3m(x,y)-HE3m(x,y))/(B-A)+HE3m(x,y);
      Egap4=(ii-A)*(AE4m(x,y)-HE4m(x,y))/(B-A)+HE4m(x,y);
      Egap5=(ii-A)*(AE5m(x,y)-HE5m(x,y))/(B-A)+HE5m(x,y);
      Ngap1=(ii-A)*(AN1m(x,y)-HN1m(x,y))/(B-A)+HN1m(x,y);
      Ngap2=(ii-A)*(AN2m(x,y)-HN2m(x,y))/(B-A)+HN2m(x,y);
      Ngap3=(ii-A)*(AN3m(x,y)-HN3m(x,y))/(B-A)+HN3m(x,y);
      Ngap4=(ii-A)*(AN4m(x,y)-HN1m(x,y))/(B-A)+HN4m(x,y);
      Ngap5=(ii-A)*(AN5m(x,y)-HN5m(x,y))/(B-A)+HN5m(x,y);
      ewgapbeam(ii)=(Egap1+Egap2+Egap3+Egap4+Egap5)/5;
      nsgapbeam(ii)=(Ngap1+Ngap2+Ngap3+Ngap4+Ngap5)/5;

      Egapd1=(ii-A)*(E1diffusesky(1)-E1diffusesky(8))/(B-
A)+E1diffusesky(8);
      Egapd2=(ii-A)*(E2diffusesky(1)-E2diffusesky(8))/(B-
A)+E2diffusesky(8);
      Egapd3=(ii-A)*(E3diffusesky(1)-E3diffusesky(8))/(B-
A)+E3diffusesky(8);
      Egapd4=(ii-A)*(E4diffusesky(1)-E4diffusesky(8))/(B-
A)+E4diffusesky(8);
      Egapd5=(ii-A)*(E5diffusesky(1)-E5diffusesky(8))/(B-
A)+E5diffusesky(8);
      Ngapd1=(ii-A)*(N1diffusesky(1)-N1diffusesky(8))/(B-
A)+N1diffusesky(8);
      Ngapd2=(ii-A)*(N2diffusesky(1)-N2diffusesky(8))/(B-
A)+N2diffusesky(8);
      Ngapd3=(ii-A)*(N3diffusesky(1)-N3diffusesky(8))/(B-
A)+N3diffusesky(8);
      Ngapd4=(ii-A)*(N4diffusesky(1)-N4diffusesky(8))/(B-
A)+N4diffusesky(8);
```

```
      Ngapd5=(ii-A)*(N5diffusesky(1)-N5diffusesky(8))/(B-
A)+N5diffusesky(8);
      ewgapdiffuse(ii)=(Egapd1+Egapd2+Egapd3+Egapd4+Egapd5)/5;
      nsgapdiffuse(ii)=(Ngapd1+Ngapd2+Ngapd3+Ngapd4+Ngapd5)/5;

      ii=ii+1;
end

x=realaltitude(18864);
y=realazimuth(18864);
ewgapbeam(18864)=(AE1m(x,y)+AE2m(x,y)+AE3m(x,y)+AE4m(x,y)+AE5m(x,y))/5;
nsgapbeam(18864)=(AN1m(x,y)+AN2m(x,y)+AN3m(x,y)+AN4m(x,y)+AN5m(x,y))/5;

for ii=18865:20015
      A=18864;
      B=20016;
      x=realaltitude(ii);
      y=realazimuth(ii);
      Egap1=(ii-A)*(BE1m(x,y)-AE1m(x,y))/(B-A)+AE1m(x,y);
      Egap2=(ii-A)*(BE2m(x,y)-AE2m(x,y))/(B-A)+AE2m(x,y);
      Egap3=(ii-A)*(BE3m(x,y)-AE3m(x,y))/(B-A)+AE3m(x,y);
      Egap4=(ii-A)*(BE4m(x,y)-AE4m(x,y))/(B-A)+AE4m(x,y);
      Egap5=(ii-A)*(BE5m(x,y)-AE5m(x,y))/(B-A)+AE5m(x,y);
      Ngap1=(ii-A)*(BN1m(x,y)-AN1m(x,y))/(B-A)+AN1m(x,y);
      Ngap2=(ii-A)*(BN2m(x,y)-AN2m(x,y))/(B-A)+AN2m(x,y);
      Ngap3=(ii-A)*(BN3m(x,y)-AN3m(x,y))/(B-A)+AN3m(x,y);
      Ngap4=(ii-A)*(BN4m(x,y)-AN1m(x,y))/(B-A)+AN4m(x,y);
      Ngap5=(ii-A)*(BN5m(x,y)-AN5m(x,y))/(B-A)+AN5m(x,y);
      ewgapbeam(ii)=(Egap1+Egap2+Egap3+Egap4+Egap5)/5;
      nsgapbeam(ii)=(Ngap1+Ngap2+Ngap3+Ngap4+Ngap5)/5;

      Egapd1=(ii-A)*(E1diffusesky(2)-E1diffusesky(1))/(B-
A)+E1diffusesky(1);
      Egapd2=(ii-A)*(E2diffusesky(2)-E2diffusesky(1))/(B-
A)+E2diffusesky(1);
      Egapd3=(ii-A)*(E3diffusesky(2)-E3diffusesky(1))/(B-
A)+E3diffusesky(1);
      Egapd4=(ii-A)*(E4diffusesky(2)-E4diffusesky(1))/(B-
A)+E4diffusesky(1);
      Egapd5=(ii-A)*(E5diffusesky(2)-E5diffusesky(1))/(B-
A)+E5diffusesky(1);
      Ngapd1=(ii-A)*(N1diffusesky(2)-N1diffusesky(1))/(B-
A)+N1diffusesky(1);
      Ngapd2=(ii-A)*(N2diffusesky(2)-N2diffusesky(1))/(B-
A)+N2diffusesky(1);
      Ngapd3=(ii-A)*(N3diffusesky(2)-N3diffusesky(1))/(B-
A)+N3diffusesky(1);
      Ngapd4=(ii-A)*(N4diffusesky(2)-N4diffusesky(1))/(B-
A)+N4diffusesky(1);
      Ngapd5=(ii-A)*(N5diffusesky(2)-N5diffusesky(1))/(B-
A)+N5diffusesky(1);
      ewgapdiffuse(ii)=(Egapd1+Egapd2+Egapd3+Egapd4+Egapd5)/5;
      nsgapdiffuse(ii)=(Ngapd1+Ngapd2+Ngapd3+Ngapd4+Ngapd5)/5;
```

```
      ii=ii+1;
end

x=realaltitude(20016);
y=realazimuth(20016);
ewgapbeam(20016)=(BE1m(x,y)+BE2m(x,y)+BE3m(x,y)+BE4m(x,y)+BE5m(x,y))/5;
nsgapbeam(20016)=(BN1m(x,y)+BN2m(x,y)+BN3m(x,y)+BN4m(x,y)+BN5m(x,y))/5;

for ii=20017:23759
      A=20016;
      B=23760;
      x=realaltitude(ii);
      y=realazimuth(ii);
      Egap1=(ii-A)*(CE1m(x,y)-BE1m(x,y))/(B-A)+BE1m(x,y);
      Egap2=(ii-A)*(CE2m(x,y)-BE2m(x,y))/(B-A)+BE2m(x,y);
      Egap3=(ii-A)*(CE3m(x,y)-BE3m(x,y))/(B-A)+BE3m(x,y);
      Egap4=(ii-A)*(CE4m(x,y)-BE4m(x,y))/(B-A)+BE4m(x,y);
      Egap5=(ii-A)*(CE5m(x,y)-BE5m(x,y))/(B-A)+BE5m(x,y);
      Ngap1=(ii-A)*(CN1m(x,y)-BN1m(x,y))/(B-A)+BN1m(x,y);
      Ngap2=(ii-A)*(CN2m(x,y)-BN2m(x,y))/(B-A)+BN2m(x,y);
      Ngap3=(ii-A)*(CN3m(x,y)-BN3m(x,y))/(B-A)+BN3m(x,y);
      Ngap4=(ii-A)*(CN4m(x,y)-BN1m(x,y))/(B-A)+BN4m(x,y);
      Ngap5=(ii-A)*(CN5m(x,y)-BN5m(x,y))/(B-A)+BN5m(x,y);
      ewgapbeam(ii)=(Egap1+Egap2+Egap3+Egap4+Egap5)/5;
      nsgapbeam(ii)=(Ngap1+Ngap2+Ngap3+Ngap4+Ngap5)/5;

      Egapd1=(ii-A)*(E1diffusesky(3)-E1diffusesky(2))/(B-
A)+E1diffusesky(2);
      Egapd2=(ii-A)*(E2diffusesky(3)-E2diffusesky(2))/(B-
A)+E2diffusesky(2);
      Egapd3=(ii-A)*(E3diffusesky(3)-E3diffusesky(2))/(B-
A)+E3diffusesky(2);
      Egapd4=(ii-A)*(E4diffusesky(3)-E4diffusesky(2))/(B-
A)+E4diffusesky(2);
      Egapd5=(ii-A)*(E5diffusesky(3)-E5diffusesky(2))/(B-
A)+E5diffusesky(2);
      Ngapd1=(ii-A)*(N1diffusesky(3)-N1diffusesky(2))/(B-
A)+N1diffusesky(2);
      Ngapd2=(ii-A)*(N2diffusesky(3)-N2diffusesky(2))/(B-
A)+N2diffusesky(2);
      Ngapd3=(ii-A)*(N3diffusesky(3)-N3diffusesky(2))/(B-
A)+N3diffusesky(2);
      Ngapd4=(ii-A)*(N4diffusesky(3)-N4diffusesky(2))/(B-
A)+N4diffusesky(2);
      Ngapd5=(ii-A)*(N5diffusesky(3)-N5diffusesky(2))/(B-
A)+N5diffusesky(2);
      ewgapdiffuse(ii)=(Egapd1+Egapd2+Egapd3+Egapd4+Egapd5)/5;
      nsgapdiffuse(ii)=(Ngapd1+Ngapd2+Ngapd3+Ngapd4+Ngapd5)/5;

      ii=ii+1;
end
```

```
x=realaltitude(23760);
y=realazimuth(23760);
ewgapbeam(23760)=(CE1m(x,y)+CE2m(x,y)+CE3m(x,y)+CE4m(x,y)+CE5m(x,y))/5;
nsgapbeam(23760)=(CN1m(x,y)+CN2m(x,y)+CN3m(x,y)+CN4m(x,y)+CN5m(x,y))/5;

for ii=23761:26831
      A=23760;
      B=26832;
      x=realaltitude(ii);
      y=realazimuth(ii);
      Egap1=(ii-A)*(DE1m(x,y)-CE1m(x,y))/(B-A)+CE1m(x,y);
      Egap2=(ii-A)*(DE2m(x,y)-CE2m(x,y))/(B-A)+CE2m(x,y);
      Egap3=(ii-A)*(DE3m(x,y)-CE3m(x,y))/(B-A)+CE3m(x,y);
      Egap4=(ii-A)*(DE4m(x,y)-CE4m(x,y))/(B-A)+CE4m(x,y);
      Egap5=(ii-A)*(DE5m(x,y)-CE5m(x,y))/(B-A)+CE5m(x,y);
      Ngap1=(ii-A)*(DN1m(x,y)-CN1m(x,y))/(B-A)+CN1m(x,y);
      Ngap2=(ii-A)*(DN2m(x,y)-CN2m(x,y))/(B-A)+CN2m(x,y);
      Ngap3=(ii-A)*(DN3m(x,y)-CN3m(x,y))/(B-A)+CN3m(x,y);
      Ngap4=(ii-A)*(DN4m(x,y)-CN1m(x,y))/(B-A)+CN4m(x,y);
      Ngap5=(ii-A)*(DN5m(x,y)-CN5m(x,y))/(B-A)+CN5m(x,y);
      ewgapbeam(ii)=(Egap1+Egap2+Egap3+Egap4+Egap5)/5;
      nsgapbeam(ii)=(Ngap1+Ngap2+Ngap3+Ngap4+Ngap5)/5;

      Egapd1=(ii-A)*(E1diffusesky(4)-E1diffusesky(3))/(B-
A)+E1diffusesky(3);
      Egapd2=(ii-A)*(E2diffusesky(4)-E2diffusesky(3))/(B-
A)+E2diffusesky(3);
      Egapd3=(ii-A)*(E3diffusesky(4)-E3diffusesky(3))/(B-
A)+E3diffusesky(3);
      Egapd4=(ii-A)*(E4diffusesky(4)-E4diffusesky(3))/(B-
A)+E4diffusesky(3);
      Egapd5=(ii-A)*(E5diffusesky(4)-E5diffusesky(3))/(B-
A)+E5diffusesky(3);
      Ngapd1=(ii-A)*(N1diffusesky(4)-N1diffusesky(3))/(B-
A)+N1diffusesky(3);
      Ngapd2=(ii-A)*(N2diffusesky(4)-N2diffusesky(3))/(B-
A)+N2diffusesky(3);
      Ngapd3=(ii-A)*(N3diffusesky(4)-N3diffusesky(3))/(B-
A)+N3diffusesky(3);
      Ngapd4=(ii-A)*(N4diffusesky(4)-N4diffusesky(3))/(B-
A)+N4diffusesky(3);
      Ngapd5=(ii-A)*(N5diffusesky(4)-N5diffusesky(3))/(B-
A)+N5diffusesky(3);
      ewgapdiffuse(ii)=(Egapd1+Egapd2+Egapd3+Egapd4+Egapd5)/5;
      nsgapdiffuse(ii)=(Ngapd1+Ngapd2+Ngapd3+Ngapd4+Ngapd5)/5;

      ii=ii+1;
end

x=realaltitude(26832);
y=realazimuth(26832);
ewgapbeam(26832)=(DE1m(x,y)+DE2m(x,y)+DE3m(x,y)+DE4m(x,y)+DE5m(x,y))/5;
nsgapbeam(26832)=(DN1m(x,y)+DN2m(x,y)+DN3m(x,y)+DN4m(x,y)+DN5m(x,y))/5;
```

```
for ii=26833:29903
      A=26832;
      B=29904;
      x=realaltitude(ii);
      y=realazimuth(ii);
      Egap1=(ii-A)*(EE1m(x,y)-DE1m(x,y))/(B-A)+DE1m(x,y);
      Egap2=(ii-A)*(EE2m(x,y)-DE2m(x,y))/(B-A)+DE2m(x,y);
      Egap3=(ii-A)*(EE3m(x,y)-DE3m(x,y))/(B-A)+DE3m(x,y);
      Egap4=(ii-A)*(EE4m(x,y)-DE4m(x,y))/(B-A)+DE4m(x,y);
      Egap5=(ii-A)*(EE5m(x,y)-DE5m(x,y))/(B-A)+DE5m(x,y);
      Ngap1=(ii-A)*(EN1m(x,y)-DN1m(x,y))/(B-A)+DN1m(x,y);
      Ngap2=(ii-A)*(EN2m(x,y)-DN2m(x,y))/(B-A)+DN2m(x,y);
      Ngap3=(ii-A)*(EN3m(x,y)-DN3m(x,y))/(B-A)+DN3m(x,y);
      Ngap4=(ii-A)*(EN4m(x,y)-DN1m(x,y))/(B-A)+DN4m(x,y);
      Ngap5=(ii-A)*(EN5m(x,y)-DN5m(x,y))/(B-A)+DN5m(x,y);
      ewgapbeam(ii)=(Egap1+Egap2+Egap3+Egap4+Egap5)/5;
      nsgapbeam(ii)=(Ngap1+Ngap2+Ngap3+Ngap4+Ngap5)/5;

      Egapd1=(ii-A)*(E1diffusesky(5)-E1diffusesky(4))/(B-
A)+E1diffusesky(4);
      Egapd2=(ii-A)*(E2diffusesky(5)-E2diffusesky(4))/(B-
A)+E2diffusesky(4);
      Egapd3=(ii-A)*(E3diffusesky(5)-E3diffusesky(4))/(B-
A)+E3diffusesky(4);
      Egapd4=(ii-A)*(E4diffusesky(5)-E4diffusesky(4))/(B-
A)+E4diffusesky(4);
      Egapd5=(ii-A)*(E5diffusesky(5)-E5diffusesky(4))/(B-
A)+E5diffusesky(4);
      Ngapd1=(ii-A)*(N1diffusesky(5)-N1diffusesky(4))/(B-
A)+N1diffusesky(4);
      Ngapd2=(ii-A)*(N2diffusesky(5)-N2diffusesky(4))/(B-
A)+N2diffusesky(4);
      Ngapd3=(ii-A)*(N3diffusesky(5)-N3diffusesky(4))/(B-
A)+N3diffusesky(4);
      Ngapd4=(ii-A)*(N4diffusesky(5)-N4diffusesky(4))/(B-
A)+N4diffusesky(4);
      Ngapd5=(ii-A)*(N5diffusesky(5)-N5diffusesky(4))/(B-
A)+N5diffusesky(4);
      ewgapdiffuse(ii)=(Egapd1+Egapd2+Egapd3+Egapd4+Egapd5)/5;
      nsgapdiffuse(ii)=(Ngapd1+Ngapd2+Ngapd3+Ngapd4+Ngapd5)/5;

      ii=ii+1;
end

x=realaltitude(29904);
y=realazimuth(29904);
ewgapbeam(29904)=(EE1m(x,y)+EE2m(x,y)+EE3m(x,y)+EE4m(x,y)+EE5m(x,y))/5;
nsgapbeam(29904)=(EN1m(x,y)+EN2m(x,y)+EN3m(x,y)+EN4m(x,y)+EN5m(x,y))/5;

for ii=29905:33071
      A=29904;
      B=33072;
```

```
      x=realaltitude(ii);
      y=realazimuth(ii);
      Egap1=(ii-A)*(FE1m(x,y)-EE1m(x,y))/(B-A)+EE1m(x,y);
      Egap2=(ii-A)*(FE2m(x,y)-EE2m(x,y))/(B-A)+EE2m(x,y);
      Egap3=(ii-A)*(FE3m(x,y)-EE3m(x,y))/(B-A)+EE3m(x,y);
      Egap4=(ii-A)*(FE4m(x,y)-EE4m(x,y))/(B-A)+EE4m(x,y);
      Egap5=(ii-A)*(FE5m(x,y)-EE5m(x,y))/(B-A)+EE5m(x,y);
      Ngap1=(ii-A)*(FN1m(x,y)-EN1m(x,y))/(B-A)+EN1m(x,y);
      Ngap2=(ii-A)*(FN2m(x,y)-EN2m(x,y))/(B-A)+EN2m(x,y);
      Ngap3=(ii-A)*(FN3m(x,y)-EN3m(x,y))/(B-A)+EN3m(x,y);
      Ngap4=(ii-A)*(FN4m(x,y)-EN1m(x,y))/(B-A)+EN4m(x,y);
      Ngap5=(ii-A)*(FN5m(x,y)-EN5m(x,y))/(B-A)+EN5m(x,y);
      ewgapbeam(ii)=(Egap1+Egap2+Egap3+Egap4+Egap5)/5;
      nsgapbeam(ii)=(Ngap1+Ngap2+Ngap3+Ngap4+Ngap5)/5;

      Egapd1=(ii-A)*(E1diffusesky(6)-E1diffusesky(5))/(B-
A)+E1diffusesky(5);
      Egapd2=(ii-A)*(E2diffusesky(6)-E2diffusesky(5))/(B-
A)+E2diffusesky(5);
      Egapd3=(ii-A)*(E3diffusesky(6)-E3diffusesky(5))/(B-
A)+E3diffusesky(5);
      Egapd4=(ii-A)*(E4diffusesky(6)-E4diffusesky(5))/(B-
A)+E4diffusesky(5);
      Egapd5=(ii-A)*(E5diffusesky(6)-E5diffusesky(5))/(B-
A)+E5diffusesky(5);
      Ngapd1=(ii-A)*(N1diffusesky(6)-N1diffusesky(5))/(B-
A)+N1diffusesky(5);
      Ngapd2=(ii-A)*(N2diffusesky(6)-N2diffusesky(5))/(B-
A)+N2diffusesky(5);
      Ngapd3=(ii-A)*(N3diffusesky(6)-N3diffusesky(5))/(B-
A)+N3diffusesky(5);
      Ngapd4=(ii-A)*(N4diffusesky(6)-N4diffusesky(5))/(B-
A)+N4diffusesky(5);
      Ngapd5=(ii-A)*(N5diffusesky(6)-N5diffusesky(5))/(B-
A)+N5diffusesky(5);
      ewgapdiffuse(ii)=(Egapd1+Egapd2+Egapd3+Egapd4+Egapd5)/5;
      nsgapdiffuse(ii)=(Ngapd1+Ngapd2+Ngapd3+Ngapd4+Ngapd5)/5;

      ii=ii+1;
end

x=realaltitude(33072);
y=realazimuth(33072);
ewgapbeam(33072)=(FE1m(x,y)+FE2m(x,y)+FE3m(x,y)+FE4m(x,y)+FE5m(x,y))/5;
nsgapbeam(33072)=(FN1m(x,y)+FN2m(x,y)+FN3m(x,y)+FN4m(x,y)+FN5m(x,y))/5;

for ii=33073:35039
      A=33072;
      B=35040;
      x=realaltitude(ii);
      y=realazimuth(ii);
      Egap1=(ii-A)*(XE1m(x,y)-FE1m(x,y))/(B-A)+FE1m(x,y);
      Egap2=(ii-A)*(XE2m(x,y)-FE2m(x,y))/(B-A)+FE2m(x,y);
```

```
      Egap3=(ii-A)*(XE3m(x,y)-FE3m(x,y))/(B-A)+FE3m(x,y);
      Egap4=(ii-A)*(XE4m(x,y)-FE4m(x,y))/(B-A)+FE4m(x,y);
      Egap5=(ii-A)*(XE5m(x,y)-FE5m(x,y))/(B-A)+FE5m(x,y);
      Ngap1=(ii-A)*(XN1m(x,y)-FN1m(x,y))/(B-A)+FN1m(x,y);
      Ngap2=(ii-A)*(XN2m(x,y)-FN2m(x,y))/(B-A)+FN2m(x,y);
      Ngap3=(ii-A)*(XN3m(x,y)-FN3m(x,y))/(B-A)+FN3m(x,y);
      Ngap4=(ii-A)*(XN4m(x,y)-FN1m(x,y))/(B-A)+FN4m(x,y);
      Ngap5=(ii-A)*(XN5m(x,y)-FN5m(x,y))/(B-A)+FN5m(x,y);
      ewgapbeam(ii)=(Egap1+Egap2+Egap3+Egap4+Egap5)/5;
      nsgapbeam(ii)=(Ngap1+Ngap2+Ngap3+Ngap4+Ngap5)/5;

      Egapd1=(ii-A)*(E1diffusesky(9)-E1diffusesky(6))/(B-
A)+E1diffusesky(6);
      Egapd2=(ii-A)*(E2diffusesky(9)-E2diffusesky(6))/(B-
A)+E2diffusesky(6);
      Egapd3=(ii-A)*(E3diffusesky(9)-E3diffusesky(6))/(B-
A)+E3diffusesky(6);
      Egapd4=(ii-A)*(E4diffusesky(9)-E4diffusesky(6))/(B-
A)+E4diffusesky(6);
      Egapd5=(ii-A)*(E5diffusesky(9)-E5diffusesky(6))/(B-
A)+E5diffusesky(6);
      Ngapd1=(ii-A)*(N1diffusesky(9)-N1diffusesky(6))/(B-
A)+N1diffusesky(6);
      Ngapd2=(ii-A)*(N2diffusesky(9)-N2diffusesky(6))/(B-
A)+N2diffusesky(6);
      Ngapd3=(ii-A)*(N3diffusesky(9)-N3diffusesky(6))/(B-
A)+N3diffusesky(6);
      Ngapd4=(ii-A)*(N4diffusesky(9)-N4diffusesky(6))/(B-
A)+N4diffusesky(6);
      Ngapd5=(ii-A)*(N5diffusesky(9)-N5diffusesky(6))/(B-
A)+N5diffusesky(6);
      ewgapdiffuse(ii)=(Egapd1+Egapd2+Egapd3+Egapd4+Egapd5)/5;
      nsgapdiffuse(ii)=(Ngapd1+Ngapd2+Ngapd3+Ngapd4+Ngapd5)/5;

      ii=ii+1;
end

x=realaltitude(35040)
y=realazimuth(35040)
ewgapbeam(35040)=(XE1m(x,y)+XE2m(x,y)+XE3m(x,y)+XE4m(x,y)+XE5m(x,y))/5;
nsgapbeam(35040)=(XN1m(x,y)+XN2m(x,y)+XN3m(x,y)+XN4m(x,y)+XN5m(x,y))/5;

ewgapdiffuseout=ewgapdiffuse';
nsgapdiffuseout=nsgapdiffuse';
ewgapbeamout=ewgapbeam';
      nsgapbeamout=nsgapbeam';
```